SEISMIC RESPONSE OF REINFORCED CONCRETE WALLS WITH STEEL BOUNDARY ELEMENTS

by

Bryce Tupper

March 1999

Department of Civil Engineering and Applied Mechanics

McGill University

Montréal, Canada

A thesis submitted to the Faculty of Graduate Studies
and Research in partial fulfilment of the requirements
for the degree of Master of Engineering

0-612-50667-3

SEISMIC RESPONSE OF REINFORCED CONCRETE WALLS WITH STEEL BOUNDARY ELEMENTS

ABSTRACT

A reinforced concrete ductile flexural wall requires the placement of well-detailed concentrated reinforcement at the ends of the wall. This often results in congestion in these heavily reinforced regions, resulting in labourious construction. Two flexural wall specimens, containing structural steel boundary elements, were constructed and tested under reversed cyclic loading to evaluate the performance of this new construction technique. For comparison, a third wall specimen meeting the requirements of a standard reinforced concrete ductile flexural wall was constructed and tested under reversed cyclic loading. One of the composite walls used rectangular hollow structural sections (HSS) as boundary elements which were connected to the wall by welding the transverse bars directly to both HSS elements. The second wall used steel channels connected to the wall with headed studs welded to the channels. These studs overlapped with the transverse reinforcing bars, which had headed ends. The details of these three walls were chosen such that all of the walls had approximately the same flexural capacity. The reversed cyclic responses of the three walls showed that each wall had similar hysteretic properties. Following significant yielding of the structural steel, local buckling of the steel boundary elements in the composite walls was observed. The design used for ductile flexural walls was modified to enable comparable design of reinforced walls with steel boundary elements.

COMPORTEMENT SISMIQUE DE MURS EN BÉTON ARMÉ AVEC DES ÉLÉMENTS EN ACIER AUX EXTRÉMITÉS

RÉSUMÉ

Il est nécessaire de bien détailler l'emplacement de l'armature d'acier aux extrémités pour les murs ductiles en béton armé en flexion. La congestion de l'armature d'acier dans ces régions fortement armées, rendent leurs construction difficile. Deux murs en flexion, avec des éléments en acier à leurs extrémités, ont été construits et soumis à des charges cycliques afin d'évaluer la performance de cette nouvelle technique de construction. A des fins comparatives, un troisième mur en flexion fut construit selon les normes usuelles et soumis à des charges cycliques réversibles. L'un des murs composites incorpore des tubes rectangulaires (HSS) comme éléments d'extrémité. Ceux-ci ont été reliés au mur eu soudant des barres transversales directement aux deux tubes HSS. Le deuxième mur utilise des profilés d'acier avec section C reliés au mur à l'aide de goujons avec tête, soudés aux profilés en C. Ces goujons chevauchent les barres transversales qui ont des têtes à leurs extrémités. Les détails pour ces trois murs ont été choisis de sorte que la capacité en flexion soit la même pour les trois murs. Le comportement cyclique des trois murs indique qu'ils ont des propriétés hystéretiques similaires. Après une importante plastification de l'acier structural, un flambement local des aciers en extrémité des murs composites fût observé. La méthode de conception des murs ductiles en flexion fut modifiée afin d'obtenir une conception équivalente pour les murs renforcés à l'aide de composites en acier en périphérie.

ACKNOWLEDGMENTS

The author would like acknowledge Professor Denis Mitchell for his encouragement and expert guidance. The assistance and advice of Dr. Bill Cook and Stuart Bristowe was extremely appreciated. The author would also like to acknowledge the contributions of Professor S. H. Cho for his insight, encouragement and for providing funding for this research project as part of the STRESS research programme in Korea.

Thanks are extended to Ron Sheppard, Marek Prykorski, Damon Kiperchuk, and John Bartczak, technicians in the Jamieson Structures Laboratory, for helping to construct the test specimens. Thanks are also extended to Kevin Li, Emmet Poon, Pierre Koch, Pedro Da Silva, Carla Ghannoum, Wassim Ghannoum and Hanaa Issa.

Lastly, the author would like to acknowledge the help of the office staff of the Department of Civil Engineering and Applied Mechanics at McGill University.

Bryce Tupper
March, 1999

TABLE OF CONTENTS

LIST OF FIGURES

Chapter 4

Appendix A

LIST OF TABLES

LIST OF SYMBOLS

A_b	area distributed longitudinal reinforcement within spacing s_v
A_{cv}	net area of concrete bounded by web thickness and length of section in the direction of lateral force consideration
A_{be}	area of structural steel boundary element
A_g	gross area of concrete wall
A_s	area of tensile reinforcement
A_{sh}	total cross-sectional area of transverse reinforcement within a distance, s_h
A_{tr}	transformed area of wall
A_v	effective area of transverse reinforcement
A_w	area of weld
b_w	width of wall
c_c	depth of the neutral axis measured from the compression edge of the wall
d	distance from extreme compression fibre to centroid of tension reinforcement
d_A	nominal diameter of aggregate
d_{cs}	the smaller of a) the distance of the concrete surface to the centre of the bar being developed or b) 2/3 the centre-to-centre spacing of the bars being developed
d_b	nominal diameter of reinforcement
d_t	nominal diameter of tie
f'_c	specified compressive strength of concrete
f_{sp}	splitting strength of concrete
f_r	modulus of rupture
f_y	specified yield strength of reinforcement
f_{yb}	specified yield strength of boundary element
f_{yh}	yield strength of transverse reinforcement
f_{ult}	ultimate strength of reinforcement
F	foundation factor of a structure
F_{app}	applied lateral load
h_s	interstorey height
h_w	height of wall
I	importance factor of a structure
k_1	bar location factor
k_2	bar coating factor
k_3	concrete density factor
k_4	bar size factor
K_{tr}	transverse reinforcement index
k_u	stiffness at a deflection of Δ_u
k_y	stiffness at a deflection of Δ_y
ℓ_d	development length for a straight bar
ℓ_p	plastic hinge length
ℓ_u	clear distance between floors or other lines of weak axis support
ℓ_w	horizontal length of wall
L	length of axial strands
M	moment at base of wall
M_{cr}	cracking moment
M_{cr}^+	positive cracking moment
M_{cr}^-	negative cracking moment
M_m	maximum resisting moment of wall
M_n	nominal moment
M_p	probable moment
M_{sw}	wall self-weight moment
M_y	moment at general yield
M_y'	moment at first yield
M_u	moment at ultimate curvature not less than 80% of M_u
n	number of bars or wires being developed along potential plane of bond splitting
N	number shear connectors
P_{axial}	applied axial load
P_x	horizontal axial load component
P_y	vertical axial load component
R	force modification factor

s	maximum centre-to-centre spacing of transverse reinforcement within ℓ_d
s_h	spacing of distributed transverse reinforcement
s_v	spacing of distributed longitudinal reinforcement
S	seismic response factor of a structure
S_{tr}	transformed sectional modulus of wall
T	fundamental period of vibration of a structure
U	calibration factor of a structure
v	zonal velocity ratio
V	seismic base shear of a structure
V_e	equivalent lateral force at the base of the structure representing elastic response
V_p	design shear
V_{peak}	load corresponding to Δ_{peak}
V_r	nominal shear resistance of one No. 10 transverse reinforcement
V_u	load corresponding to Δ_u
V_y	load corresponding to Δ_y
W	dead load of a structure plus 25% of design snow load plus 60% of the storage load for areas used for storage and the full contents of tanks
X_u	ultimate tensile strength of electrode
Z_a	acceleration-related seismic zone
Z_v	velocity-related seismic zone
Δ_{peak}	cycle peak tip deflection
Δ	tip deflection
Δ_u	maximum recorded tip deflection
Δ_y	deflection at general yielding
Δ_y'	deflection at first yielding
Δ_y^+	deflection at general yielding in the positive direction
Δ_y^-	deflection at general yielding in the negative direction
ε	strain
ε_1	principal tensile strain
ε_2	principal compression strain
ε_c'	concrete strain corresponding to f_c'
ε_s	strain in reinforcement
ε_y	yield strain of reinforcement
ϕ	diameter
ϕ_c	resistance factor for concrete
ϕ_s	resistance factor for reinforcement
ϕ_w	resistance factor for weld
γ	shear strain in the plastic hinge region of wall
γ_w	wall overstrength factor equal to the ratio of the load corresponding to nominal moment resistance of the wall system to the factored load on the wall system
φ	wall curvature
φ_m	curvature at maximum moment
φ_u	ultimate curvature
φ_y	general yield curvature
φ_y'	first yield curvature
λ	factor to account for density of concrete
μ	coefficient of friction
ρ	ratio of reinforcement to concrete

CHAPTER 1

INTRODUCTION

The research reported in this thesis is aimed at investigating alternative construction techniques for shear walls incorporating structural steel boundary elements, interconnected to the reinforced concrete web of the wall. The reversed cyclic loading performance of this new type of construction is compared to the performance of concrete shear walls with conventional reinforcement details.

1.1 Seismic Design Criteria for Structural Walls

According to Paulay (1980) "the primary requirement for an earthquake-resisting shearwall structure is that it should ensure survival during the largest ground shaking that can be expected in the locality". The National Building Code of Canada (NBCC 1995), gives provisions for the design of structures to achieve an acceptable level of safety. Specifically, the code prescribes the minimum lateral seismic force at the base of the structure, V, as follows:

$$V = \frac{V_e}{R} U \qquad (1\text{-}1)$$

where,
- V_e = equivalent lateral force at the base of the structure representing elastic response
- R = force modification factor
- U = factor representing level of protection based on experience, 0.6

The equivalent lateral force, V_e, is calculated as:

$$V_e = v \cdot S \cdot I \cdot F \cdot W \qquad (1\text{-}2)$$

where,
- v = zonal velocity ratio = the specified zonal horizontal ground velocity expressed as a ratio of 1 m/s
- I = seismic importance factor of the structure
- F = foundation factor

W = dead load plus 25% of the design snow load plus 60% of the storage load for areas used for storage and the full contents of tanks

S = seismic response factor, for unit value of zonal velocity ratio, based on
- fundamental period of vibration of the structure
- acceleration-related seismic zone
- velocity-related seismic zone

The force modification factor, R, defines the ability of a structure to dissipate energy through inelastic behaviour. The NBCC categorizes a number of different types lateral-force-resisting systems having varying values of R. Reinforced concrete walls are categorized as "ductile coupled walls" (R=4.0), "other ductile wall systems" (R=3.5), "walls with nominal ductility" (R=2.0) and other structural walls without special seismic design or detailing requirements (R=1.5).

In addition to strength requirements, the NBCC limits the interstorey drift of structures under seismic actions. In determining the interstorey drifts the estimated lateral deflections are first determined using an elastic analysis with the loads found from Eq. 1-1. The resulting elastic deflections multiplied by the force modification factor, R, are limited to 0.01 h_s for post-disaster buildings and 0.02 h_s for all other buildings, where h_s is the interstorey height.

The Canadian design and detailing requirements for "ductile flexural walls" (R=3.5) and for walls with nominal ductility (R=2.0), given in the Canadian Standards Association A23.3 "Design of Concrete Structures" (1994), are discussed below.

1.1.1 Ductile Flexural Walls

Clause 21.5 of the CSA A23.3 Standard (1994) prescribes the design and detailing requirements for reinforced concrete ductile flexural walls. These requirements are based mainly on the requirements developed for the New Zealand Standard (NZS 3101) "Concrete Structures Standard" (1982, 1995). These provisions are based on the capacity design philosophy developed by Park and Paulay (1975) to ensure that significant flexural hinging can occur without the formation of brittle failure modes. The plastic hinge region is typically located at the base of a cantilever wall where significant flexural deformations occur. Figure 1.1[1], adapted from the CSA Standard A23.3 Commentary (1994), indicates the region of potential plastic hinging and includes a method for estimating the plastic hinge length. In order to ensure that plastic hinging can occur, the CSA Standard assumes that at the hinge location the wall can develop its probable moment resistance, M_p. This probable moment resistance is defined as the moment resistance of the section using 1.25 f_y as the equivalent yield stress of the tension reinforcement and the specified values of f'_c, with material resistance factors, ϕ_c and ϕ_s, taken as 1.0.

The primary longitudinal reinforcement used to develop the resisting moment is concentrated at both ends of the wall (see Fig. 1.2). The minimum amounts and detailing requirements for this concentrated reinforcement and other distributed reinforcement are summarized in Fig. 1.2 and Table 1.1, which are both taken from the CSA Standard A 23.3 Commentary (1994). For example, the concentrated reinforcing bars have to be tied within confining hoops, which are detailed like column transverse reinforcement according to Clause 7.6 of the CSA Standard A23.3. All the reinforcing bars used in ductile flexural walls must be weldable grade in accordance with CSA Standard G30.18 (1992).

To ensure that the plastic hinge has opportunity to develop fully without other brittle failure modes occurring, the CSA Standard has requirements to avoid shear failure and instability problems. The factored shear resistance of a ductile flexural wall must be greater than the applied shear corresponding to the development of the probable moment resistance at the base of the wall. In determining this factored shear resistance the contribution of the tensile stresses in the concrete are neglected in the plastic hinge region. The horizontal reinforcement must be sufficiently anchored into the confined regions of the concentrated longitudinal reinforcement (see Fig. 1.2 and Table 1.1). In order to limit instability of the compression zone of ductile flexural walls a minimum wall thickness, b_w, of $\ell_u/10$ must be provided, where ℓ_u is the clear storey height of the wall.

Clause 21.5.6.7 of the CSA Standard limits the calculated depth of compression, c_c, to a maximum value of $0.55\ell_w$ in order to provide the desired level of ductility. If c_c exceeds this value, the wall will have insufficient plastic rotational capabilities needed to reach the desired ductility.

	Plastic Hinge	Other Region
Distributed reinforcement		
Amount	$\rho \geq 0.0025$	$\rho \geq 0.0025$
Spacing	≤ 300 mm	≤ 450 mm
Horizontal reinforcement anchorage	develop f_y within region of concentrated reinforcement	extend into region of concentrated reinforcement
Concentrated reinforcement		
Where required	at ends of walls and coupling beams, corners, and junctions	at ends of the walls and coupling beams
Amount (at least 4 bars)	$\rho \geq 0.002\ b_w\ \ell_w$ $\rho \leq 0.06$ x area of concentrated reinforcement region	$\rho \geq 0.001\ b_w\ \ell_w$ $\rho \leq 0.06$ x area of concentrated reinforcement region
Hoop requirements	must satisfy Clauses 7.6 and 21.5.6.5	hoop spacing according to Clause 7.6
Splice requirements	1.5 ℓ_d and not more than 50% of the same location. Unless lap length less than 1/4 storey height lap alternate floors	1.5 ℓ_d and 100% at the same location.

Table 1.1 CSA A23.3 requirements for ductile flexural wall reinforcement

1.1.2 Walls with Nominal Ductility

The design criteria for walls with nominal ductility are based on similar design principles as that for ductile flexural walls. However, there are some relaxation in the requirements in keeping with the smaller force modification factor (R=2.0) for walls with nominal ductility. The minimum thickness for walls with nominal ductility is $\ell_u/14$. The required factored shear resistance is the shear corresponding to the attainment of the nominal moment resistance instead of the shear corresponding to the probable moment resistance. The reinforcement used in walls with nominal ductility need not be weldable grade meeting CSA Standard G30.18 (1992). In order to ensure sufficient ductility in the plastic hinge region of a wall with nominal ductility the neutral axis depth, c_c, shall not exceed $0.33\ell_w\gamma_w$ (where γ_w is the wall overstrength factor, equal to the ratio of the load corresponding to nominal moment resistance of the wall system to the factored load on the wall system). This limit may be exceeded if concentrated vertical reinforcement having a minimum reinforcement ratio of 0.005, tied in accordance with Clause 21.4.4, is provided over the outer half of the compression zone.

1.2 Brief Summary of Previous Research

1.2.1 Reinforced Concrete Shear Walls

Cardenas and Magura (1973) studied the advantages of using vertical steel, concentrated at the ends of walls, in improving the ductility (see Fig. 1.3). They carried out analytical predictions of the monotonic responses of a series of walls with varying percentages and distributions of vertical reinforcement. These monotonic predictions indicated that with concentrated reinforcement at the ends of the walls, rather that uniformly distributed reinforcement, larger ductilities could be attained.

Park and Paulay (1975) contributed significantly to the development of capacity design procedures and important detailing concepts for the design of beams, columns and shear wall systems. This research led to the development of the progressive design codes given in the New Zealand Standards (NZS 1982, 1995). A comprehensive summary of shear wall design considerations, along with corresponding research, is given by Paulay and Preistley (1992).

The ductility characteristics of structural walls were reported by Paulay and Uzumeri in 1975. They established a relationship between the curvature and displacement ductilities of walls with different wall height to length aspect ratios (see Fig. 1.4). The range of required curvature ductilities for each aspect ratio and displacement ductility is derived from an upper and lower estimate of plastic hinge length. The plastic hinge lengths are in turn a function of the wall dimensions or aspect ratio. It is seen that as shear walls become more slender they develop a greater plastic hinge length resulting in more rotational capacity and in turn greater ductility.

Wall stability becomes a concern when thin wall sections are subjected to high compressive strains which could possibly lead to out-of-plane buckling. It is explained in the NZS Commentary on The Design of Concrete Structures (1982, 1995) that this concern is based on concepts of Eulerian buckling of struts. The resulting solution to reducing the occurrence of instability was to limit the wall thickness, b_w, to about one-tenth the height of the wall in the first storey. This solution is also reflected in the CSA Standard A23.3 (1984, 1994). More recent research by Goodsir (1985) and Goodsir, Paulay and Carr (1983) shows that out-of-plane buckling of thin walls is more dependent on high inelastic tensile strains in the tensile steel. It is believed that upon initial moment reversal, all compressive stresses will be resisted by the steel because the cracks, formed in the concrete from the previous tensile cycle, will not have completely closed. The result may be a flexural compressive force that does not coincide with the centre of the wall thickness, b_w. This eccentricity together with small dislocated concrete particles and unaligned crack surfaces could lead to instability.

One of the consequences of Park and Paulay's (1975) concern over achieving large ductility led to the suggestion that the concentrated steel at the ends of the wall should be tied as columns. Confined concrete at the end of a walls would increase the allowable strain in the compression zone of the wall where strains exceeding 0.004 are required to reach larger curvature ductilities. In addition, more closely spaced ties at the ends of walls prevent buckling of the concentrated vertical reinforcement (Park and Paulay, 1975; ACI 318, 1989).

Several issues must be considered to ensure that shear failure in a structural wall will be avoided so that the desired ductility and energy dissipation can be achieved. The shear resistance of a wall system must first be sufficient to withstand potential flexural overstrength. Markevicius and Ghosh (1987) examined the effects of shear from the influence of second and third modes of vibration on the a cantilever wall system. They stated that dynamic shear magnification will occur, moving the maximum shear lower in the wall compared to the first mode of vibration. Blakeley, Cooney and Meggett (1975) showed that as the fundamental period of the wall increases, so does the shear contributions from higher modes. Iqbal and Derecho (1980) have also proposed shear force envelopes based on inelastic dynamic analyses. In an attempt to understand the reversed cyclic shear-resisting mechanisms of concrete, Corely, Fiorato and Oesterle (1981) observed that uniformly distributed horizontal and vertical reinforcement helped to preserve the shear capacity of the concrete web. Tests on the reversed cyclic loading performance of shear walls by Bertero et al. (1977), and Vallenas et al. (1979) and Oesterle et al. (1980) showed that despite limitations applied to maximum shear stress in the wall web, web crushing in the plastic hinge region may occur after a few cycles of reversed cyclic loading.

1.2.2 Composite Members

Composite members, especially columns, have been extensively used for seismic resistance in Japan. Wakabayashi (1986) explained that "buildings of composite construction showed good earthquake resistant capacity under the Kanto earthquake (1923) as compared with ordinary reinforced concrete structures". However, in the 1995 Kobe earthquake a large number of failures occurred in structures with composite members built before 1981. There were many examples of failures in concrete encased steel columns, due to poor confinement. In addition, there were failures of columns at the transition between encased steel construction and reinforced concrete construction, which usually occurred at the sixth storey level (Hiraishi and Kaminosono, 1996; Mitchell et al. 1996). In 1974 Wakabayashi showed that experimental flexural strengths could be accurately predicted with the theoretical assumption that "plane sections remain plane". The experimental results from testing composite columns indicated that the strengths were similar to that of reinforced concrete members. In addition, Wakabayashi and Minami (1976) observed that reinforced concrete encased columns had improved shear behaviour when compared to traditional reinforced concrete columns. The hysteretic loops, governed by shear distortion, of a concrete-encased steel column produced greater ductility and less strength degradation compared to a reinforced concrete column. Wakabayashi's composite research was supported by other surveys on composite members (e.g., Viest, 1974). Viest pointed out the increased stiffness and energy absorption that is developed by encasing a steel beam with concrete. He also commented on the reduction of torsional instability and local buckling that is associated with the use of concrete encased steel beams.

Composite shear walls originated as reinforced concrete shear walls with encased flat steel bars, steel trusses and steel plates (Tall Building Committee A41, 1979). The deformation capacity produced by the steel truss and steel plate composite walls compared to reinforced concrete walls is shown in Fig. 1.5. The use of composite construction resulted in greater ductility with the load-carrying capacity being limited by the buckling of the concrete-encased steel.

Composite lateral load resisting systems incorporating moment-resisting steel frames with an infill of reinforced concrete were also studied. Chrysostomou (1991) pointed out the importance of composite shear connection between the infilled concrete and steel boundary elements. Without adequate shear connection, the storey shear is primarily resisted by a compression struts in the concrete panel. This compressive strut has finite width and is aligned with the corners of the panel. In contrast, frames with adequate shear connection are able to resist the shear with a field of diagonal compression in the concrete rather than one single strut.

The Composite Structural Steel and Reinforced Concrete Buildings Provisions of the AISC (1997) and the National Earthquake Hazards Reduction Program (NEHRP, 1997) provide some design provisions for boundary element shear walls. One consideration is that the structural steel sections shall meet dimensional limitations to produce significant inelastic deformations without local buckling. Another, tentative recommendation suggests that the static yield strength of the composite shear connectors be reduced 25% as a conservative measure, until further research is performed.

1.3 Research Objectives

The overall objective of this research project is to investigate the feasibility of reinforced concrete shear walls incorporating structural steel boundary elements having adequate shear connection to the reinforced concrete. Two very different types of composite shear walls were investigated: one with total prefabrication of the boundary elements, shear connection and wall reinforcement, while the other specimen had prefabricated boundary elements and shear connectors, with additional reinforcement to be added in the field. The construction of these two composite walls, including prefabrication and on-site activities, were compared with the construction of a typical reinforced concrete ductile flexural wall.

In order to compare the seismic responses of the two composite shear walls with the response of the reinforced concrete ductile flexural wall all three walls were subjected to reversed cyclic loading. The response characteristics that were examined include:

1. load versus deflection responses;
2. crack patterns and crack development;
3. moment versus curvature responses;
4. extent of flexural yielding;
5. shear responses and
6. failure modes.

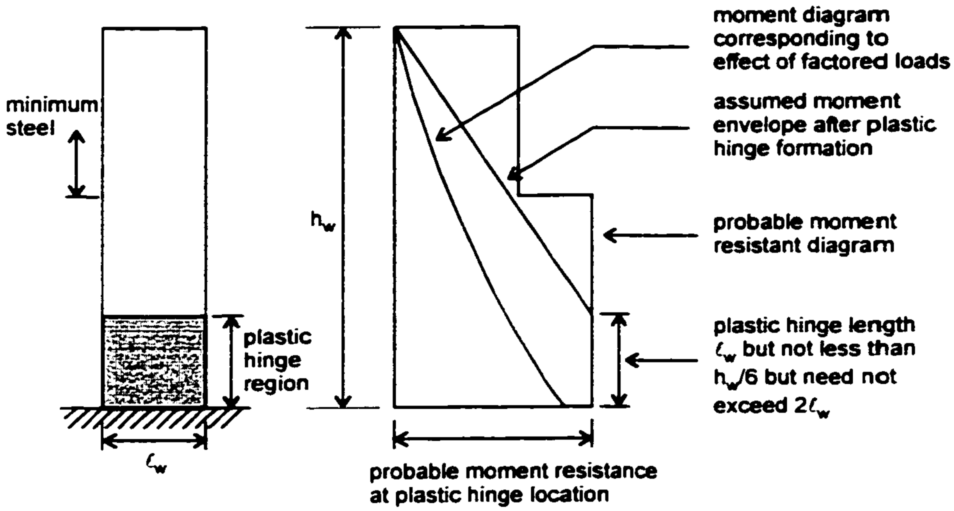

Figure 1.1 Determination of potential plastic hinging (adapted from CSA Standard A23.3-94)

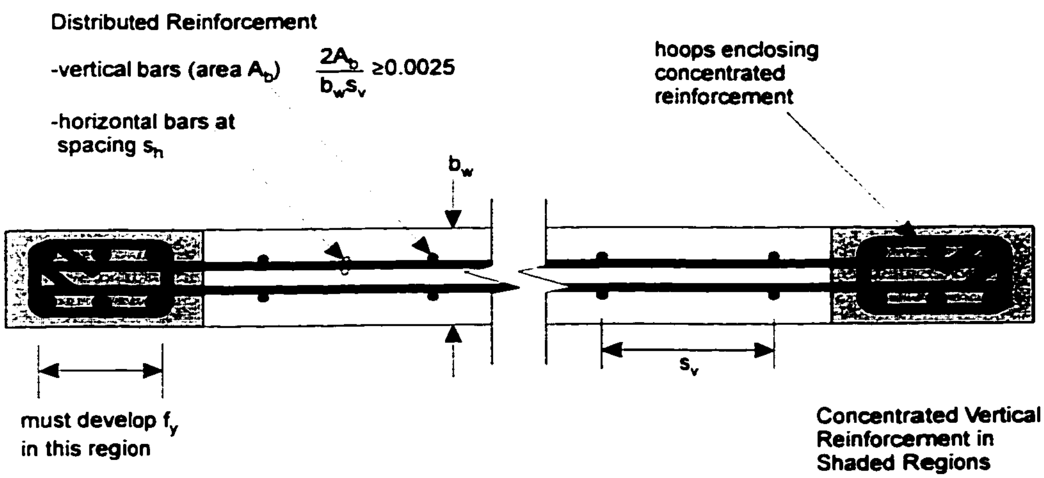

Figure 1.2 Concentrated and distributed reinforcement (adapted from CSA Standard A23.3-94)

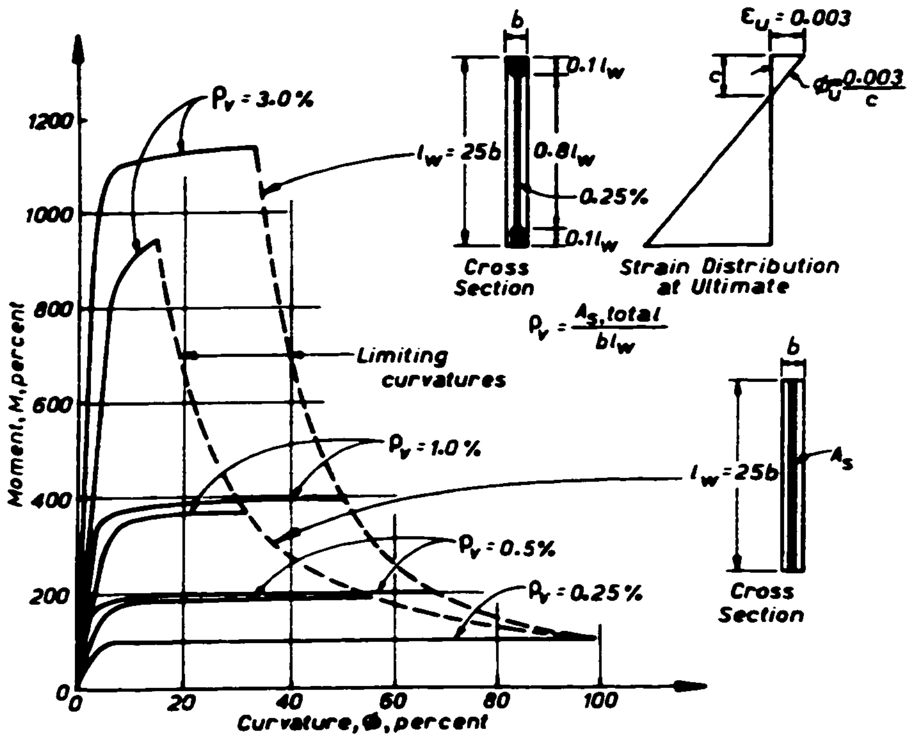

Figure 1.3 Effect of distributed vertical reinforcement on curvature (Cardenas and Magura, 1973)

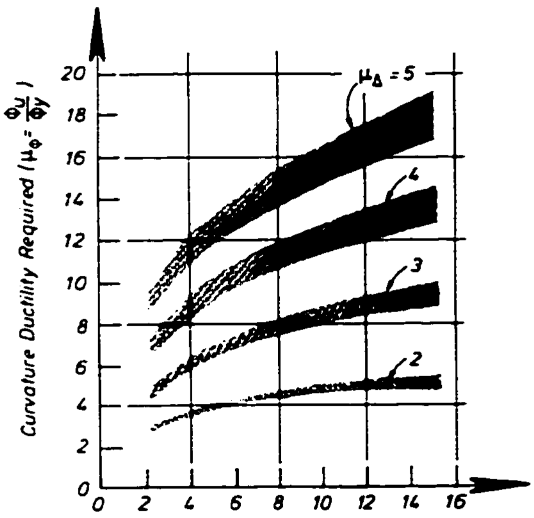

Figure 1.4 Variation of the curvature ductility ratio at the base of cantilever walls with the aspect ratio and imposed displacement ductility demand (Paulay and Uzumeri, 1975)

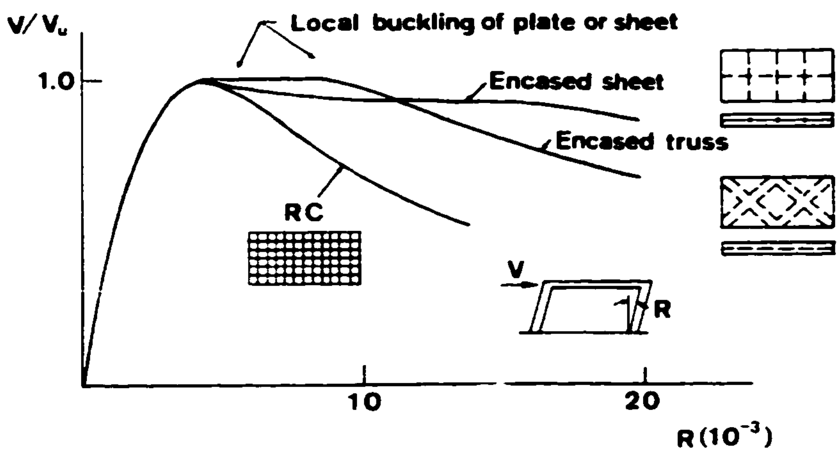

Figure 1.5 Idealized envelope curves of the load-deflection relationship of shear walls failing in shear under repeated loading (Tall Building Committee A41, 1979)

CHAPTER 2

EXPERIMENTAL PROGRAMME

Three shear wall specimens were constructed and tested in the Jamieson Structures Laboratory of the Department of Civil Engineering at McGill University. Two specimens containing different types of steel boundary elements and one typical reinforced concrete wall were subjected to reversed-cyclic loading. In addition to the seismic loading responses, different stages of construction for each specimen were monitored to enable comparisons of the construction techniques.

2.1 Design of Test Specimens

The design of the walls followed the philosophy and design requirement described in Clause 21.5 of the CSA Standard A23.3 (1994) for ductile flexural wall systems. The walls were designed as ductile flexural walls with force modification factors, R, of 3.5.

The test specimens had the same overall dimensions, representing approximately half scale of a typical prototype shear wall. The dimensions were chosen to accommodate the shear wall testing facility. The cross-sectional dimensions of each wall were 1000 mm by 152 mm, with the shear wall cantilevering 3900 mm from the end block (see Fig. 2.1). The potential hinge length, assumed as 1000 mm, was equal to the wall length in conformance with the CSA. Each wall emerged from a heavily reinforced end block, representing a foundation, with dimensions of 1400 mm by 2500 mm by 400 mm, as shown in Fig. 2.1.

The design of the test specimens is given in Appendix A. A minimum concrete compressive strength of 35 MPa was used for design. For all three walls, the 300 mm spacing of distributed longitudinal reinforcement was taken from the minimum requirement necessary for plastic hinge regions. The spacing of distributed transverse reinforcement used for shear resistance varied with each wall. However, the same shear design expression was used to determine the spacing, s_h, of the transverse reinforcement. This spacing was calculated as:

$$s_h = \frac{\phi_s A_{sh} f_y d}{V_p} \qquad (2\text{-}1)$$

where, ϕ_s = resistance factor for reinforcing bars (0.85)
A_{sh} = area of transverse steel within a distance s (200 mm^2 - 2 No. 10 bars)
f_y = actual yield stress of No. 10 transverse reinforcement (488 MPa)
d = effective depth of specimen
V_p = design shear corresponding to the formation of plastic hinging in the wall

Differences in spacing arose from variations in effective depth and design shear force of the three specimens. The effective depths are the distances from extreme concrete compression fibre to the centroid of the tension reinforcement. The design shear was determined using the program RESPONSE (Collins & Mitchell, 1991). The flexural response was determined for each specimen assuming monotonic loading.

An axial load level was also chosen to represent an expected compressive load for a twelve storey structure. The resulting compressive load was 600 kN (see Appendix A), which is approximately 9 % of nominal axial capacity or 11% of gross concrete strength, $A_g f'_c$, of the typical reinforced concrete wall specimen. This axial load of 600 kN was also used with the walls containing boundary elements.

2.2 Specimen Detailing

2.2.1 Reinforcement Details for Specimen W1

The design details of Specimen W1 are presented in Figs 2.2 and 2.3. Specimen W1 was designed and constructed with hollow structural sections (HSS) at the wall boundaries. These HSS sections were not filled with concrete during casting. The transverse reinforcing bars were placed in two layers, 180 mm apart as calculated from Eq. 2-1 in order to provide sufficient shear resistance (see Appendix A). Each pair of transverse bars were welded to the inner flanges of the HSS elements, separated by a clear spacing of 66 mm (see Fig 2.2).

Additional transverse reinforcement, spaced at 90 mm, located at the tip of the wall was used to ensure full flexural development and composite shear connection of the HSS elements. A clear concrete cover of 15 mm was provided over the longitudinal reinforcing bars which were tied to the outside of the transverse bars (see Fig 2.2). The heavily reinforced end block details were chosen to ensure proper anchorage and force transfer.

2.2.2 Reinforcement Details for Specimen W2

The second specimen was constructed with steel channel sections as boundary elements. Figures 2.4 and 2.5 present the details of Specimen W2. Shear studs, 207 mm in length, were welded at the interior face of the channel webs to provide the necessary composite connection. Each stud had a diameter of 12.7 mm with a 25 mm diameter head. Spacing of the studs was 220 mm to match the spacing of the transverse reinforcement (see Appendix A). Each pair of studs was separated by a 63 mm clear spacing. Extra studs were welded to the channels near the tip of the wall to provide extra shear connection and ensure full flexural development of the channels. In order to guarantee development of the transverse reinforcement, each transverse bar had a 37 mm x 37 mm x 9.5 mm plate welded to each end and were overlapped 175 mm with the headed studs (see Fig. 2.4). The clear concrete cover was 15 mm to the longitudinal reinforcement. As with Specimen W1, the channel sections, longitudinal reinforcement and shear reinforcement continued into the footing end block to provide proper anchorage.

2.2.3 Reinforcement Details of Specimen W3

The typical reinforced concrete shear wall, Specimen W3, was designed to have a similar flexural capacity to that of the boundary element walls (see Appendix A). Specimen W3 had eight No. 20 bars concentrated at each end of the wall that were confined by 6 mm diameter ties (see Figs 2.6 and 2.7). The confining ties were spaced at a distance of one half the wall thickness, 76 mm, in the plastic hinge region and were spaced at a distance equal to the wall thickness, 152 mm, elsewhere. A clear concrete cover of 15 mm was used on the ties, while 30 mm was used on the longitudinal reinforcement. The pairs of No. 10

transverse bars were placed at 215 mm throughout the wall height, as calculated by Eq. 2-1. These bars extended into the confined regions of concentrated reinforcement, conforming to the development requirement of CSA Standard A23.3 (see Appendix A).

2.2.4 Foundation End Block

The end block for each wall was identical. The end blocks were heavily reinforced to provided adequate anchorage for the reinforcement of each wall, while responding elastically during flexural hinging of the walls. The flexural capacity of the end block was provided by eight No. 25 headed bars. In addition, closed stirrups were used to confine the longitudinal reinforcement anchored in the wall and to provide adequate shear resistance.

2.3 Construction Sequence

The same formwork was used in the casting of each of the specimens and the construction sequence for the end blocks of each wall was identical. The details of the construction sequence for each specimen are discussed below.

2.3.1 Specimen W1

The first step in the construction of Specimen W1 was to drill holes in the HSS elements for the placement and welding of the No. 10 transverse bars (see Figs 2.2 and 2.3). After placement of the bars in the holes, the steel sections were properly aligned and leveled. During the alignment stage, several welded connections were made to help position the HSS elements. Following this, the remaining welds were completed and the resulting frame was inserted into the formwork. Once in place, longitudinal reinforcement was tied to the outside of the transverse reinforcement. The concrete was placed into the formwork with the wall in a horizontal position (see Fig. 2.3a). The HSS elements provided the formwork for the ends of the wall and remained "hollow" after casting.

2.3.2 Specimen W2

The No. 10 transverse bars of Specimen W2 were fabricated by welding plates to their ends resulting in headed bars, 930 mm in length. Standard stud welding procedures enabled the rapid welding of the stud shear connectors to the channel boundary elements (see Fig. 2.8). Following the stud welding, the channels where aligned and the headed reinforcing bars were tied to each pair of adjacent studs. The steel frame was placed into the formwork and the longitudinal reinforcing bars were tied to the outside of the transverse reinforcement. The steel channels served as formwork at the ends of the wall during the placing of the concrete.

2.3.3 Specimen W3

The first stage of the construction of Specimen W3 was the fabrication of the tied column cages forming the concentrated reinforcement. The fabrication of the two column cages required considerable effort to tie the confining hoops to the longitudinal bars. The concentrated reinforcement cages were aligned and the transverse bars were tied into the confined cores. Unlike Specimens W1 and W2, Specimen W3 required additional formwork at the ends of the wall.

2.4 Material Properties

2.4.1 Reinforcing Steel

The reinforcement used in the construction of each of the specimens was in conformance with CSA Standard G30.18. All reinforcement was weldable grade, which is required for structures having a force modification factor greater than 2.0. Three samples of each reinforcing bar size were tested in order to determine their stress-strain characteristics. The test samples of the 6 mm and 10 mm diameter bars were 250 mm in length and the No. 20 bars were 500 mm in length. With the 6 mm diameter bars and the No. 10 bars, a 25 mm long extensometer was used to measure strain. The No. 20 bars were instrumented with a 150 mm long extensometer. The 6 mm diameter bars and No. 20 bars were used in the design and construction of Specimen W3 and the No. 10 bars were used in all of the specimens. Figure 2.9 shows typical stress versus strain curves for these reinforcing bars while Table 2.1 summarizes the mechanical properties.

Bar Size	Bar Description	f_y, MPa (std. deviation)	ε_y, mm/mm (std. deviation)	f_{ult}, MPa (std. deviation)
6 mm diameter	W3 confining hoops	381.2 (0.6)	0.00174 (0.00014)	445.2 (3.6)
No. 10	distributed reinforcement	487.8 (6.6)	0.00285 (0.00030)	597.5 (2.7)
No. 20	W3 flexural reinforcement	450.1 (1.1)	0.00246 (0.00053)	610.0 (0.5)

Table 2.1 Properties of reinforcing steel

2.4.2 Structural Steel

Two types of structural steel were used, rectangular hollow steel sections in Specimen W1 and channel sections in Specimen W2. Coupons, 250 mm in length, were fabricated from the two different steel sections in order to perform tensile tests from which typical stress versus strain curves were found (see Fig. 2.10). The stress-strain relationship for the HSS samples have no defined yield plateau and hence the 0.2 percentage offset stress was used for the equivalent yield stress. The mechanical properties are summarized in Table 2.2. Both the HSS and channel sections conformed to the Class 1 requirements of the CSA S16.1 (see Table 2.2). A Class 1 section is defined as an member that will attain plastic moment capacity, reduced for the presence of axial load, prior to local buckling of the plate elements. It is indicated in Table 2.2, that the flange of the HSS and the web of the channel section are closest to the CSA requirements and will undergo local buckiling first. The effective slenderness ratios of each of the sections are a function of the transverse reinforcement spacing, s_h, and are also presented in Table 2.2

Property	Specimen W1	Specimen W2
Steel Description (Area, mm^2)	HSS 152x102x6.4 (2960)	C 150x19 (2450)
f_y, MPa (std. deviation)	377.0 (18.3)	402.2 (2.1)
ε_y, mm/mm (std. deviation)	0.00500 (0.00005)	0.0028 (0.00130)
f_{ult}, MPa (std. deviation)	442.5 (16.6)	555.0 (3.7)
Flange b/t ratio = (b-2t)/t	21.9	12.1
CSA Class 1 Flange b/t limit	21.6 ($420\sqrt{F_y}$)	20.9 ($420\sqrt{F_y}$)
Web h/w ratio	14.1	6.2
CSA Class 1 Web h/w limit	21.6 ($420\sqrt{F_y}$)	7.2 ($145\sqrt{F_y}$)
s_h, mm	180	220
Effective Slenderness Ratio, s_h/t	28.3	19.3

Table 2.2 Properties of structural steel

2.4.3 Studs

Three stud specimens were fabricated at the same time the studs were welded to the channels. Each stud specimen consisted of two studs each welded to opposite sides of a steel plate (see Fig. 2.10). The head of each stud was removed and then direct tension was applied to the specimens to determine the yield stress and ultimate strength of the studs and the adequacy of the stud welds. Two of the specimens failed by yielding of the stud and one failed in a brittle manner at the weld. The specimen that failed in the weld reached a load level exceeding the yield force, corresponding to 90% of the stud capacity. An additional stud specimen was tested (Fig. 2.10) to determine the stress-strain relationship. The results of the testing of these four specimens are summarized in Table 2.3. The large standard deviation in the ultimate strength of the studs, given in Table 2.3, is due to the lower ultimate strength of the specimen that failed in the weld.

Stud	Description	f_y, MPa (std. deviation)	f_{ult}, MPa (std. deviation)
12.7 mm diameter	shear connection in W2	402.0 (11.9)	500.7 (29.3)

Table 2.3 Properties of studs

2.4.4 Concrete

Ready-mix concrete with a specified 28 day compressive strength of 30 MPa was used for all three specimens. Table 2.4 shows the components of the mix and indicates the proportions as specified by the supplier.

A series of field cured standard cylinders and flexural beams were prepared from each of the three casts and tested to determine the concrete properties. The compressive strengths, f'_c, and compressive stress-strain relationships (see Fig. 2.11) were determined from three 150 mm diameter by 300 mm cylinders for each batch. The modulus of rupture, f_r, was determined from 150 x 150 x 600 mm long flexural beams subjected to three-point loading. The splitting tensile strength, f_{sp}, was determined from three 150 x 300 mm cylinders. Table 2.5 summarizes the test results.

Shrinkage measurements for each concrete batch were taken on two standard 50 mm by 50 mm shrinkage specimens over a gauge length of 275 mm (see Fig. 2.12). The readings were taken between two small studs embedded in either end of the concrete prisms. The concrete from Specimen W1 underwent approximately 40% more shrinkage than the other Specimen's concrete, which is consistent with the lower concrete compressive strength observed for the concrete of Specimen W1 (see Fig. 2.11). If excessive water was added to the concrete mix of Specimen W1 the result would be greater shrinkage and lower compressive strength.

Component	Specified quantity
cement (kg/m^3)	*340
fine aggregate (kg/m^3)	795
coarse aggregate (kg/m^3)	**1055
water (kg/m^3)	160
water-cement ratio	0.47
superplasticizer (L/m^3)	2.9
retarding agent (L/m^3)	0.28
slump (mm)	170
Air content	5 %
density (kg/m^3)	2350

*Type 30 high early strength cement
**20 mm maximum aggregate

Table 2.4 Mix proportions for all specimens

Specimen	f'_c, MPa (std. deviation)	ε_c, mm/mm (std. deviation)	f_r, MPa (std. deviation)	f_{sp}, MPa (std. deviation)
W1	25.8 (0.8)	0.0022 (0.00029)	3.8 (0.4)	2.2 (0.2)
W2	38.1 (0.0)	0.0020 (0.00012)	3.9 (0.3)	3.0 (0.2)
W3	38.7 (2.4)	0.0022 (0.00001)	3.7 (0.5)	3.2 (0.3)

Table 2.5 Concrete properties

2.5 Test Setup

The wall specimens were tested in their horizontal positions due to the available shear wall testing apparatus (see Figs 2.13 and 2.14). Each wall end block was placed on four steel supports and then post-tensioned to the reaction floor with eight 37 mm diameter high-strength threaded rods.

Two pairs of 250 mm stroke hydraulic jacks were used to provide the reversed cyclic loading at a distance of 3750 mm from the wall base. To produce downward loading (positive shear) a reaction beam on top of the wall was pulled down with 32 mm diameter threaded rods using jacks, which were bearing against the under-side of the reaction floor (see Fig. 2.13). Negative shear loading was produced with upward forces provided by two jacks bearing against the top surface of the reaction floor. Upward loading was transmitted to the underside of each specimen through a distribution plate and a 50 mm diameter roller.

The constant axial load of 600 kN was provided with four hydraulic jacks and four 15 mm diameter prestressing strands (see Figs 2.13 and 2.14).

A steel frame near the tip of the wall was used to prevent out-of-plane movement of the wall. As shown in Fig. 2.14, the out-of-plane movement was resisted by two rollers on each side of the wall, which reacted against vertical extension arms attached to the wall. The rollers permitted vertical movement of the walls while preventing side to side movement.

2.6 Instrumentation

A computerized data acquisition system was used to record load, displacement and strain values at small intervals throughout testing. In addition, some strain measurements were taken manually using a demountable strain indicator.

2.6.1 Load Measurements

Load cells were used to measure the positive and negative shear forces on each wall and to monitor the axial load. In total, eight load cells were used in each test to collect the load measurements (see Fig. 2.13). The axial load was recorded using four 350 kN load cells and the applied shear was recorded using 445 kN load cells.

2.6.2 Deflection Measurements

Linear voltage differential transducers (LVDTs) were used to measure the deflections of each wall. Two ±125 mm range LVDTs, located 3650 mm from the base of the wall, were used to monitor the tip deflections (see Fig. 2.15). The two LVDTs were offset 75 mm in opposite directions allowing for a total available tip travel of ±175 mm ensuring the acquisition of all deflection data.

Two sets of four LVDTs were attached to the tension and compression chords along the height of each wall (see Fig. 2.15) in order to determine curvature. In addition. each wall had LVDTs configured to form a rosette over the length of the expected plastic hinge region. A slightly different configuration was used for Specimen W2 than that used for Specimens W1 and W3 (see Fig. 2.15).

A pair of LVDTs was also used to measure the movement of the end blocks relative to the reaction floor. No significant movement was observed.

2.6.3 Strain Measurements

Strain measurements were collected using both electrical resistance strain gauges and demountable mechanical targets. The gauge lengths of the electrical resistance strain gauges were 5 mm and 2 mm dependent on the surface to which they were mounted (see Fig. 2.16). The gauge length between the mechanical targets was 200 mm (8 inches). The mechanical strain measurements were taken manually at the peak load of each cycle and at zero loads.

Two rosettes composed of mechanical targets with 200 mm gauge lengths were attached to the concrete in the plastic hinge region. Each rosette enabled determination of local shear strains and principal strains in the concrete. These rosettes were centred in the middle of the web at distances of 500 mm and 700 mm from the base of the wall (see Fig. 2.16). Specimens W1 and W2 had mechanical targets attached to the structural steel and concrete in order to measure any separation between the structural steel boundary elements and the concrete. These targets were located at 50 mm and 900 mm from the base of the wall on both sides of the walls (see Fig. 2.16).

Seven electrical resistance strain gauges were placed on the outer faces of the tension and compression steel chords of each wall (see Fig. 16). The gauges were located along the lengths of the hollow sections, channel sections and the No. 20 reinforcing bars for the respective walls. In each wall, the first strain gauge was placed at the base of the wall while the others were spaced 200 mm along the wall. These gauges allowed the progression of yielding along the height of each wall to be monitored.

Electrical resistance strain gauges with 2 mm gauge lengths were placed on specific transverse reinforcement in each wall. Figure 2.16 shows the locations of the strain gauges, which were glued to the two No. 10 transverse reinforcing bars. Only one transverse bar was instrumented in the plastic hinge region of Specimen W3, however, two 6 mm diameter confining hoops, located 126 mm from the base of the wall were instrumented (see Fig 2.7).

2.7 Test Procedure

Throughout testing, the axial load was monitored and adjusted to give a constant load of 600 kN. The reversed cyclic lateral loading was applied in small steps at a distance of 3750 mm from the base of the wall. One complete cycle consisted of a downward and then upward loading sequence. Downward loading and deflection were chosen as positive quantities as positive moments were created. Consequently, upward loading and deflections were assigned negative quantities.

Figure 2.17 shows the proposed loading sequence for each wall. The first two cycles were load-control sequences with essentially elastic response. The first cycle was to produce the pre-calculated moment, $0.5M_{cr}$, equal to half of the cracking moment. The second cycle loaded the walls to the theoretical cracking moment, M_{cr}. The next cycle was determined by the first yielding of flexural steel in the wall, monitored by the electrical resistance strain gauges. The peak of the fourth cycle was taken as the load and deflection corresponding to general yield, Δ_y, of the wall. General yielding is determined by the point at which a significant drop in stiffness occurs, indicated by the load versus tip deflection relationship for the specimen. The cycles after general yielding were controlled by deflection limits, based on multiples of the general yield deflection. It should be noted, for the load-controlled cycles a correction for self-weight was made.

During the experiments, manual measurements of the mechanical strain gauges, photographs and crack widths were taken at the peak of each half cycle. All other electronic readings were taken by a computerized data acquisition system at short intervals during both the loading and unloading.

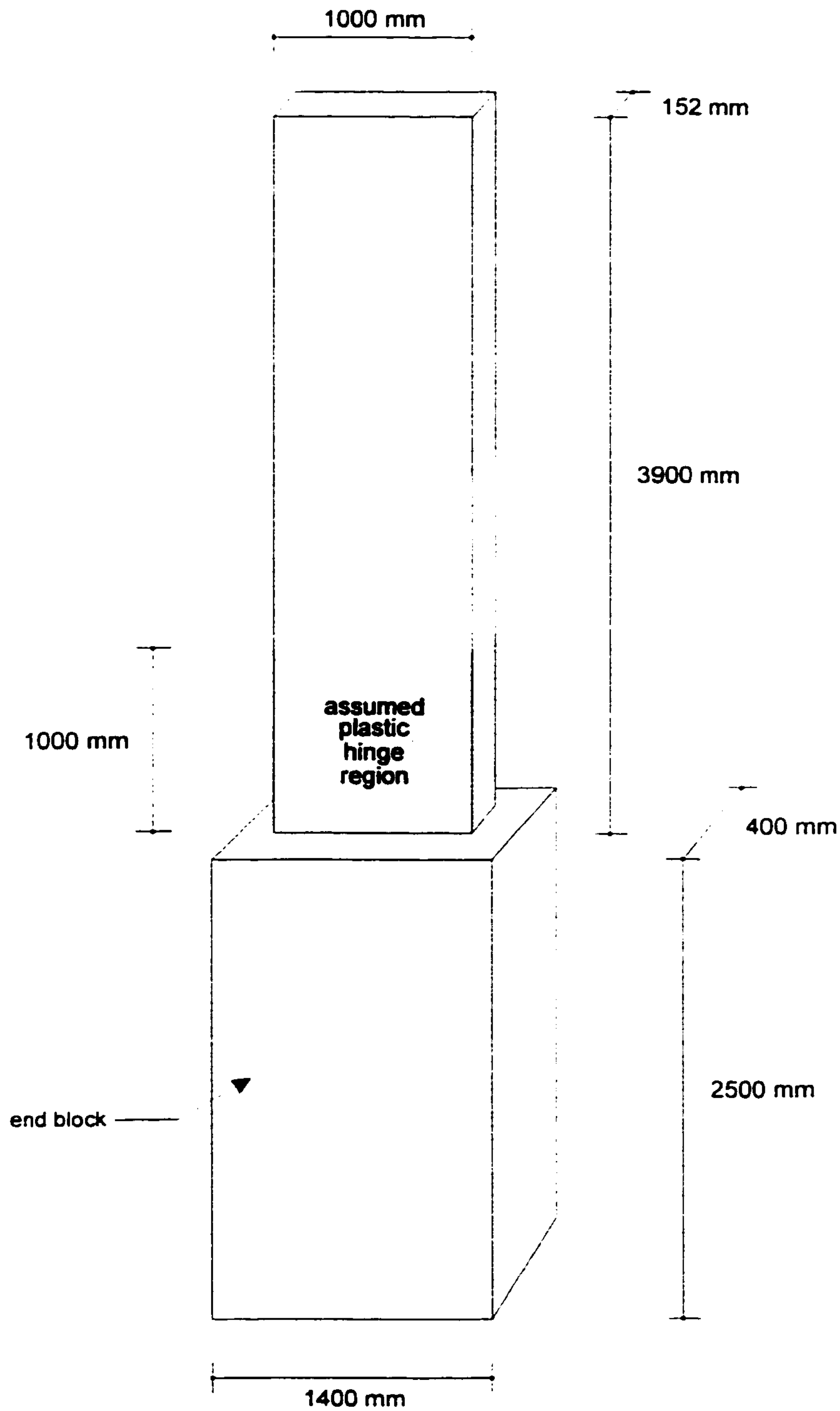

Figure 2.1 Typical wall dimensions

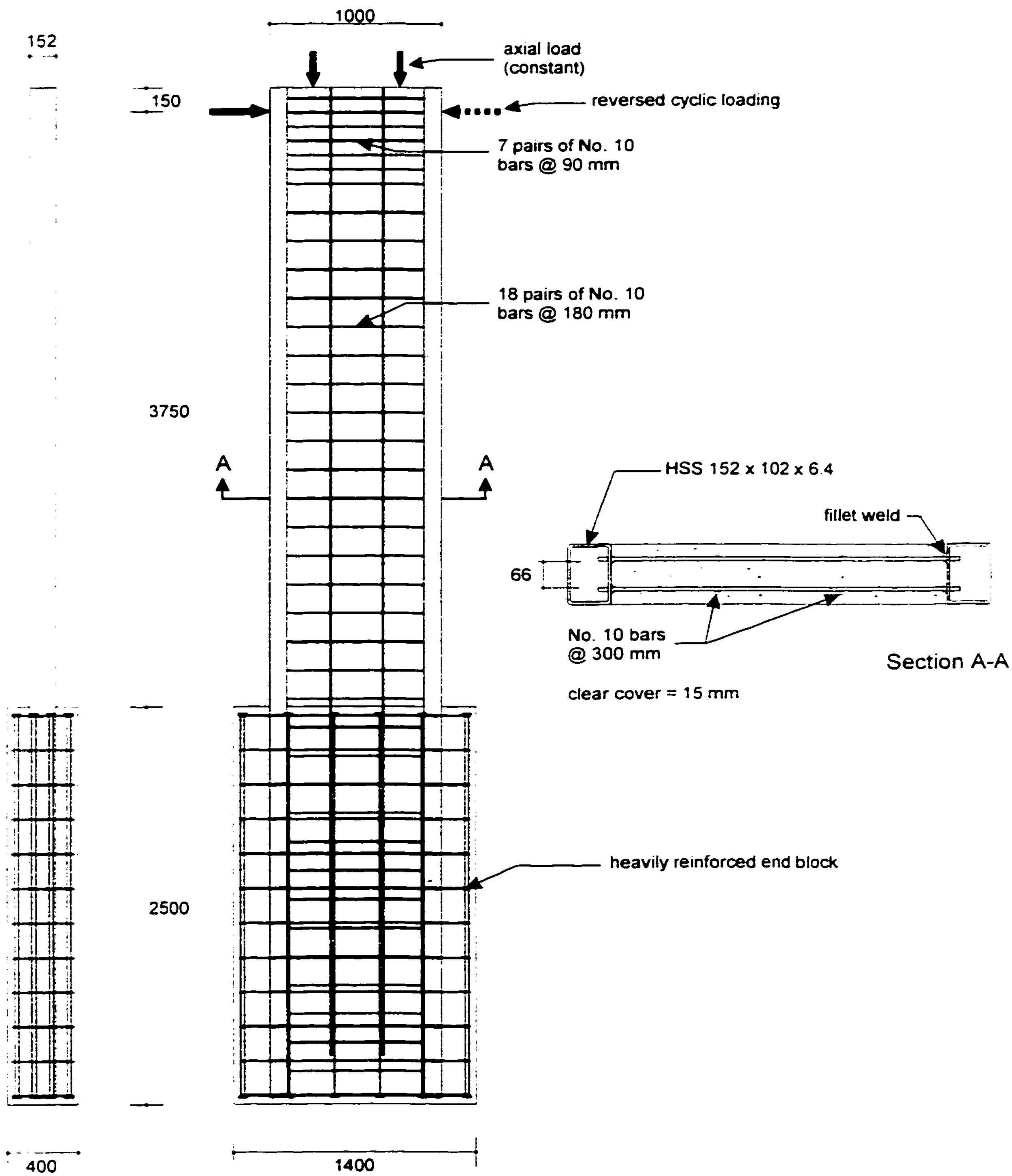

Figure 2.2 Details of reinforcement for Specimen W1

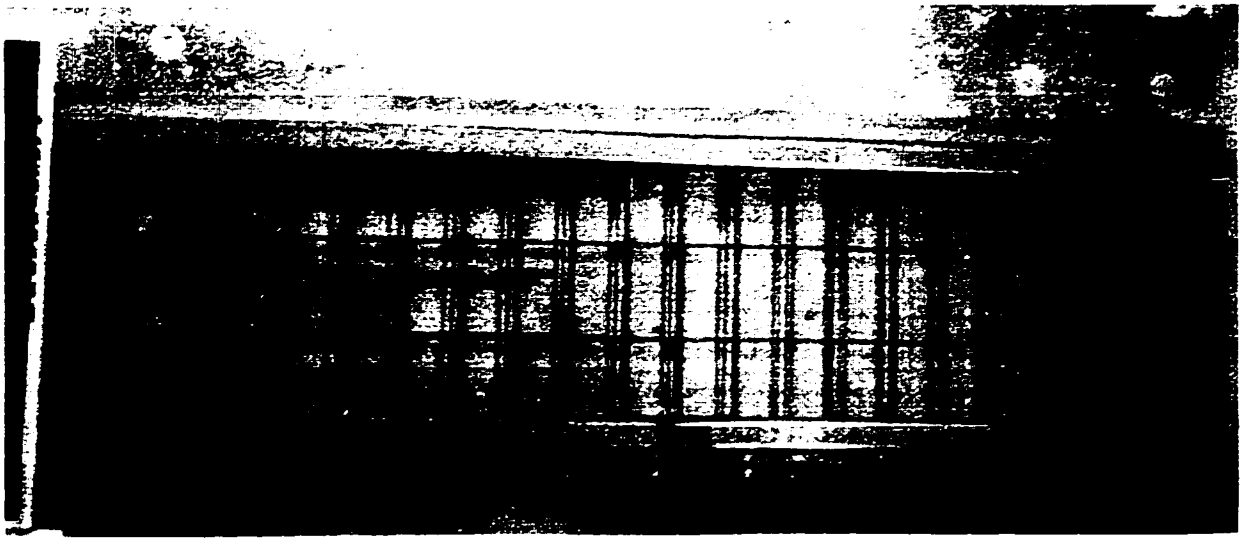

a) reinforcement before casting

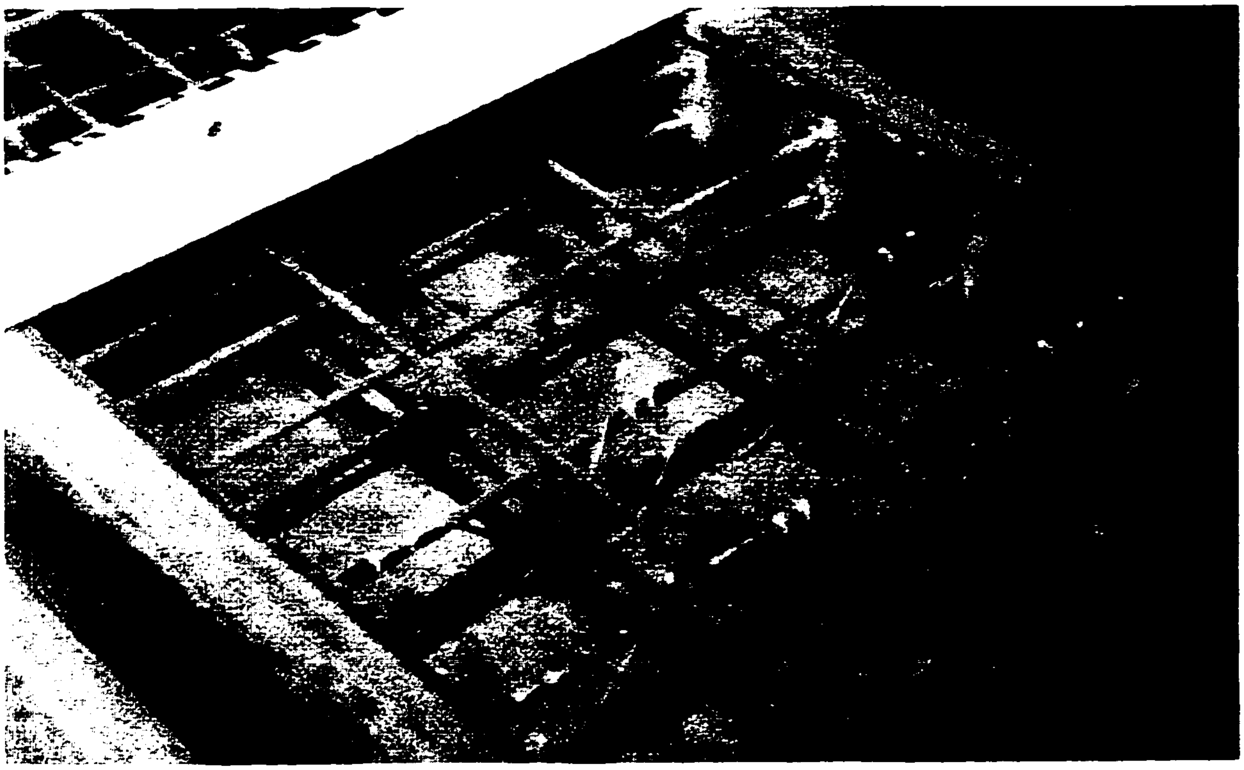

b) close-up of reinforcement

Figure 2.3 Specimen W1 reinforcing cage

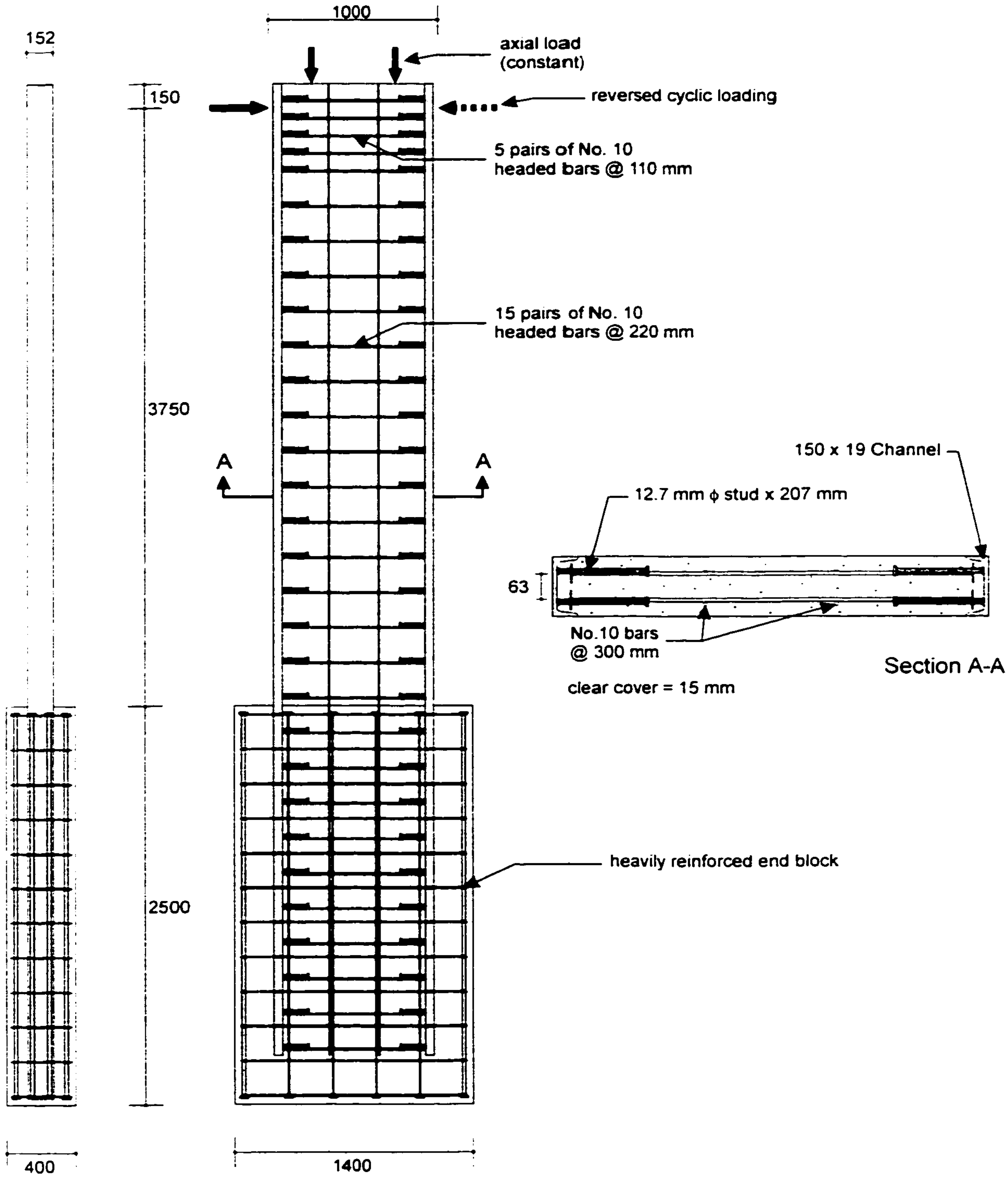

Figure 2.4 Details of reinforcement for Specimen W2

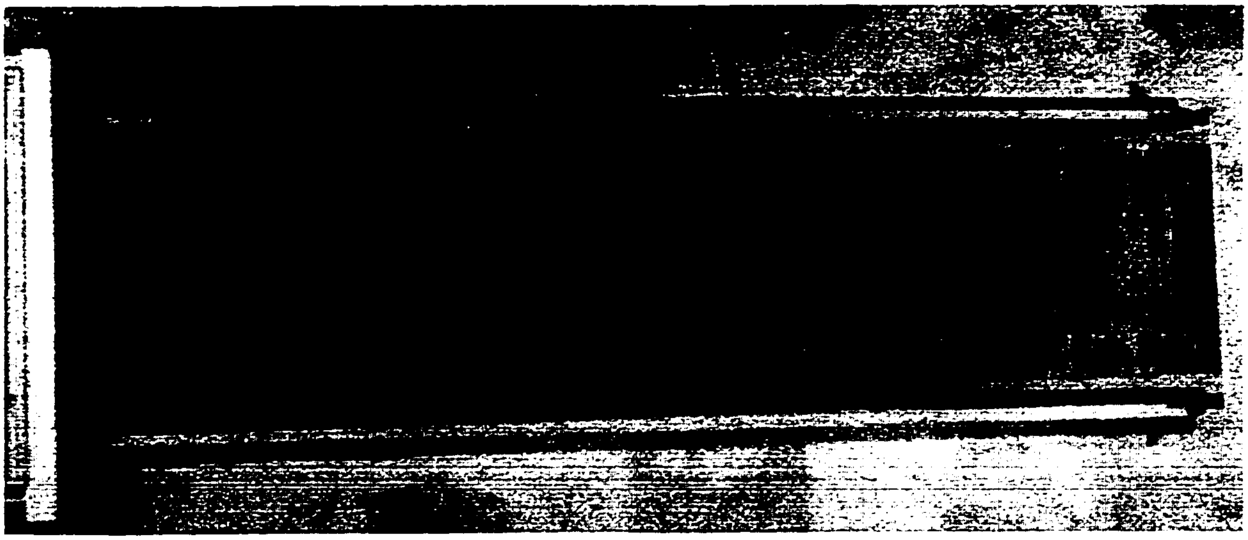

a) reinforcement before casting

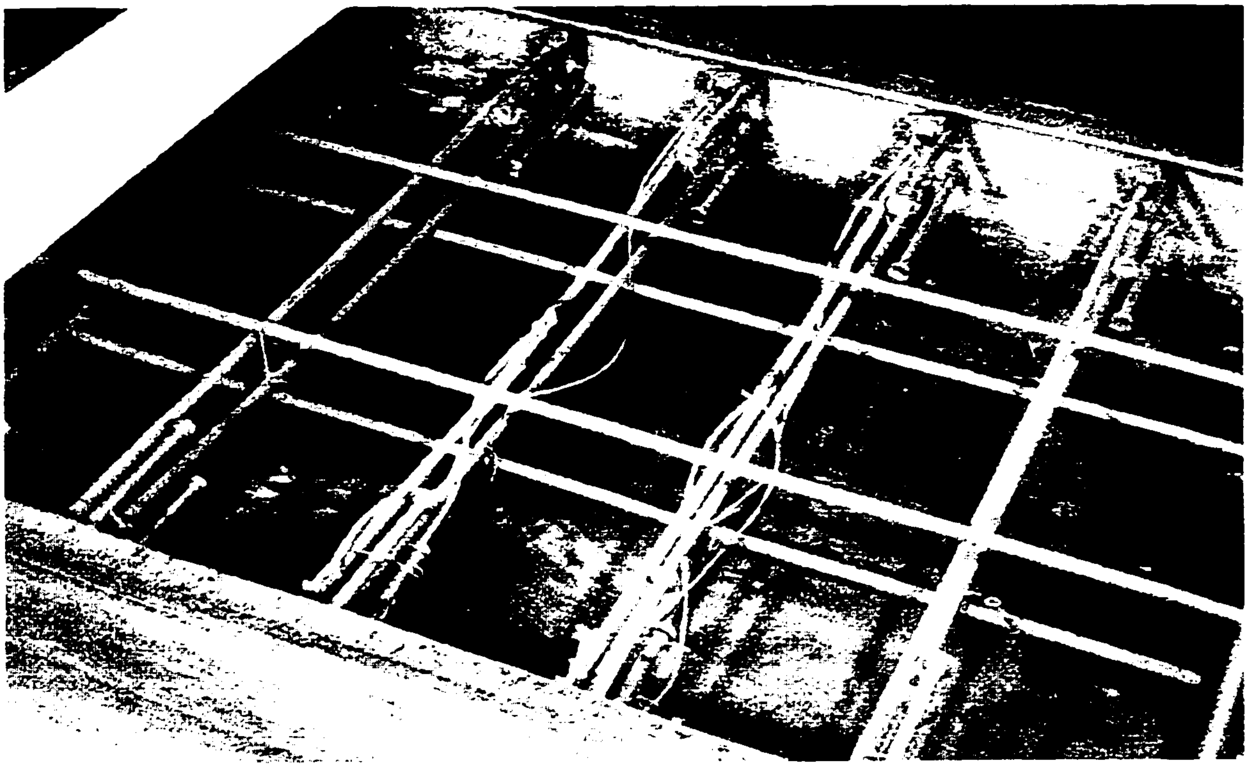

b) close-up of reinforcement

Figure 2.5 Specimen W2 reinforcing cage

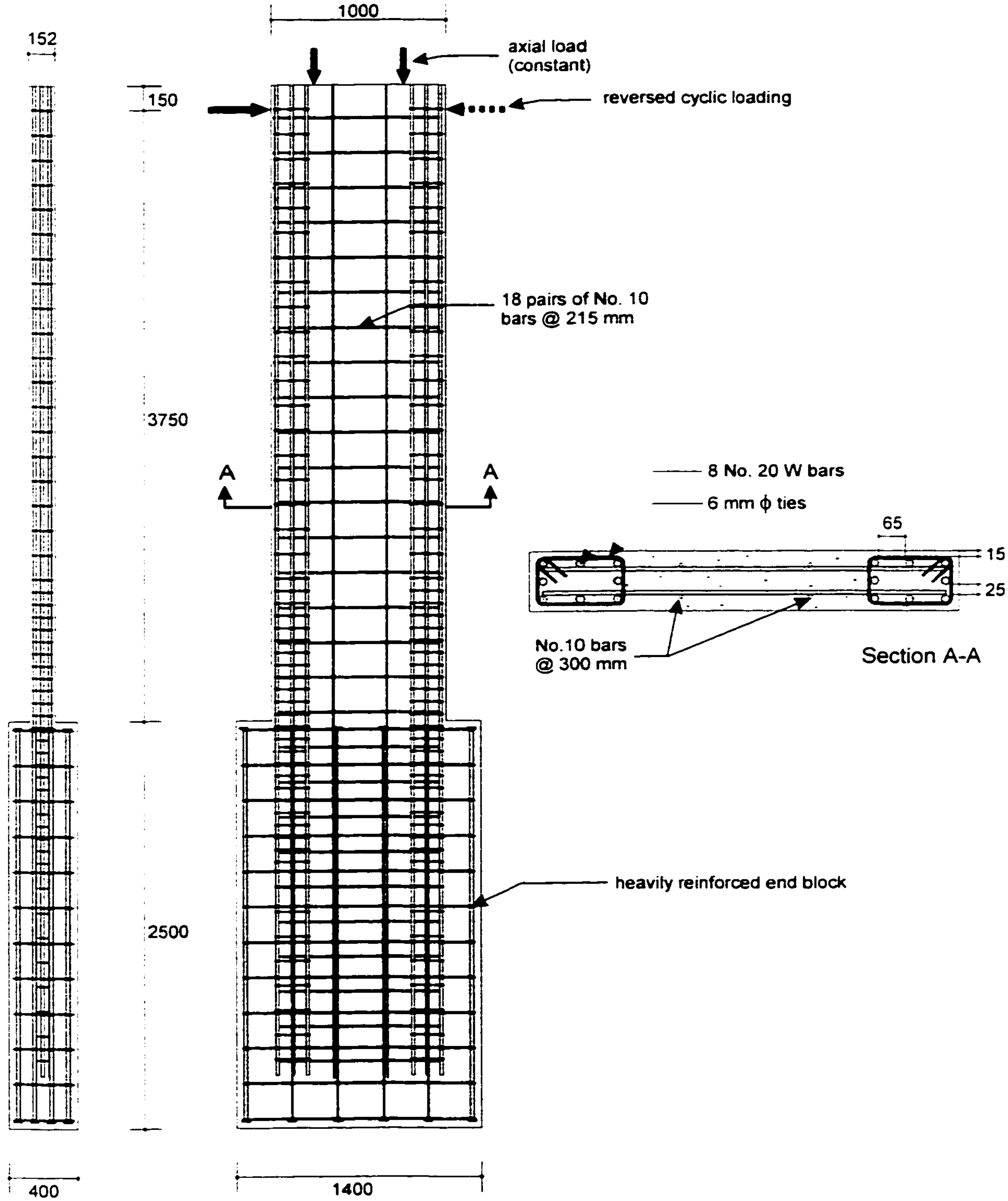

Figure 2.6 Details of reinforcement for Specimen W3

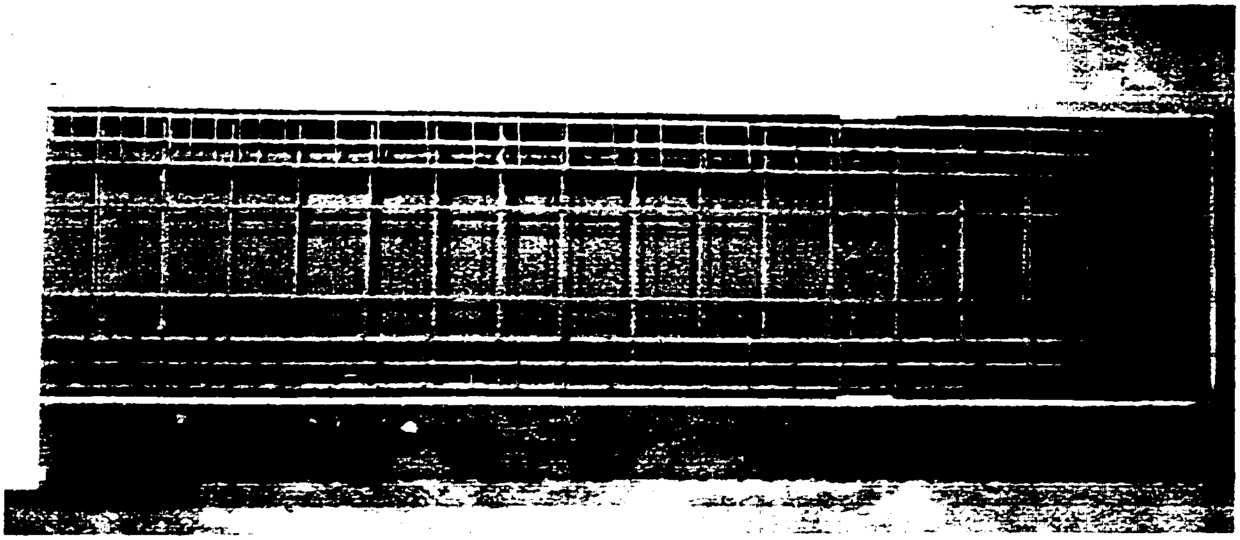

a) reinforcement before casting

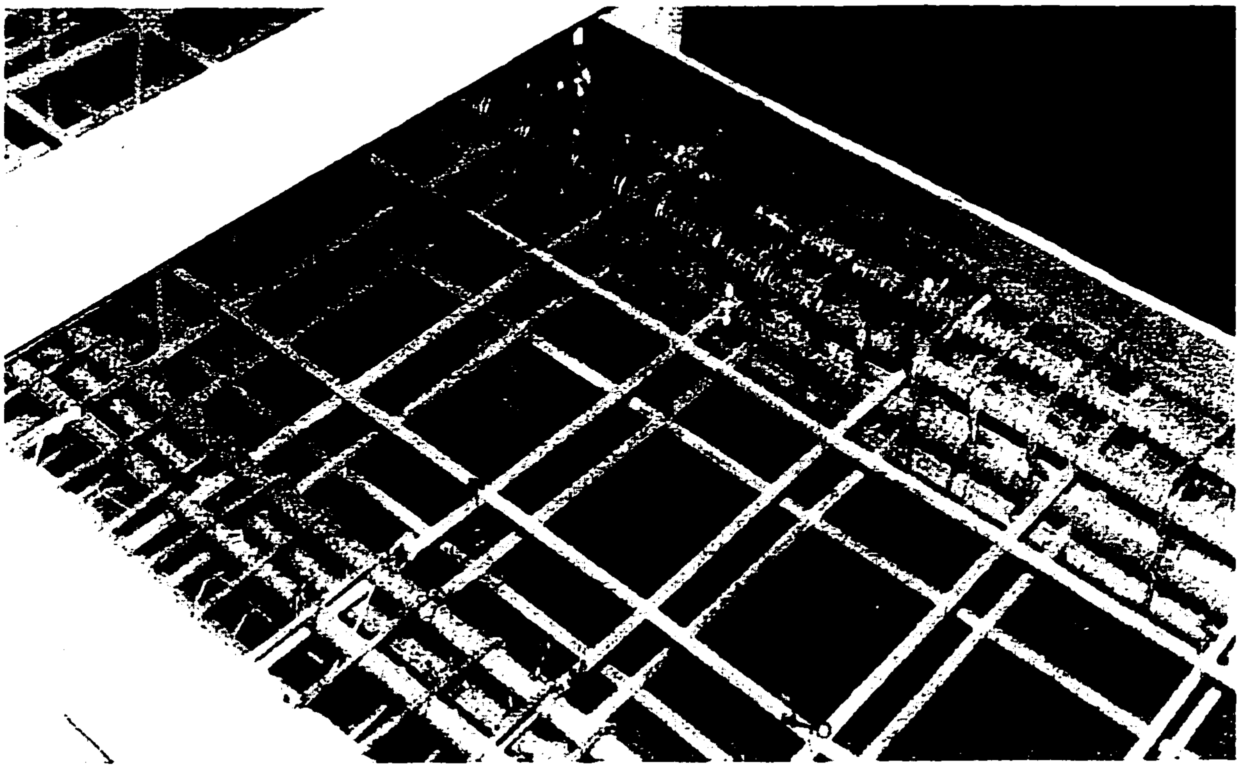

b) close-up of reinforcement

Figure 2.7 Reinforcing cage for Specimen W3

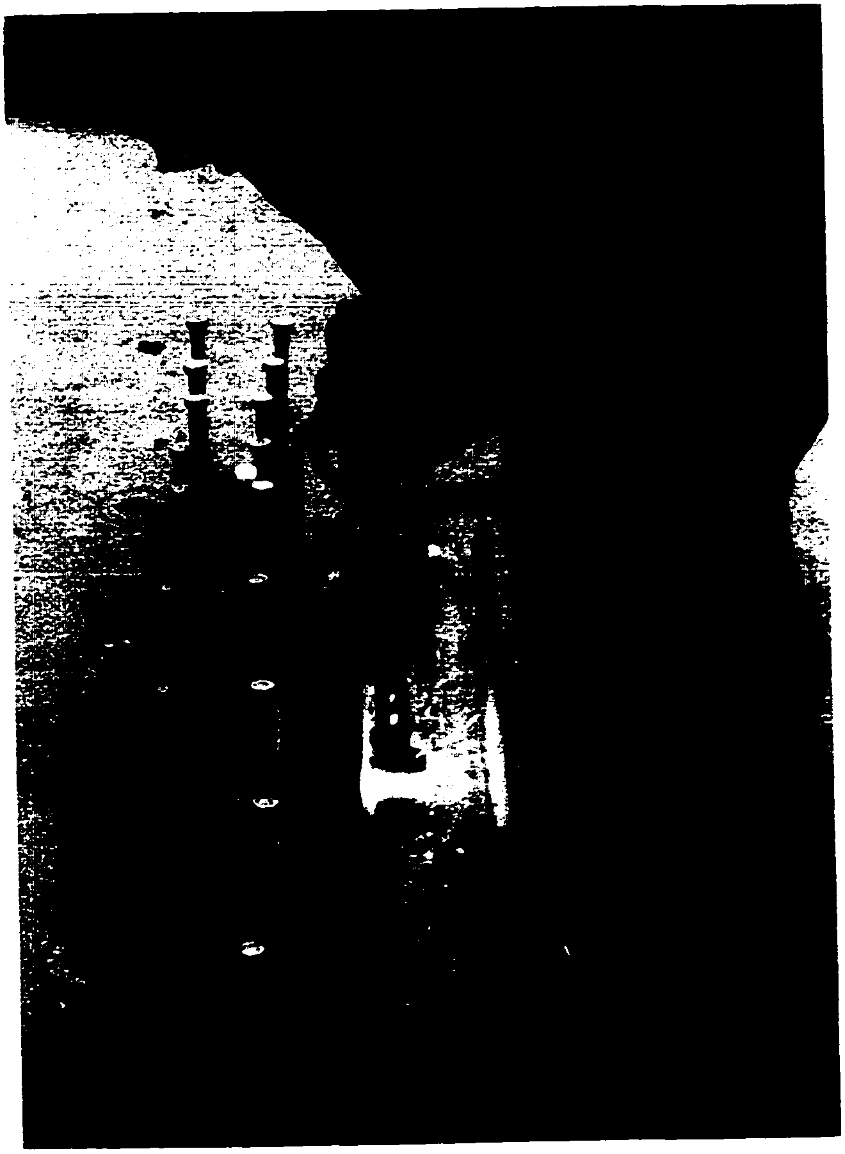

Figure 2.8 Welding studs to channel (Specimen W2)

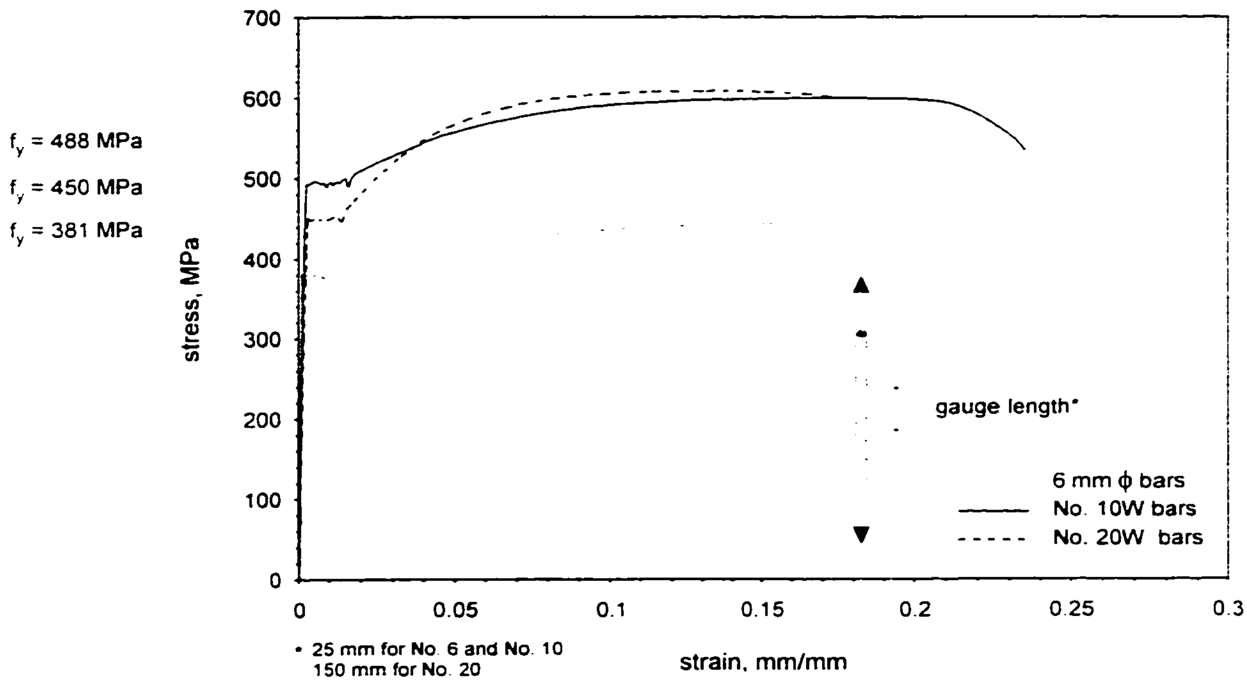

Figure 2.9 Stress-strain responses for reinforcing bars

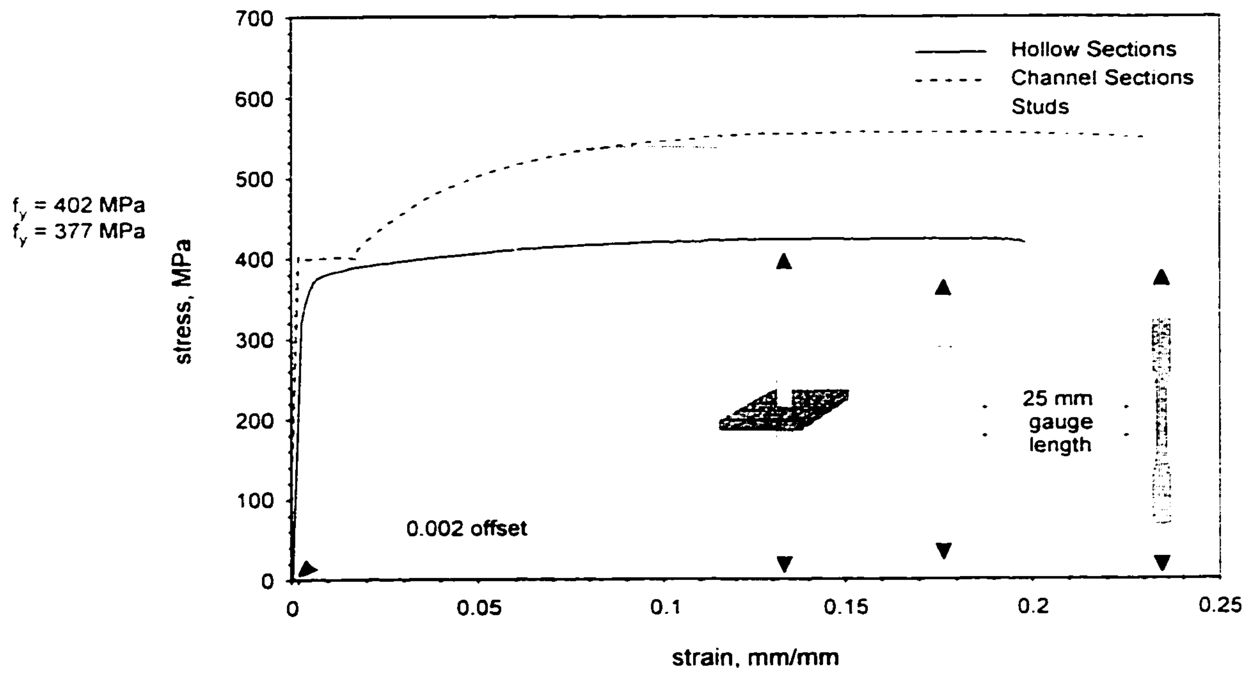

Figure 2.10 Stress-strain responses for structural steel and studs

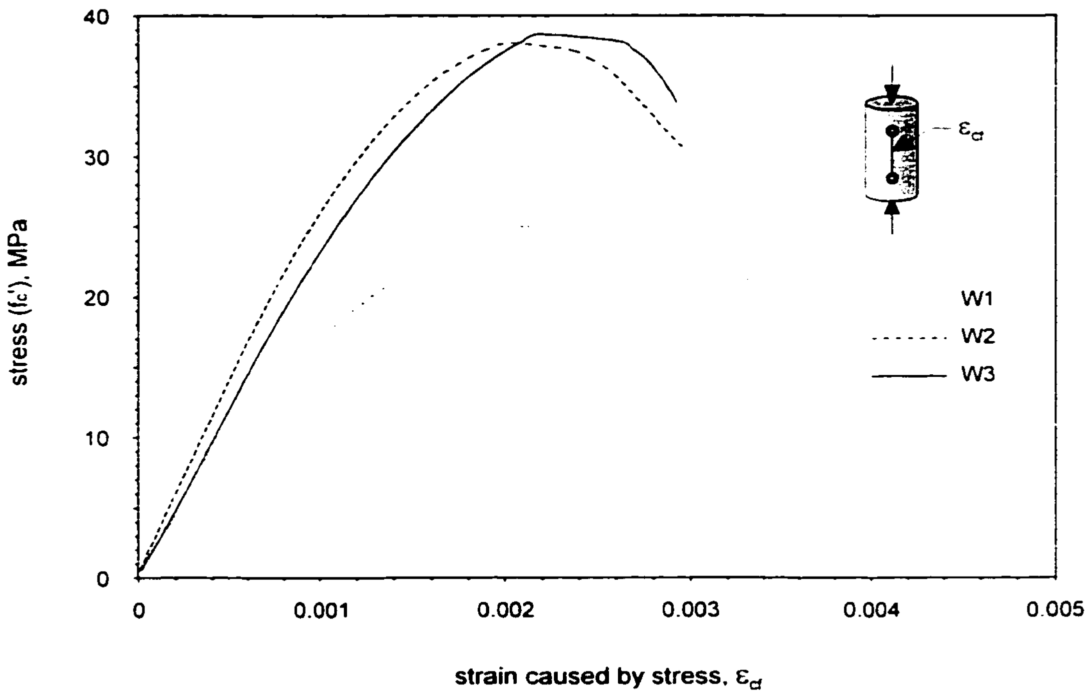

Figure 2.11 Compressive stress-strain responses for concrete

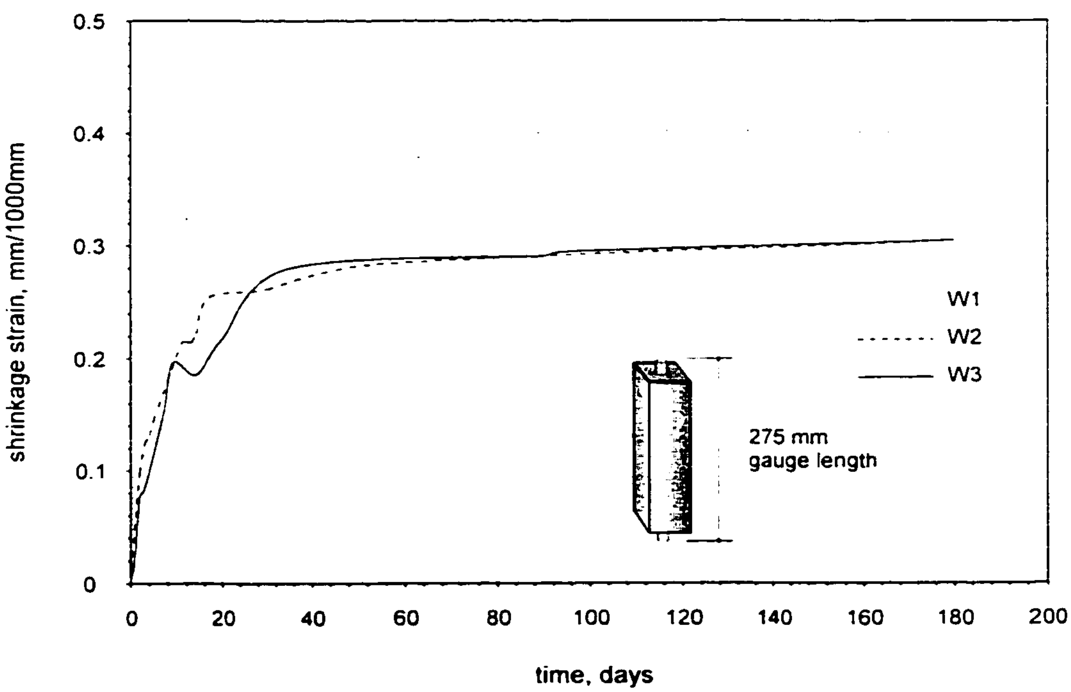

Figure 2.12 Shrinkage strains measured in the concrete over time

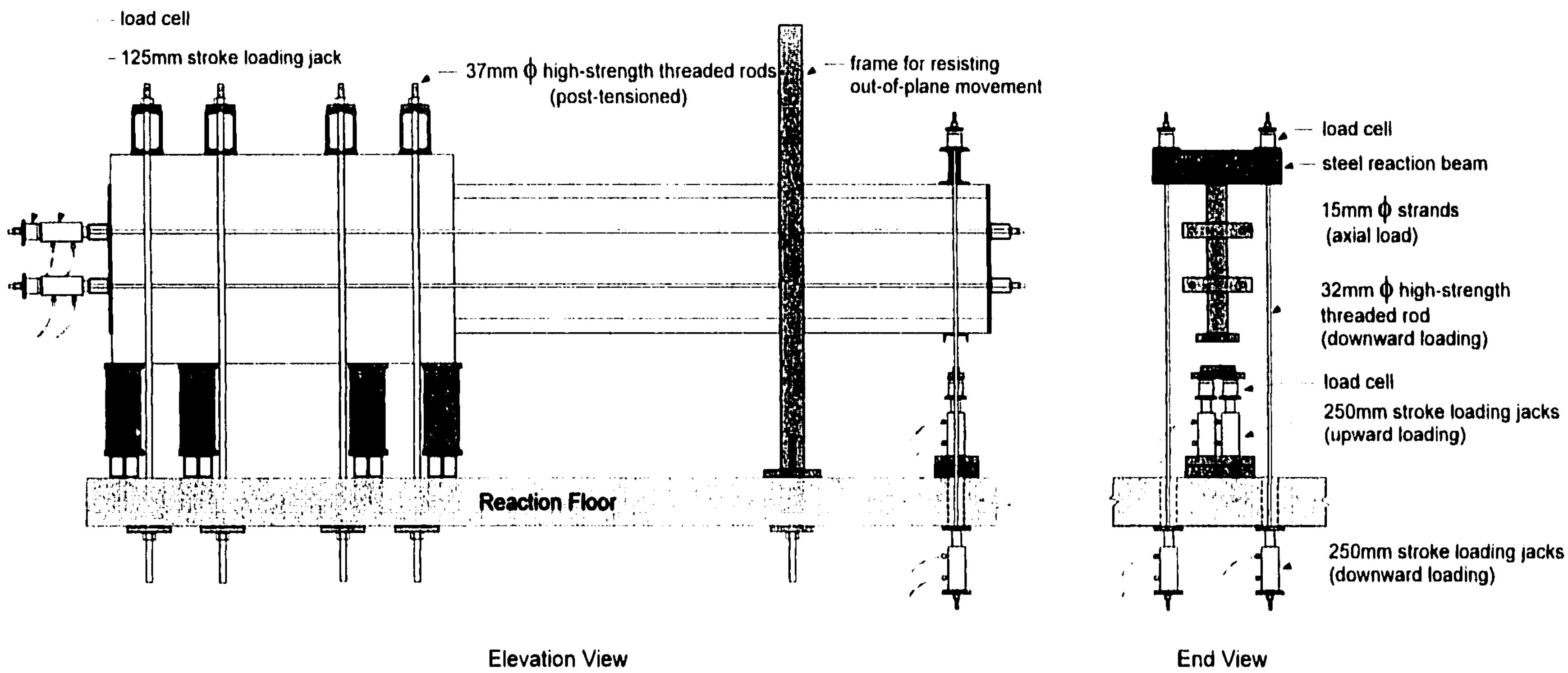

Figure 2.13 Test setup for reversed cyclic loading of specimens

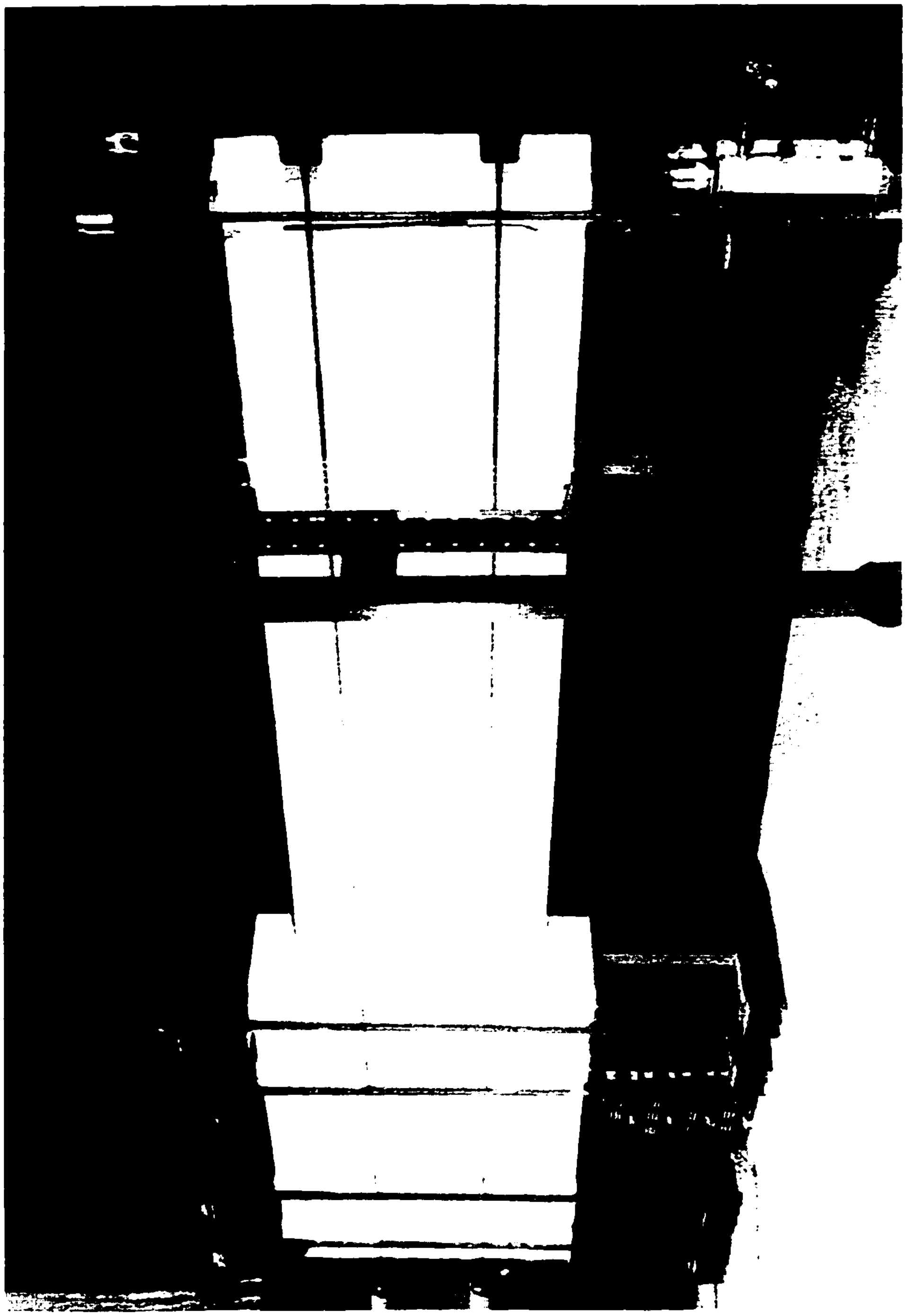

Figure 2.14 Test setup before loading

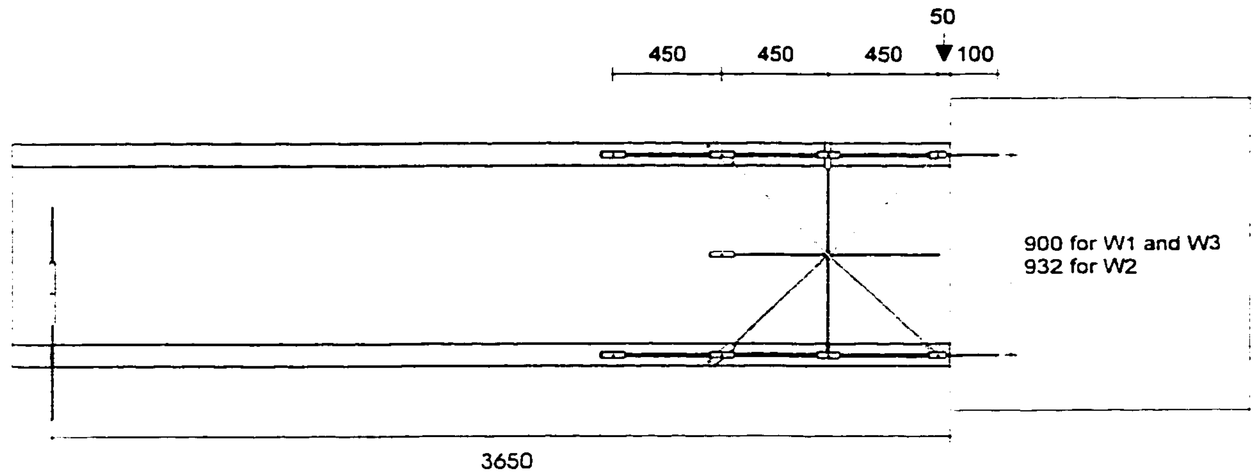

Figure 2.15 LVDT assembly (view of back side of wall)

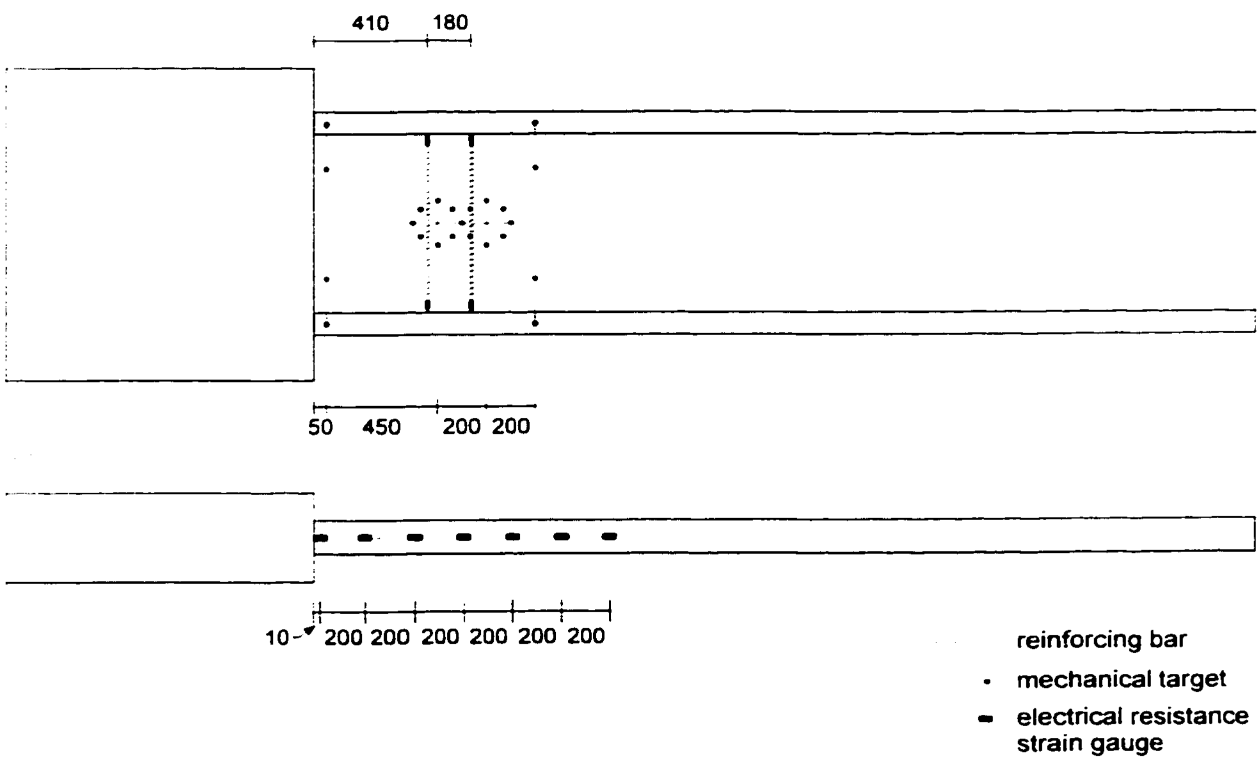

Figure 2.16 Strain measuring instrumentation

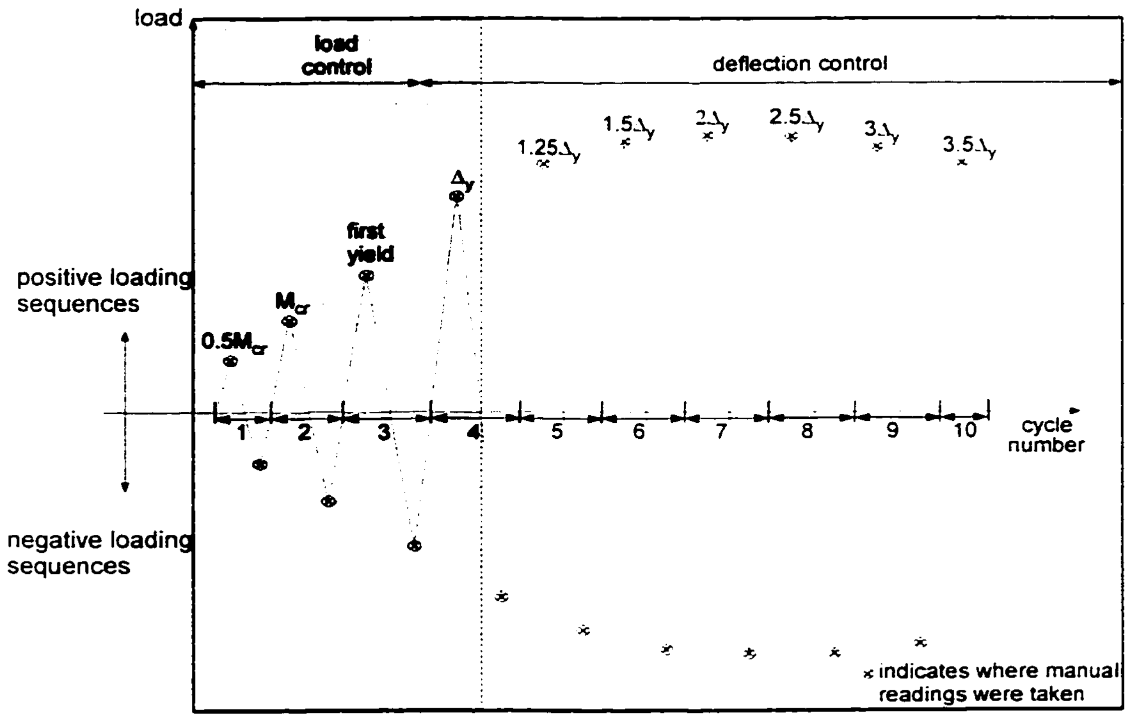

Figure 2.17 Loading sequence for specimens

CHAPTER 3

EXPERIMENTAL RESULTS

This chapter describes the behaviour of the three specimens that were tested under reversed cyclic loading. The general response of each wall was monitored by plotting the applied lateral load versus tip deflection throughout each test. The lateral load was applied at 3750 mm from the base of the wall, while the tip deflection was measured at a distance of 3650 mm to avoid the loading apparatus. The reported deflections were increased slightly (2.7%) from the measured deflections to account for this small difference.

Due to the horizontal orientation of each wall during testing, it was necessary to include the wall self-weight in determining the shears and moments acting on the wall. The self-weights of the cantilever portions were 15.8 kN, 17.5 kN and 16.7 kN for Specimens W1, W2 and W3, respectively. The corresponding base moments were 35.0 kN·m, 38.7 kN·m and 36.7 kN·m.

3.1 P-Δ Effect Considerations

As described in Chapter 2, a constant axial load, P_{axial}, was applied to each wall during testing using four prestressing strands. As the wall deflected due to the applied lateral load, F_{app}, the strands also deflected from their original horizontal orientation. The resulting eccentricity creates an additional vertical load component, P_y, and horizontal load component, P_x, due to the axial load. Figure 3.1 illustrates the second order effects resulting from the tip deflection of the wall. The base shear, V, includes the shear from applied loads, the shear arising from self-weight and the vertical component of prestressing, P_y. In order to determine the base moment, M, it was necessary to include the self-weight moment and the secondary effects from the components of P_{axial} (P_x and P_y).

3.2 Specimen W1

3.2.1 Load-Deflection Response

Figure 3.2 shows the base shear, V, versus tip deflection and base moment, M, versus tip deflection curves. The base shear at the peak of the cycles and corresponding tip deflections are given in Table 3.1.

Cycle	Cycle Description	Base Shear, kN	Tip Deflection, mm
1A	M_{cr}^{+}	76.1	6.8
1B	M_{cr}^{-}	-59.5	-6.5
2A	2.0 M_{cr}^{+}	137.2	13.6
2B	2.0 M_{cr}^{-}	-140.0	-16.0
3A'	Δ_y	257.5	36.6
3A	$1.4\Delta_y$	295.6	51.3
3B'	Δ_y	-278.0	-32.4
3B	$1.5\Delta_y$	-296.6	-48.9
4A	$1.7\Delta_y$	317.5	62.5
4B	$1.8\Delta_y$	-313.2	-59.9
5A	$2.1\Delta_y$	324.3	77.6
5B	$2.0\Delta_y$	-314.1	-74.9
6A	$2.8\Delta_y$	326.4	102.4
6B	$3.1\Delta_y$	-321.6	-100.1
7A	$3.3\Delta_y$	182.6	120.3

Table 3.1 Peak base shears and tip deflections for Specimen W1

Specimen W1 was loaded to the theoretically calculated cracking moment (see Appendix A) during the first cycle, however, cracks were not obvious until the following cycle. During the loading of the 2A and 2B cycles, which increased the applied load on the wall to twice the cracking moment, hairline flexural cracks began forming (see Fig 3.3a).

The base shear at peak 3A reached 295.6 kN, which produced a 51.3 mm positive tip deflection. The first yielding of Specimen W1 occurred during this positive loading cycle at a base shear of 191.2 kN and a corresponding deflection of 22 mm. General yielding also occurred during this loading cycle at a base shear of 257.5 kN and a deflection of 36.6 mm. Both points are indicated on the base moment versus tip deflection curve (see Fig. 3.2b).

The location of general yielding, representing flexural yielding was determined from Fig. 3.2b using a bilinear approximation; the elastic portion defined by the secant stiffness at first yield (Paulay and Priestley, 1992). The crack development during this stage was significant with many flexural cracks forming perpendicular to the concrete and HSS interface. These cracks formed at the location of each transverse reinforcing bar. The largest flexural crack at peak 3A, located 430 mm from the base of the wall, was 0.6 mm wide. A series of shear cracks also developed during this cycle propagating from the flexural cracks. The slope and width of the cracks decreased as the distance from the base of the wall increased.

Subsequent cycles were deflection controlled, based on predetermined deflections. The fourth cycle had target peak deflections of ±60 mm, which produced an increase in both the number and the size of the flexural and shears cracks (see Fig. 3.3b). Important notes for this cycle were crushing of the concrete near the compression face of the wall and the opening of a 3 mm wide crack just inside the end block. During cycle five, local buckling began in the outer flange followed by the webs of the HSS subjected to compression. The shear cracks produced earlier were fully developed during the fifth cycle and reached 1 mm in width near the wall base. The sixth loading cycle deflected Specimen W1 to 100 mm; approximately three time the general yielding deflection. During this loading, the HSS experienced further buckling of the compression side and pullout from the end block on the tension side. The crack in the footing block at the peak load of 6A reached a width of 8 mm (see Fig. 3.3c). The final half-cycle, 7A, was an attempt to reach beyond the previous 100 mm deflection. However, at 98.8 mm a sudden reduction in load occurred as the bottom HSS completely buckled, brought on by excessive crushing of the concrete (see Fig. 3.4).

3.2.2 Strains and Deformations

A series of LVDTs were used to determine curvatures at three different regions along the wall. Figure 3.5 shows the three regions where these LVDTs were located and the moment versus curvature plots for each region. The majority of flexural deformations occurred in region 1, with the curvature progressively increasing in each cycle. The maximum curvature in this region reached approximately 30 rad/1000m. The curvature response of region 2 indicates that although yielding occurred, general yielding was not apparent. Region 3 responded essentially elastically with no yielding.

Figure 3.6 shows the strains measured from the series of electrical resistance strain gauges glued on the surface of both hollow sections. These readings provide confirmation to the extent of yielding along the steel sections. The upper and lower graphs of Fig. 3.6 show the strain measurements along each steel section at the peak shear of each positive cycle. Tension and compression yielding of both steel sections occurred during the third cycle. Subsequent cycles show the development of the plastic hinging near the wall base. These strain measurements indicate that tension yielding occurred over a wall length of about 1.2 m while compression yielding took place over a distance of approximately 1 m.

Strain measurements in the plastic hinge region were recorded using a full depth LVDT rosette (see Fig 2.15). Figure 3.7 shows the various strain components determined from this rosette, including the transverse strain, ε_t, the shear strain, γ, the principal tensile strain, ε_1, and the principal compression strain, ε_2. The measured transverse strains indicate that the transverse reinforcing bars reached about 80% of their yield strain. The shear strains and the principal tensile strains indicate that significant shear deformation and significant shear cracking occurred in this region.

The electrical resistance strain gauges glued to two transverse reinforcing bars (see Section 2.6.3) also indicate that the maximum strains reached were approximately 80% of their yield strain (see Fig. 3.8).

The mechanical targets used to determine the separation between the hollow structural sections and concrete confirmed the results of the electrical strain gauges on the transverse bars. Apart from the transverse bar straining no significant separation occurred. These measurements help to verify that the welding of the transverse bars provided adequately shear connection to the hollow steel sections.

3.3 Specimen W2

3.3.1 Load-Deflection Response

The base moment and base shear versus tip deflection curves for Specimen W2 are shown in Fig. 3.9. Table 3.2 shows the base shears at the peak of each cycle and corresponding tip deflections.

Cycle	Cycle Description	Base Shear, kN	Tip Deflection, mm
1A	$0.5M_{cr}^{+}$	48.5	2.1
1B	$0.25M_{cr}^{-}$	-13.3	-1.4
2A	M_{cr}^{+}	83.5	4.8
2B	M_{cr}^{-}	-68.6	-5.3
3A	$2.0M_{cr}^{+}$	158.5	11.6
3B	$2.0M_{cr}^{-}$	-141.8	-12.3
4A	$<M_y$	293.0	28.9
4B	M_y	-279.8	-30.9
5A	$0.97\Delta_y$	307.9	33.1
5B'	Δ_y	-292.8	-33.7
5B	$1.1\Delta_y$	-305.0	-36.5
6A'	Δ_y	314.0	34.3
6A	$1.2\Delta_y$	319.8	41.6
6B	$1.3\Delta_y$	-319.5	-42.9
7A	$1.8\Delta_y$	326.7	62.2
7B	$1.8\Delta_y$	-336.2	-61.4
8A	$2.1\Delta_y$	346.5	77.5
8B	$2.3\Delta_y$	-341.3	-76.8
9A	$3.0\Delta_y$	322.2	103.1
9B	$3.1\Delta_y$	-351.2	-104.9
10A	$2.5\Delta_y$	113.7	87.5

Table 3.2 Peak base shears and tip deflections for Specimen W2

The first full cycle performed a loading sequence in the pre-cracking range of Specimen W2. The second cycle loaded Specimen W2 to the moments predicted to develop cracking of the extreme concrete fibre. Several small flexural cracks became evident at the peak shears of this cycle. The third cycle was a stage in the elastic response range of the specimen with maximum loads producing positive and negative moments equaling twice the cracking moment. Figure 3.10a shows the crack pattern of Specimen W2 at the peak of the 3A cycle. Cycle 4 was carried out to a maximum deflection slightly less than the deflection at general yielding with first yielding occurring in cycle 4B. During cycle 5A, first yielding occurred in the positive cycle at a deflection of 32.1 mm. General yielding occurred in the positive loading cycle at 34.3 mm and in the negative loading cycle at a deflection of 33.7 mm. As can been seen from Fig. 3.7 first yielding and general yielding are very close together. The crack development for the fourth and fifth cycles included significant flexural and shear cracking with the flexural cracks developing at the locations of the transverse reinforcing bars.

The cycles following the fifth cycle were deflection controlled, based on the tip deflections applied to Specimen W1. During cycle 6, horizontal cracks formed along the steel and concrete interface, parallel to the steel sections, indicating that some separation was taking place. This observation was confirmed by the data from the mechanical targets that spanned this interface. The largest cracks in the sixth cycle were flexural and were located close to the base of the wall. During the seventh cycle, significant cracking and the first noticeable concrete crushing occurred close to the base of the wall (see Fig. 3.10b). Also noticeable during this cycle was a 2 mm pullout of the tensile steel section, relative to the end block. During cycle eight, cracks extended and further concrete crushing was observed. Channel yielding was also indicated by surface flaking of the mill scale over a length of 580 mm, originating from the base of the wall. At the peak loading of 9A, yielding of the tensile channel had propagated to 790 mm from the wall base and local buckling was first noticed in the compression channel. The local buckling began as outward buckling of the web followed by the flanges. In addition, during cycle nine, concrete crushing and some spalling was evident along with the development of several large shear cracks (see Fig. 3.10c).

Specimen W2 failed on the positive loading of the tenth cycle when the compression loaded channel underwent local buckling, 50 mm from the base of the wall (see Fig. 3.11). The applied load decreased rapidly as the tip deflection passed 75 mm (see Fig. 3.9).

3.3.2 Strains and Deformations

The same LVDT setup that was used with Specimen W1 was used to determine the curvature responses of Specimen W2. As shown in Fig 3.12, the majority of the flexural deformations occurred in region 1, at the base of the wall. The plots also indicate that region 2 underwent general yield in the latter loading cycles. Region 3 in Specimen W2 did not undergo any significant deformations, responding elastically throughout the experiment.

The strain readings, measured with the electrical resistance strain gauges on the channels, are shown in Fig. 3.13. The upper channel, loaded in tension during the positive cycles, started to yield significantly during the 7A cycle. By the completion of the test, this tension chord had yielded over a length of about 800 mm from the base of the wall. The yielding of the corresponding compression chord occurred over a length of 400 mm.

The LVDT rosette assemblage of Specimen W2 (see Fig. 2.15) allowed for the calculation of the transverse, principal and shears strains in the wall during the testing. Figure 3.14 shows the shear strains and principal strains, which indicate that significant shear deformations occurred in the plastic hinge region during testing. Although the strains in the transverse direction, ε_t, indicate that yielding may have occurred in the transverse headed reinforcing bars, the results presented Fig. 3.15 indicate that the strains in these bars only reached about one-half of their yield strain. The mechanical targets that measured the separation between the channels and the concrete gave separations of about 1.0 mm toward the end of the testing. This separation accounts for the very high apparent transverse strains since the vertical transducer in the strain rosette also measured separation.

3.4 Specimen W3

3.4.1 Load-Deflection Response

Figure 3.16 shows the base shear and base moment versus tip deflection responses for Specimen W3. A summary of the peak base shears and corresponding tip deflections are shown in Table 3.3.

Cycles 1 and 2 were performed in the elastic response range of Specimen W3. The first cracking was noticeable at the positive and negative peak loads of the second cycle. These cracks were small, hairline flexural cracks. During the third cycle, many flexural cracks developed at the location of the confining ties (see Fig. 3.17a). First yielding of Specimen W3 was estimated to have occurred just before the peak of cycle 4A at a base shear level of 251.2 kN and corresponding tip deflection of 28 mm. This stage also corresponded to compression yielding of the lower No. 20 reinforcing bars. The first appearance of shear cracks in Specimen W3 also occurred during load stage four. General yielding during the positive loading occurred at a deflection of 35.8 mm, at the peak of the fifth cycle (see Fig. 3.16).

Cycle	Cycle Description	Base Shear, kN	Tip Deflection, mm
1A	$0.5M_{cr}^{+}$	58.3	3.0
1B	$0.5M_{cr}^{-}$	-46.8	-3.7
2A	$1.0M_{cr}^{+}$	86.2	4.9
2B	$1.0M_{cr}^{-}$	-73.0	-5.8
3A	$2.0M_{cr}^{+}$	158.3	12.6
3B	$2.0M_{cr}^{-}$	-140.4	-13.1
4A	$0.8\Delta_y$	262.0	29.7
4B	$0.8\Delta_y$	-223.9	-29.1
5A	Δ_y	293.1	35.8
5B	$0.9\Delta_y$	-269.7	-35.2
6A	$1.2\Delta_y$	322.1	42.5
6B'	Δ_y	-288.1	-38.4
6B	$1.1\Delta_y$	-294.3	-40.8
7A	$1.7\Delta_y$	334.9	62.5
7B	$1.6\Delta_y$	-325.2	-61.7
8A	$2.1\Delta_y$	329.0	77.7
8B	$2.0\Delta_y$	-326.7	-76.6
9A	$2.9\Delta_y$	331.1	103.7
9B	$2.7\Delta_y$	-330.5	-102.6
10A	$3.2\Delta_y$	317.1	114.0

Table 3.3 Peak base shears and tip deflections for Specimen W3

Subsequent cycles were deflection controlled, based on the tip deflections reached during the cycles applied to Specimens W1 and W2. By this stage, the crack patterns of Specimen W3 were significantly different from the crack patterns of Specimens W1 and W2. At the wall ends, in the area of the concentrated longitudinal reinforcement, there were a large number of closely spaced small cracks. Moreover, the shear crack widths in cycle six reached a maximum of only 0.4 mm. General yielding of Specimen W3 under negative loading also occurred in the sixth cycle at a deflection of 38.4 mm. During the seventh cycle, several shear and flexural cracks merged (see Fig. 3.17b), while concrete crushing began in the compression zone. Cycle 8 did not reach the same peak loads as the previous cycles, which was most likely due the concrete crushing. At this stage, the maximum width of the shear cracks was measured at 1.5 mm. In the last full cycle before failure, cycle 9: further widening of the cracks occurred along with continued concrete crushing (see Fig. 3.17c).

Specimen W3 failed abruptly during positive loading of the tenth cycle (see Fig.

3.16) at a load of 317.1 kN and a tip deflection of 114 mm. Figure 3.18 shows the appearance of the wall after failure. It is clear that failure occurred due to severe distress in the compression zone, with concrete crushing, rupturing of one of the confining hoops and local buckling of the longitudinal bars.

3.4.2 Strains and Deformations

Moment versus curvature responses for the three regions of Specimen W3 are shown in Fig. 3.19. These responses have a very similar shape to those associated with Specimen W2. The majority of the flexural deformations occurred in region 1 with general yielding propagating into region 2 in the last loading cycles.

The positive cycle strain measurements for the compression and tension chords are shown in Fig. 3.20. It is evident that yielding of the tension chord occurred over a length of 800 mm from the base of the wall while the compression chord yielded over a length of 550 mm.

The LVDT rosette assembly was identical to that of Specimen W1 (see Fig. 2.15) and the strain plots are shown in Fig. 3.21. The results indicate that the transverse strains were small throughout most of the experiment reaching the yield strain at the very end of the test. The shear strains and principle tensile strains indicate that significant shear deformation and shear cracking had taken place.

The responses of the transverse steel instrumented in Specimen W3 (see Section 2.6.3) are shown in Fig. 3.22. Strain measurements indicate that neither of the No. 10 transverse bars yielded until failure of the specimen. The steel ties responded similar to that of the transverse bar, in that yielding did not occur until the last cycle.

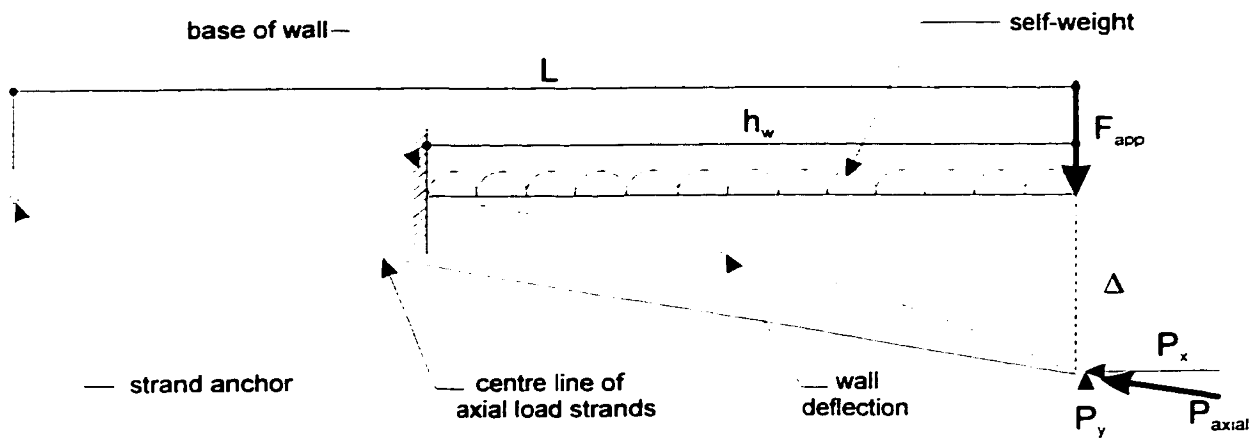

a) applied loads

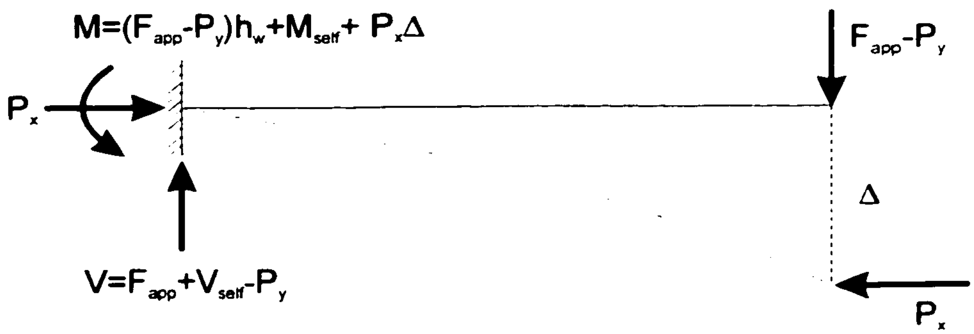

b) base shear and moment, including self-weight and P-Δ effects

Figure 3.1 Accounting for P-Δ effect

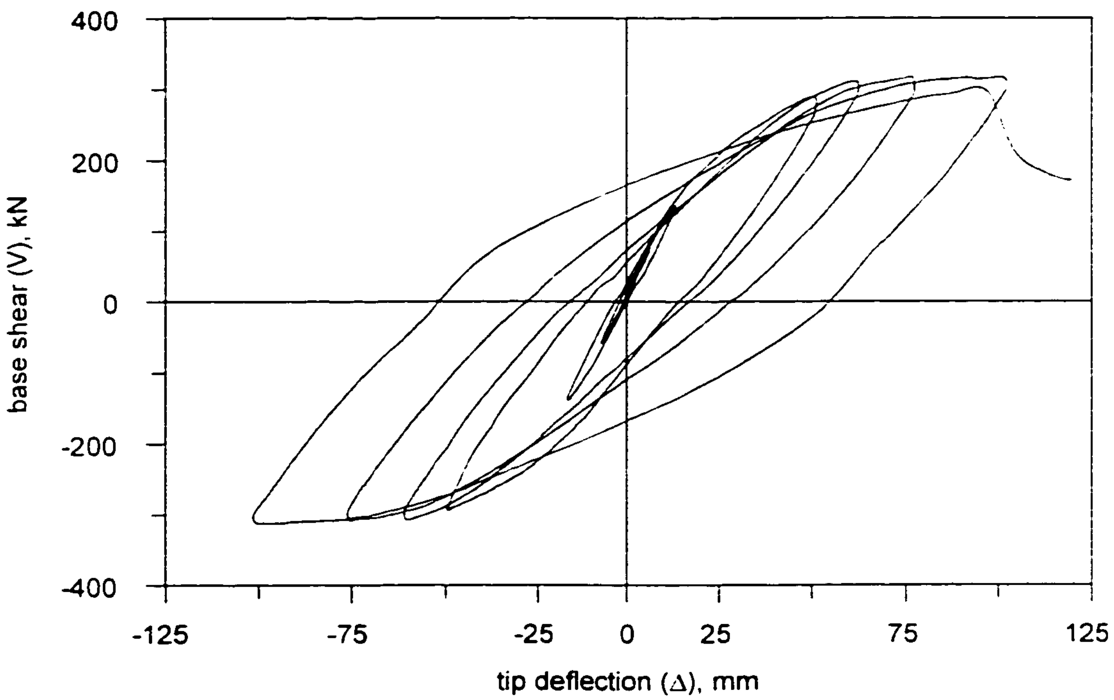

a) base shear vs. tip deflection

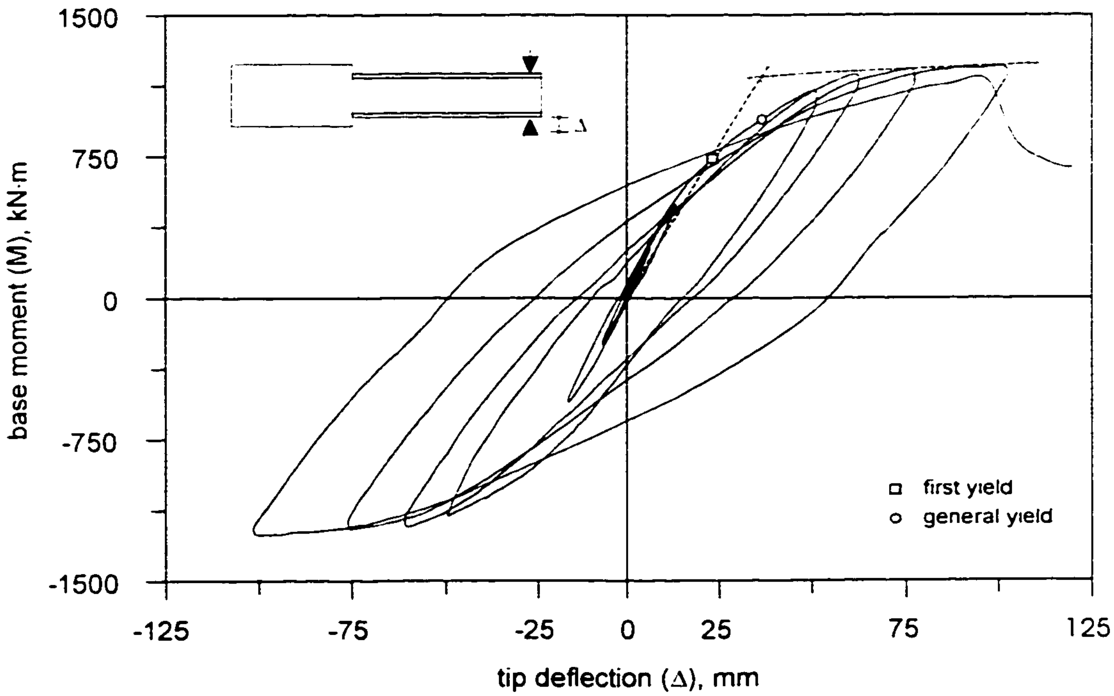

b) base moment vs. tip deflection, including P-Δ

Figure 3.2 Shear and moment vs. tip deflection responses of Specimen W1

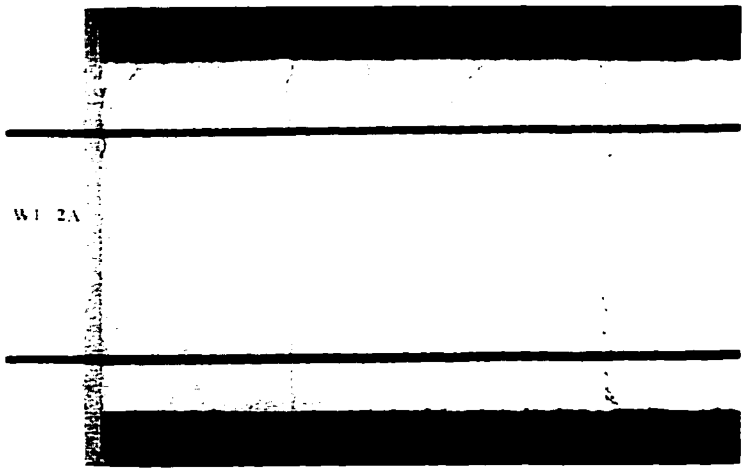

c) load of approximately $2M_{cr}$

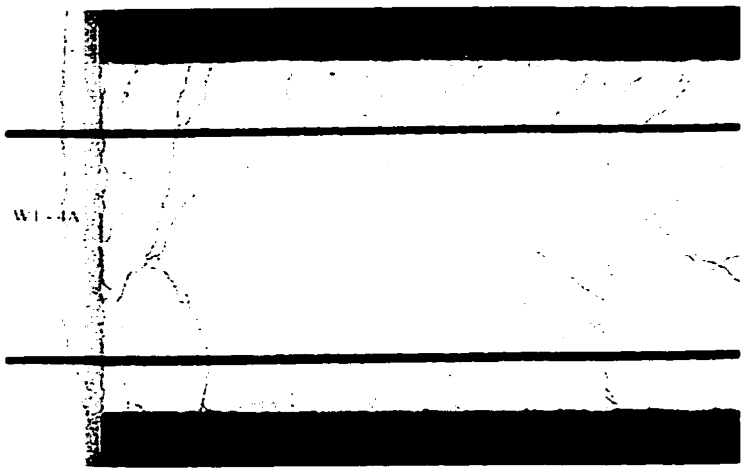

c) deflection of approximately $1.75\Delta_y$

c) deflection of approximately $3\Delta_y$

Figure 3.3 Crack patterns for Specimen W1

a) close-up of HSS local buckling

b) plastic hinge region at failure

Figure 3.4 Failure of Specimen W1

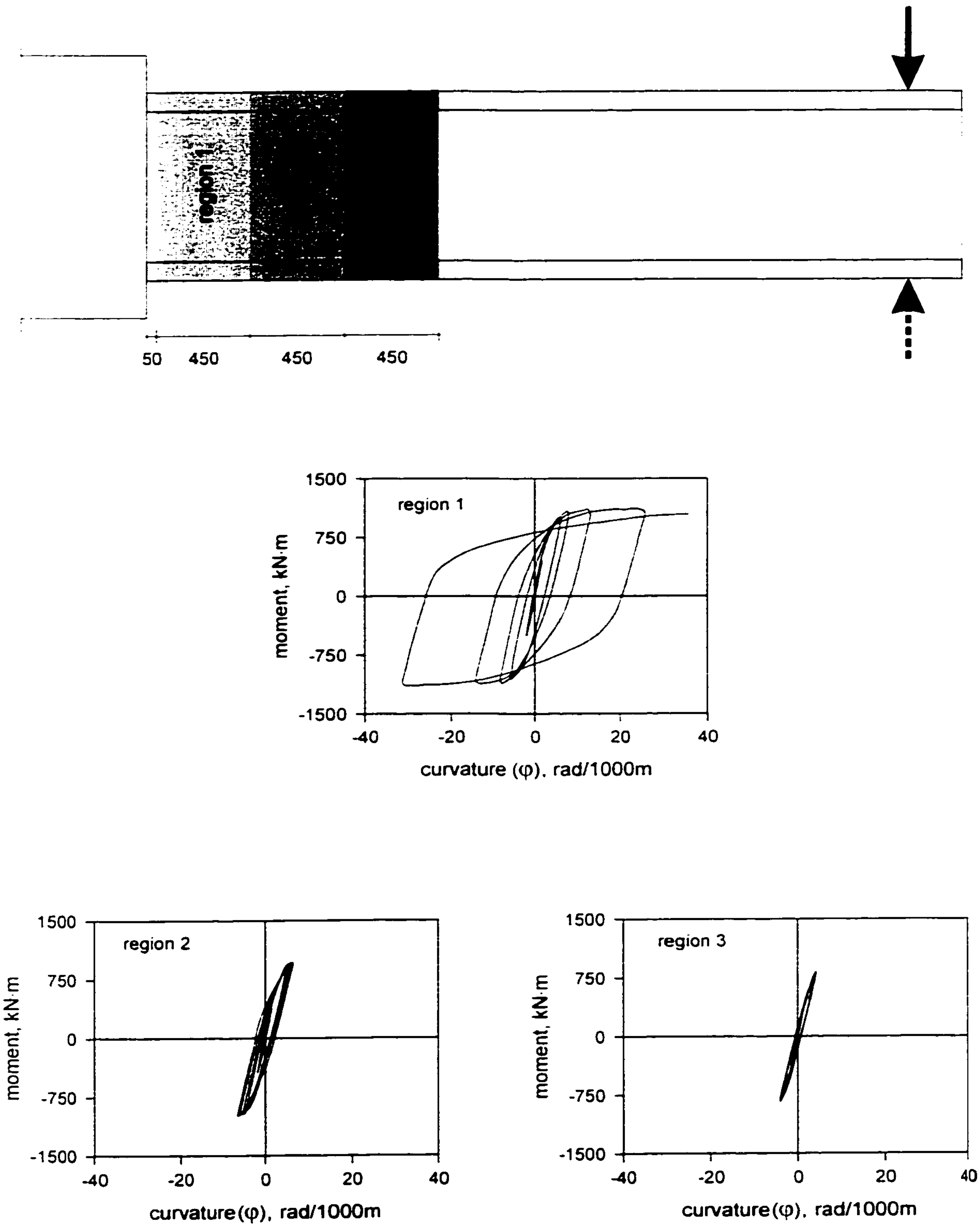

Figure 3.5 Curvature response of Specimen W1

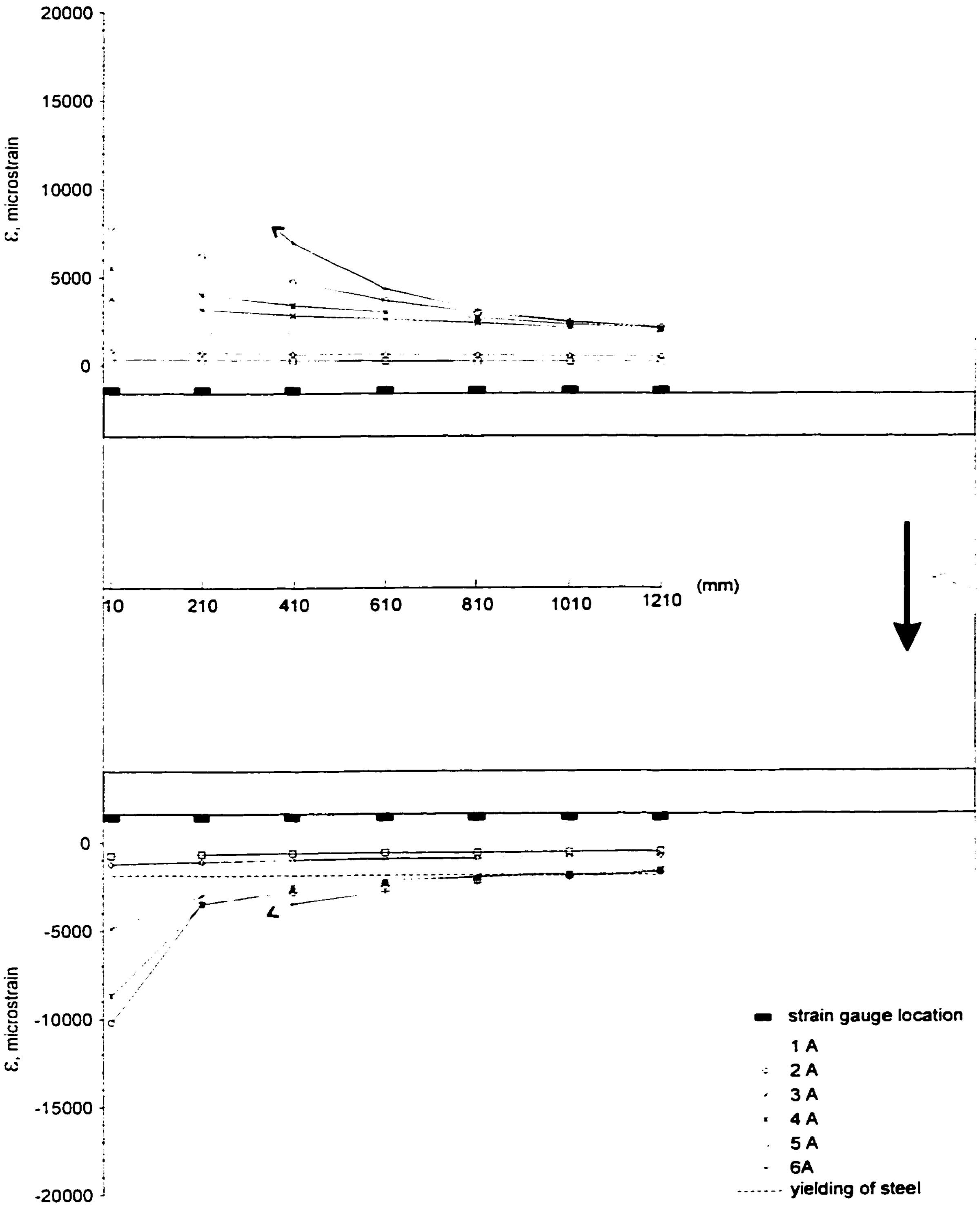

Figure 3.6 HSS strain distribution at peak positive cycles for Specimen W1

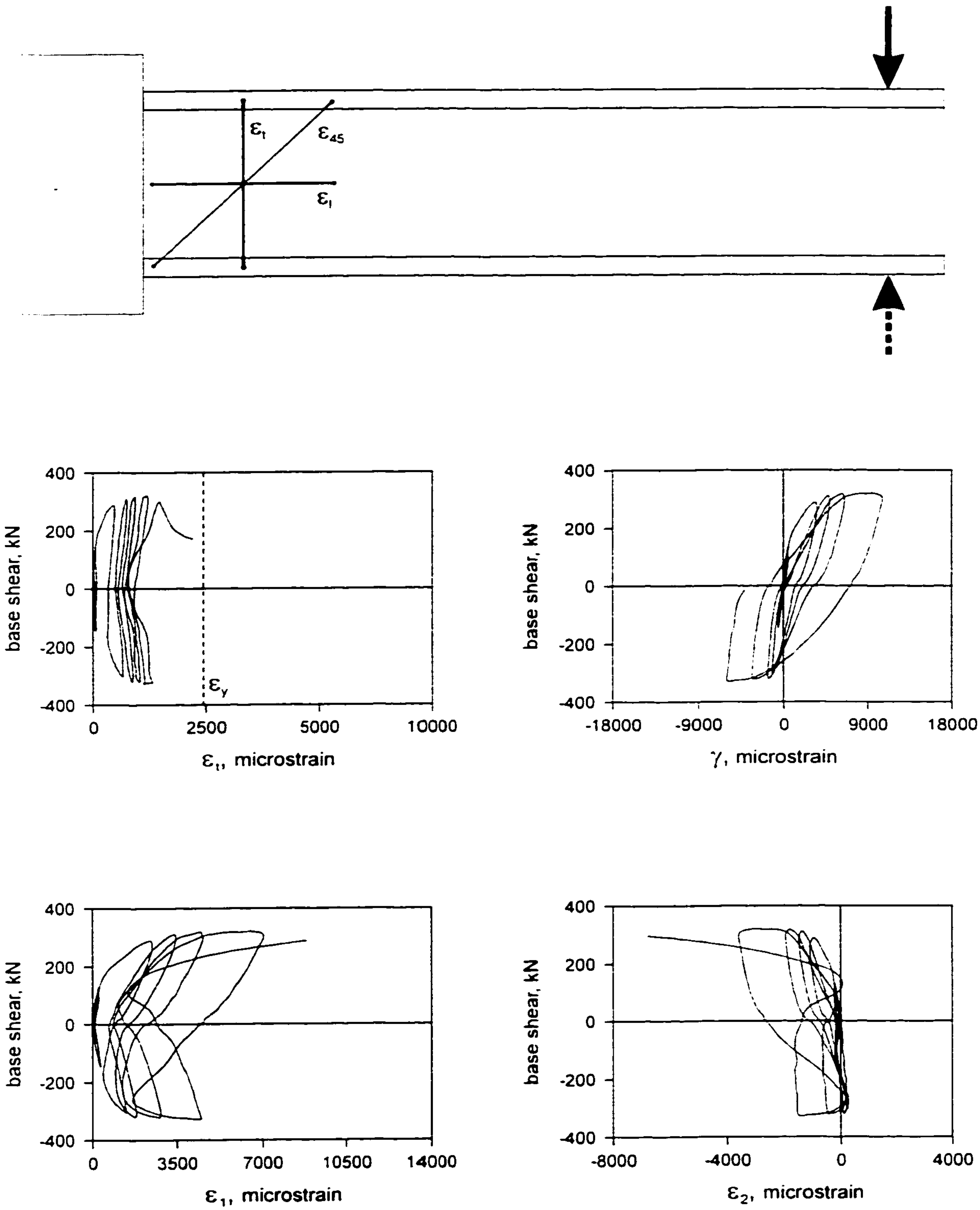

Figure 3.7 Strain conditions for Specimen W1

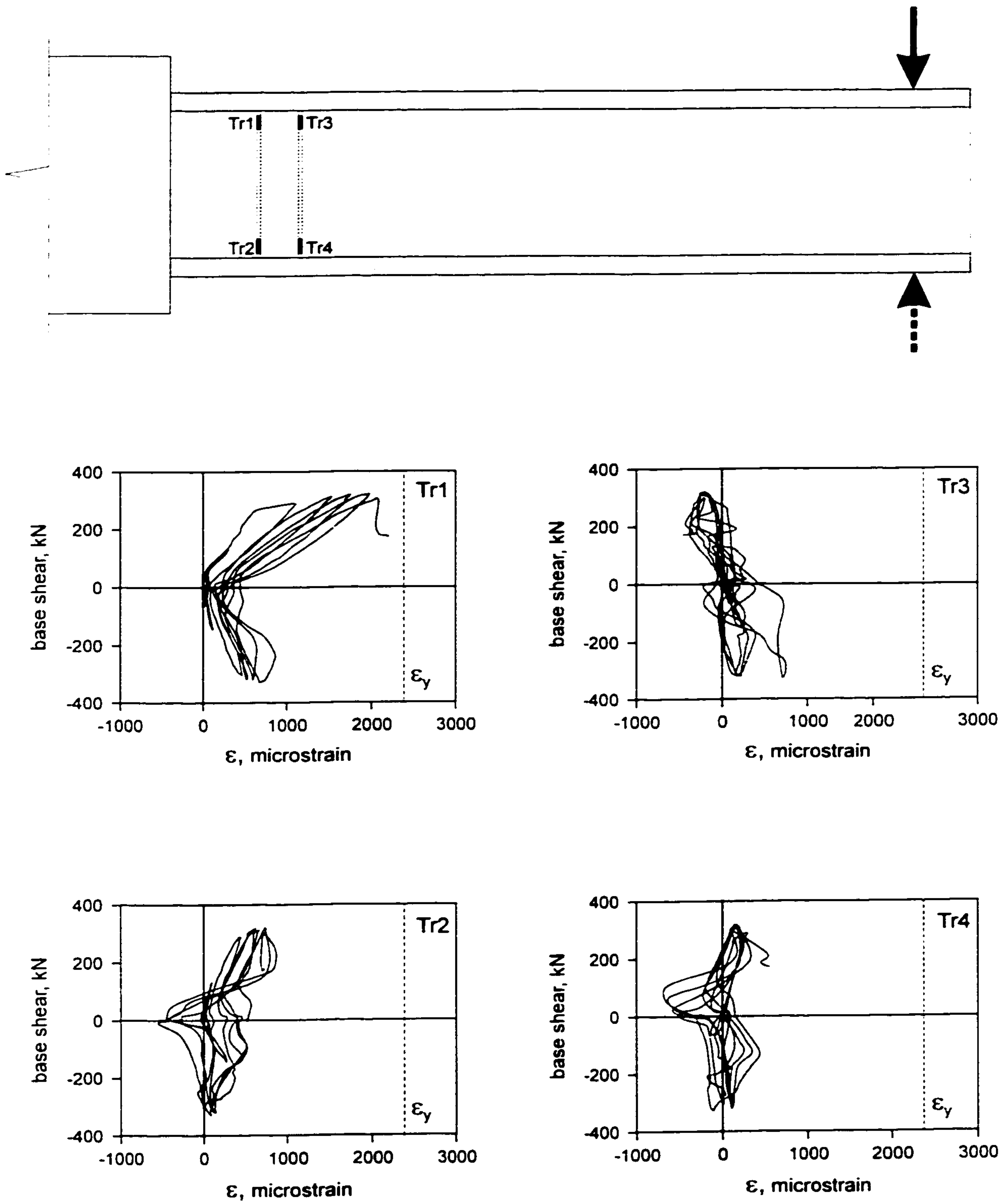

Figure 3.8 Response of Specimen W1 reinforcement

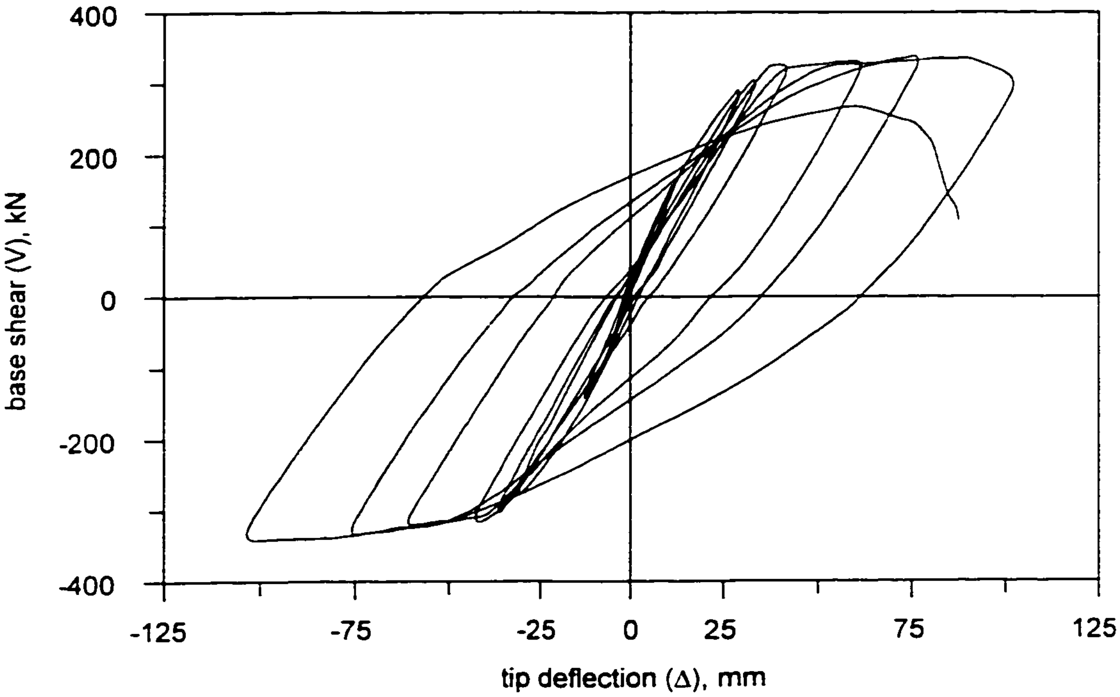

a) base shear vs. tip deflection

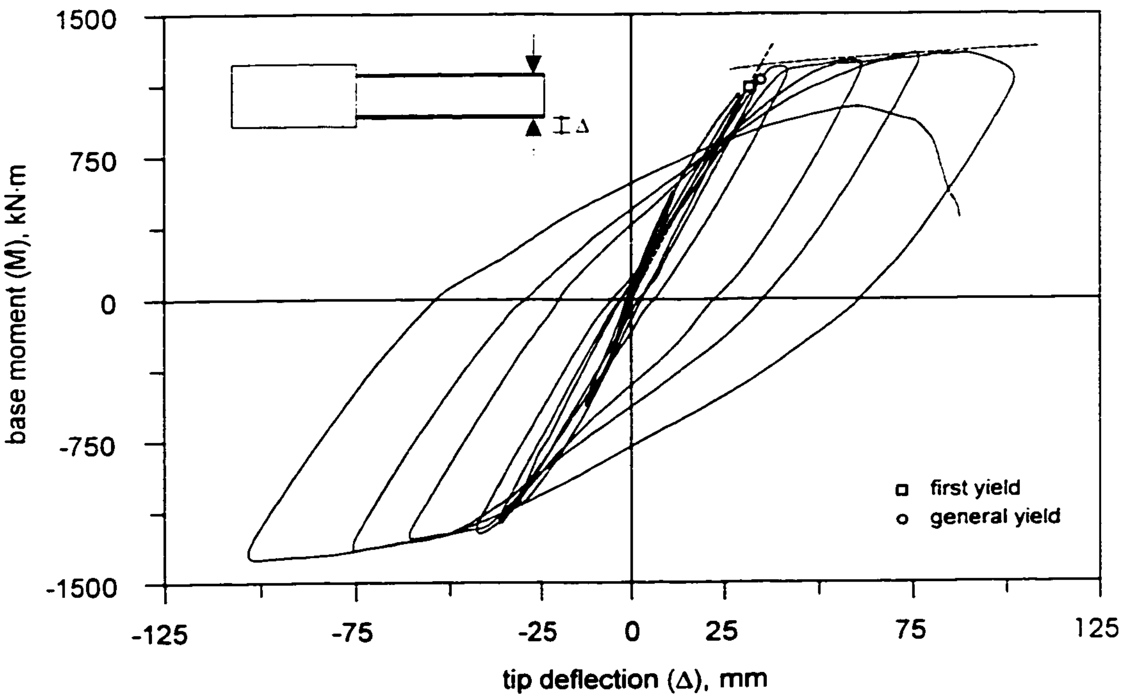

b) base moment vs. tip deflection, including P-Δ

Figure 3.9 Shear and moment vs. tip deflection responses of Specimen W2

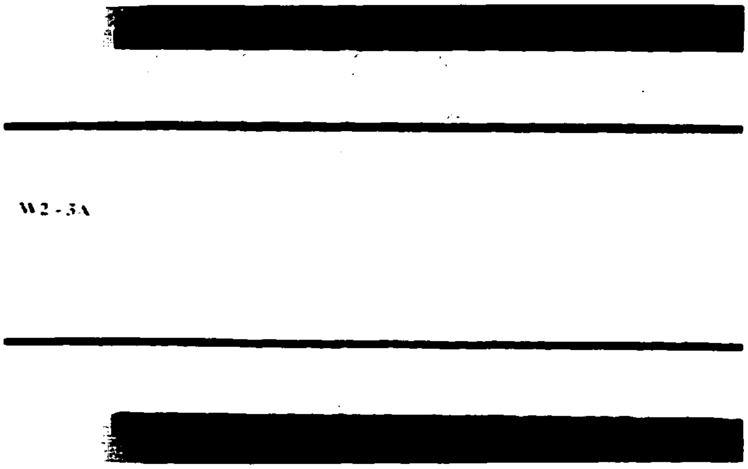

a) load of approximately $2M_{cr}$

b) deflection of approximately $1.75\Delta_y$

c) deflection of approximately $3\Delta_y$

Figure 3.10 Crack patterns for Specimen W2

a) close-up of channel local bucking

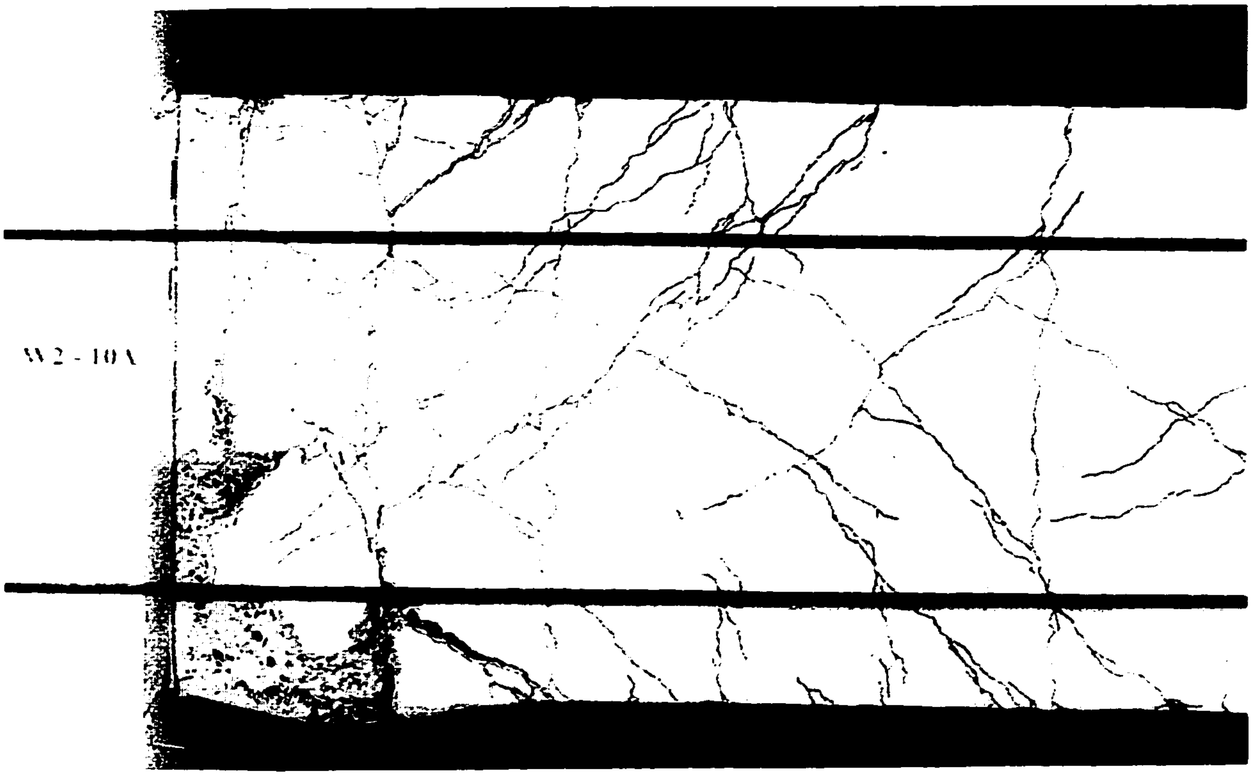

b) plastic hinge region at failure

Figure 3.11 Failure of Specimen W2

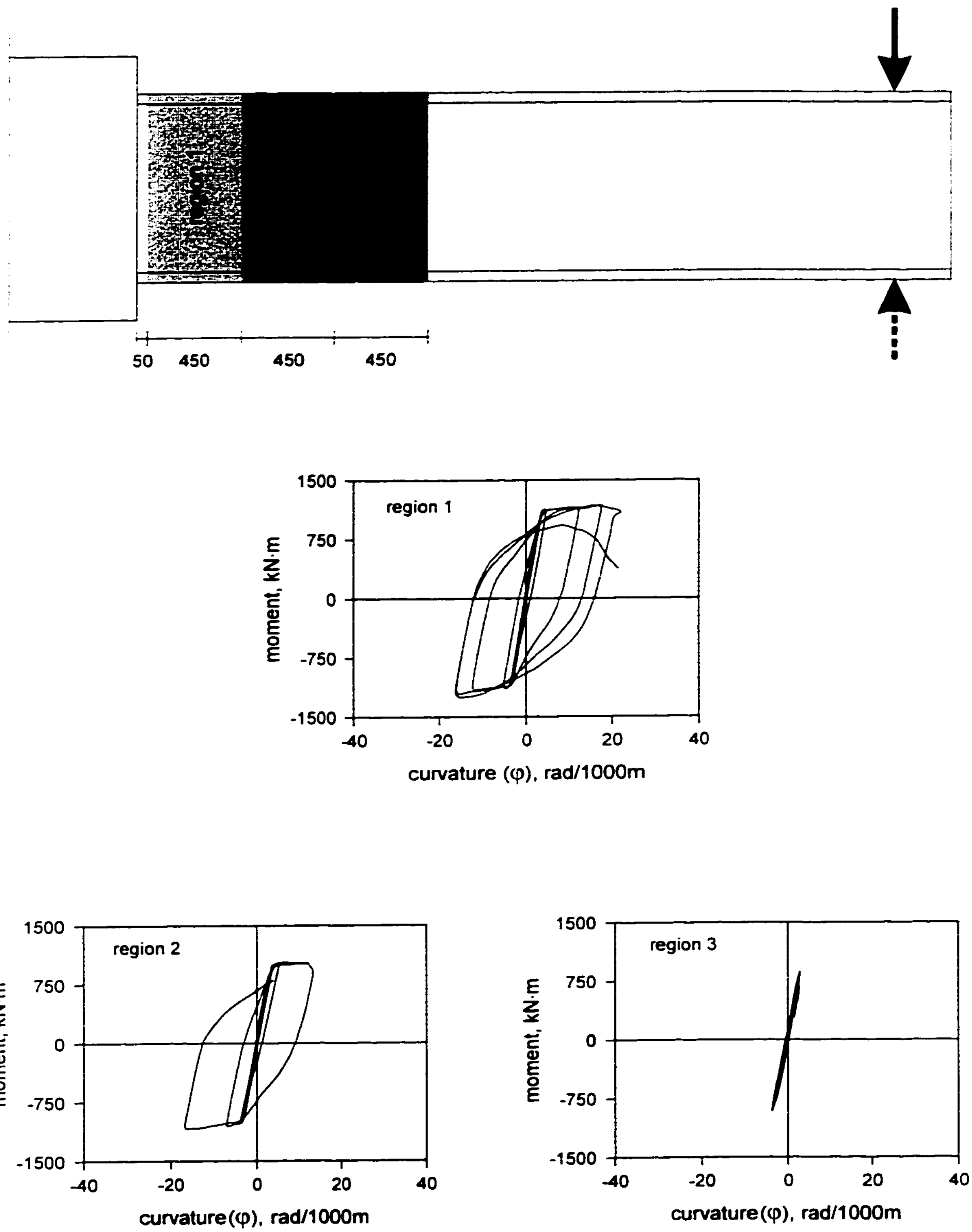

Figure 3.12 Curvature response of Specimen W2

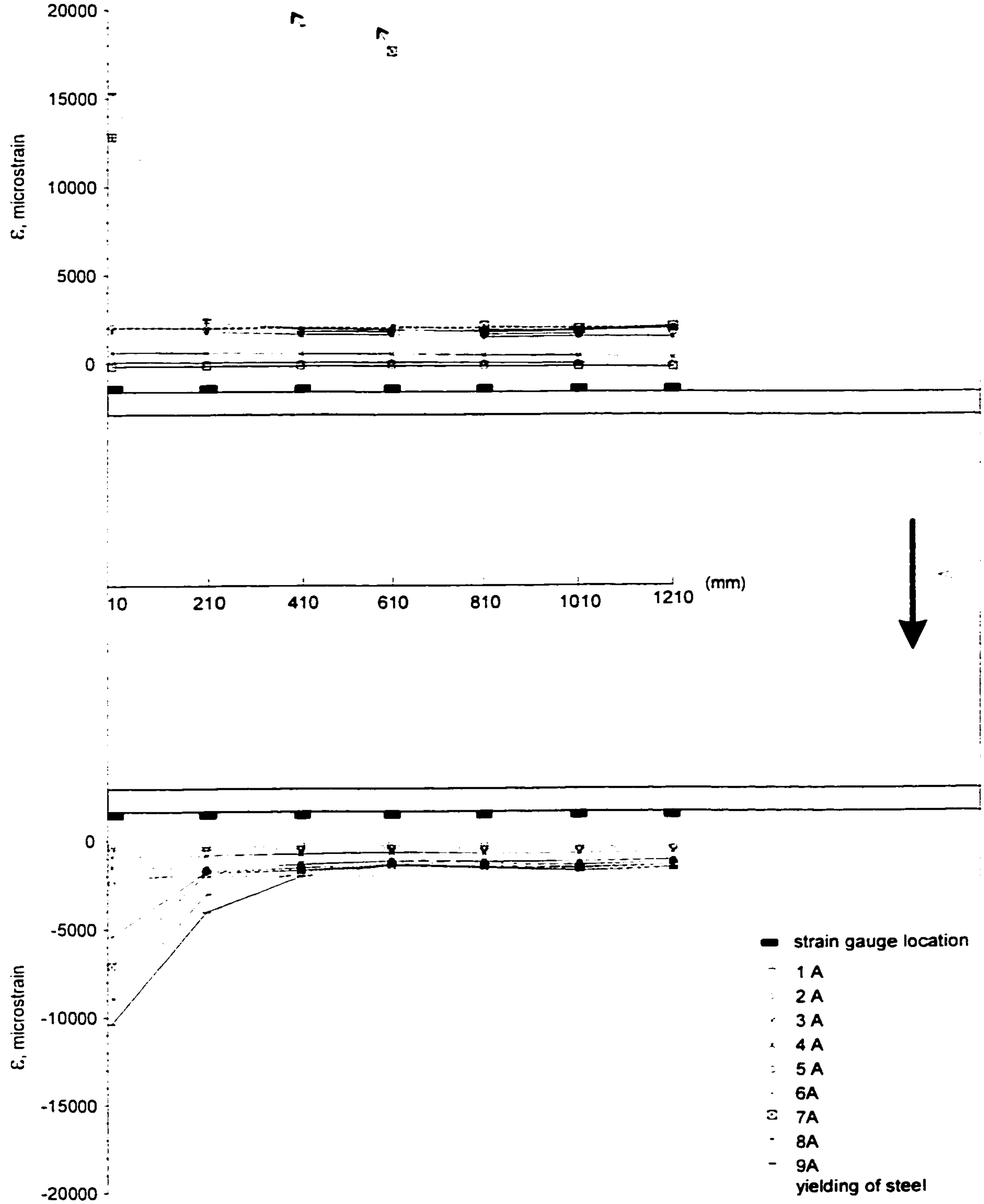

Figure 3.13 Channel strain distribution at peak positive cycles for Specimen W2

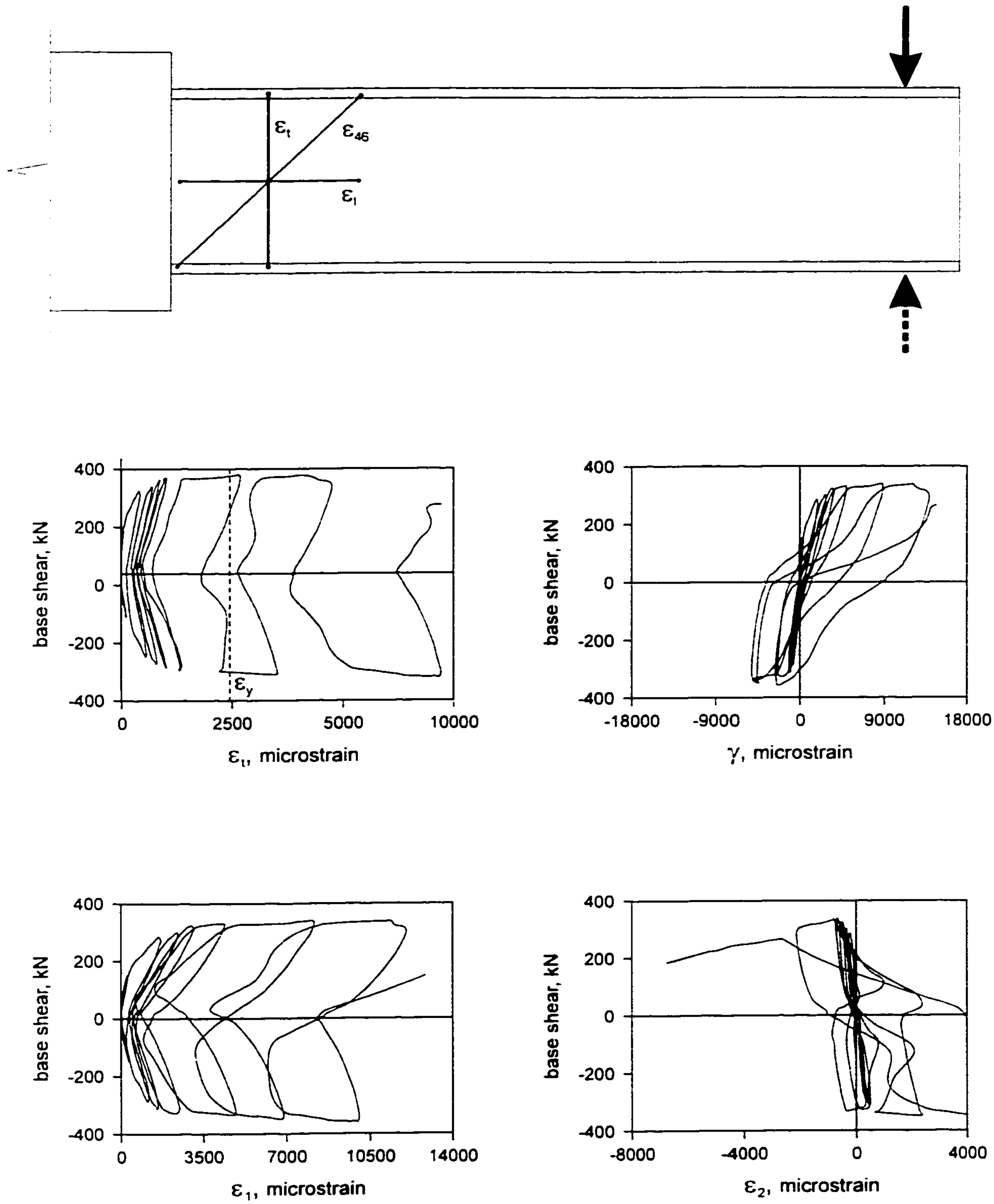

Figure 3.14 Strain conditions for Specimen W2

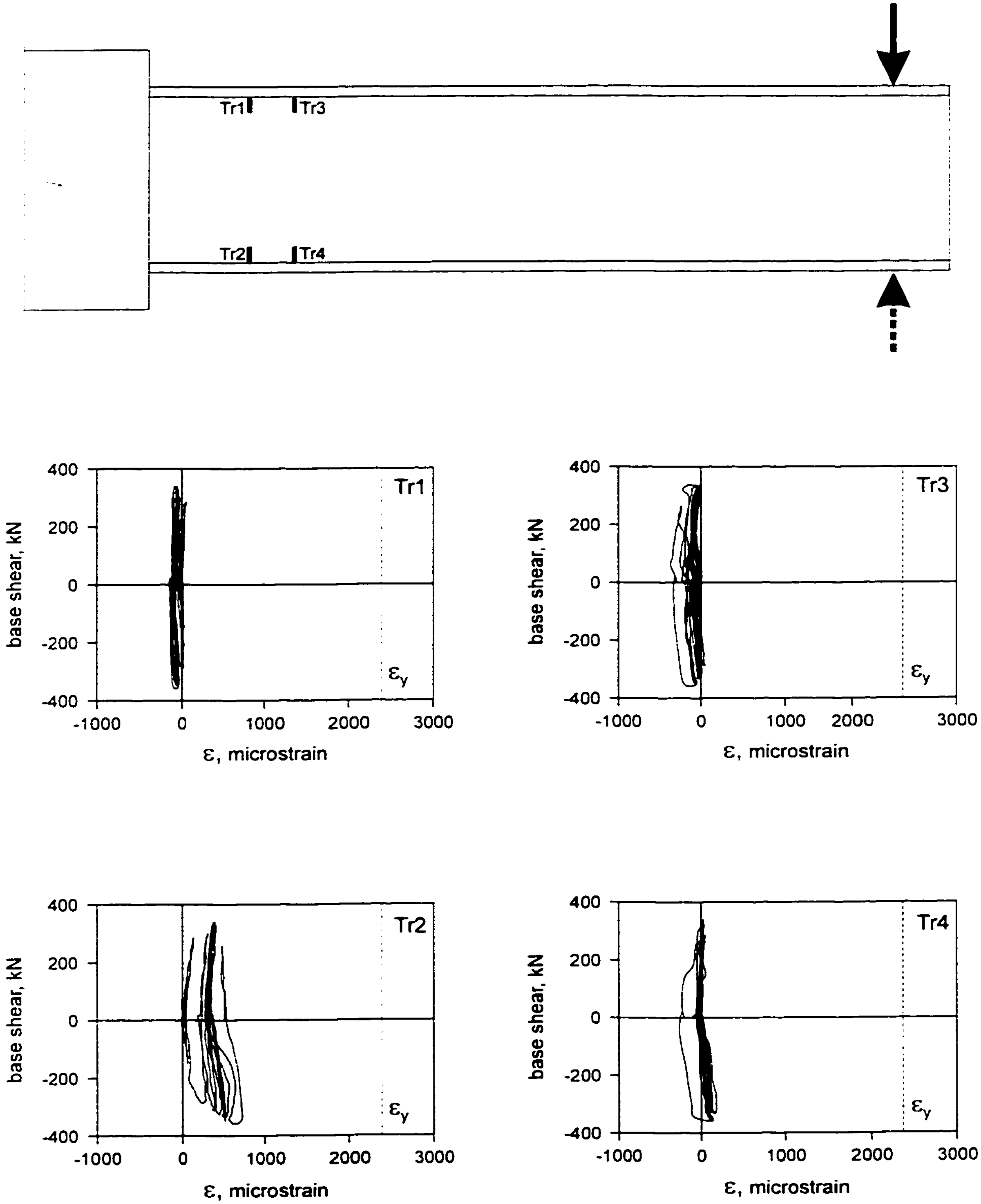

Figure 3.15 Response of Specimen W2 reinforcement

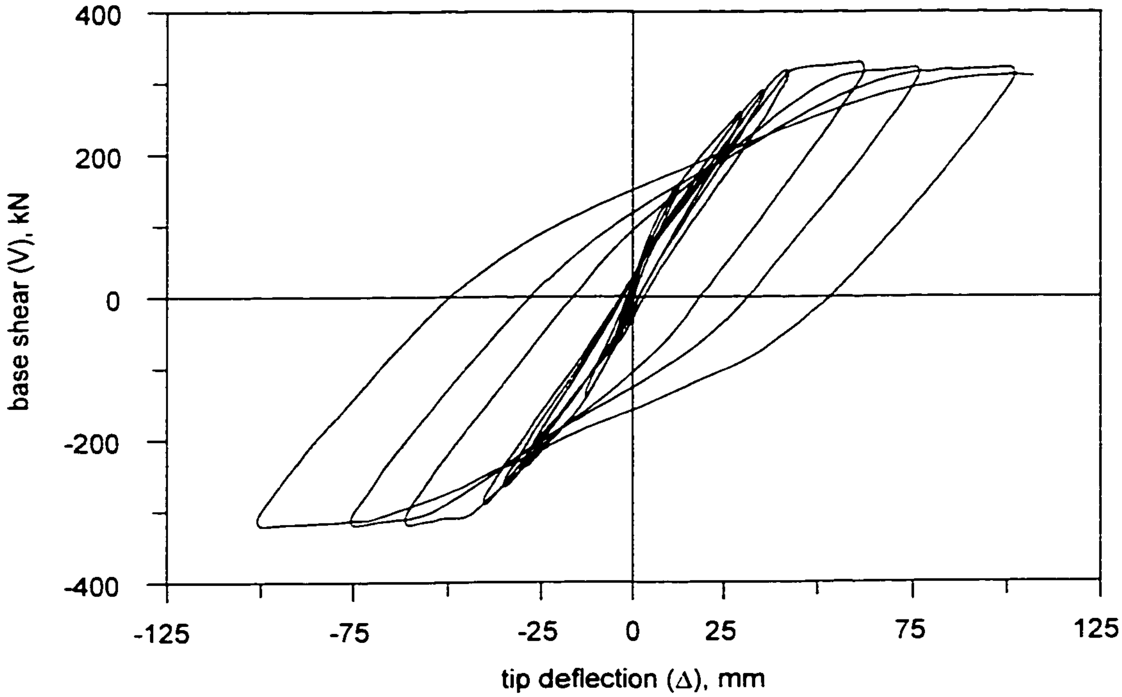

a) base shear vs. tip deflection

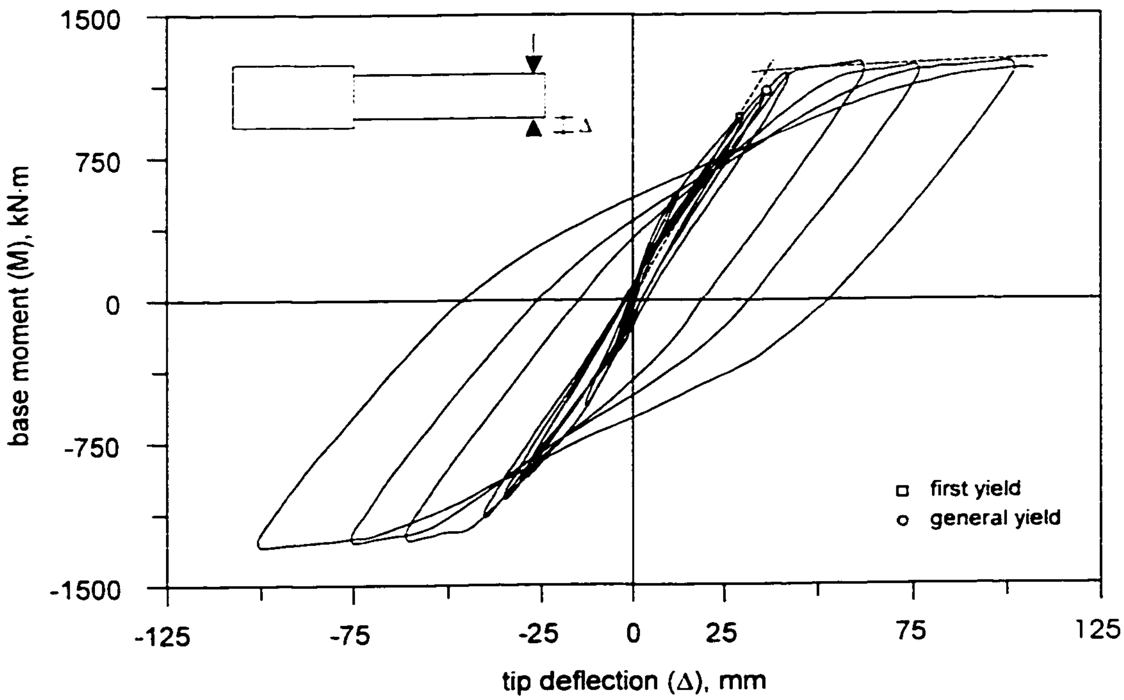

b) base moment vs. tip deflection, including P-Δ

Figure 3.16 Shear and moment vs. tip deflection responses of Specimen W3

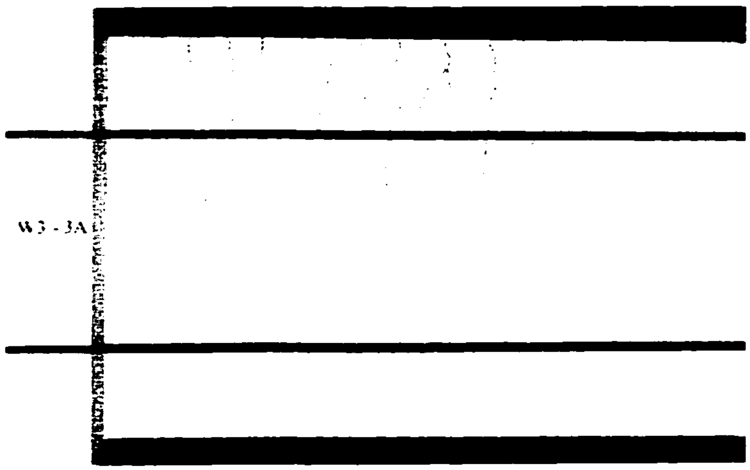

a) load of approximately $2M_{cr}$

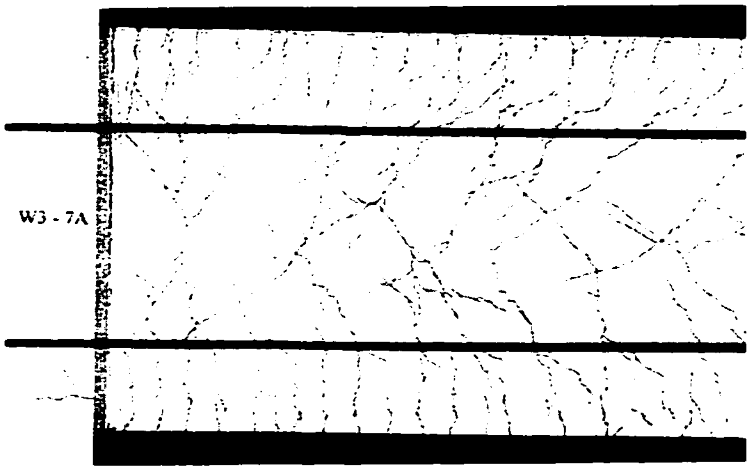

b) deflection of approximately $1.75\Delta_y$

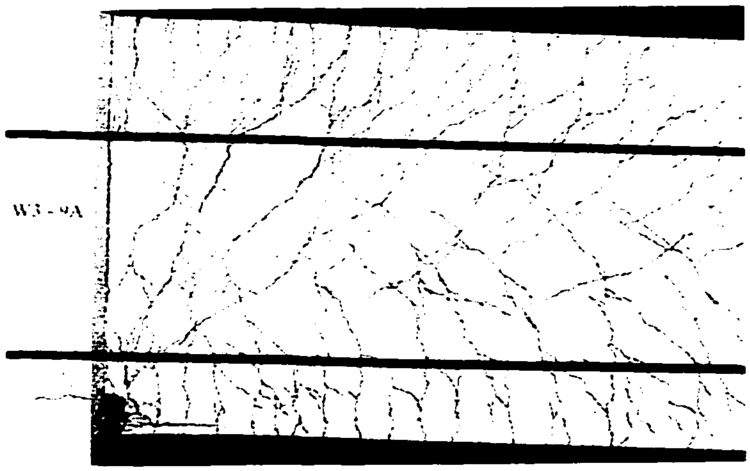

c) deflection of approximately $3\Delta_y$

Figure 3.17 Crack patterns for Specimen W3

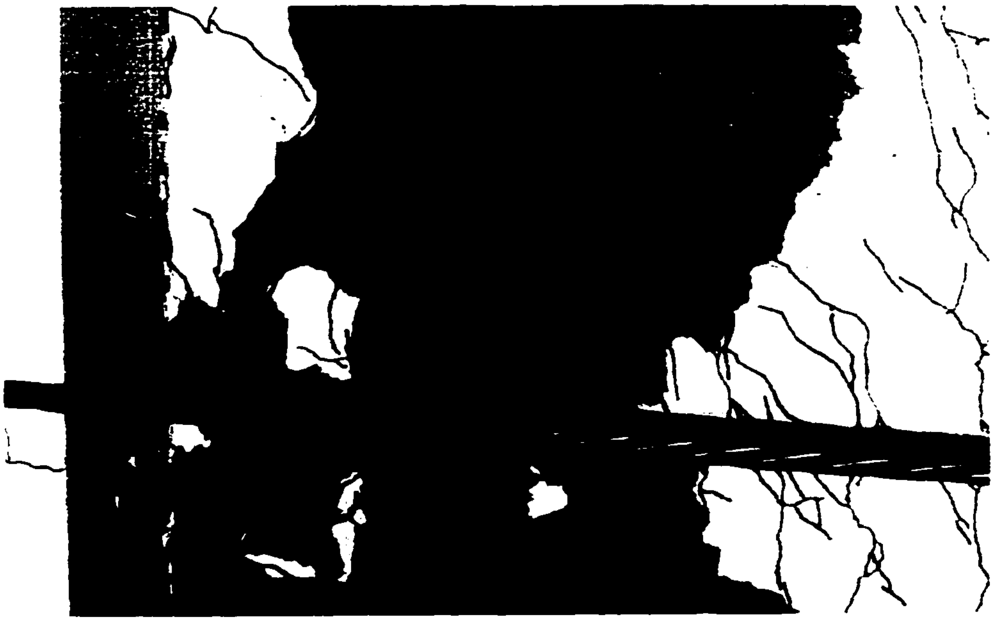

a) close-up of bucked reinforcement

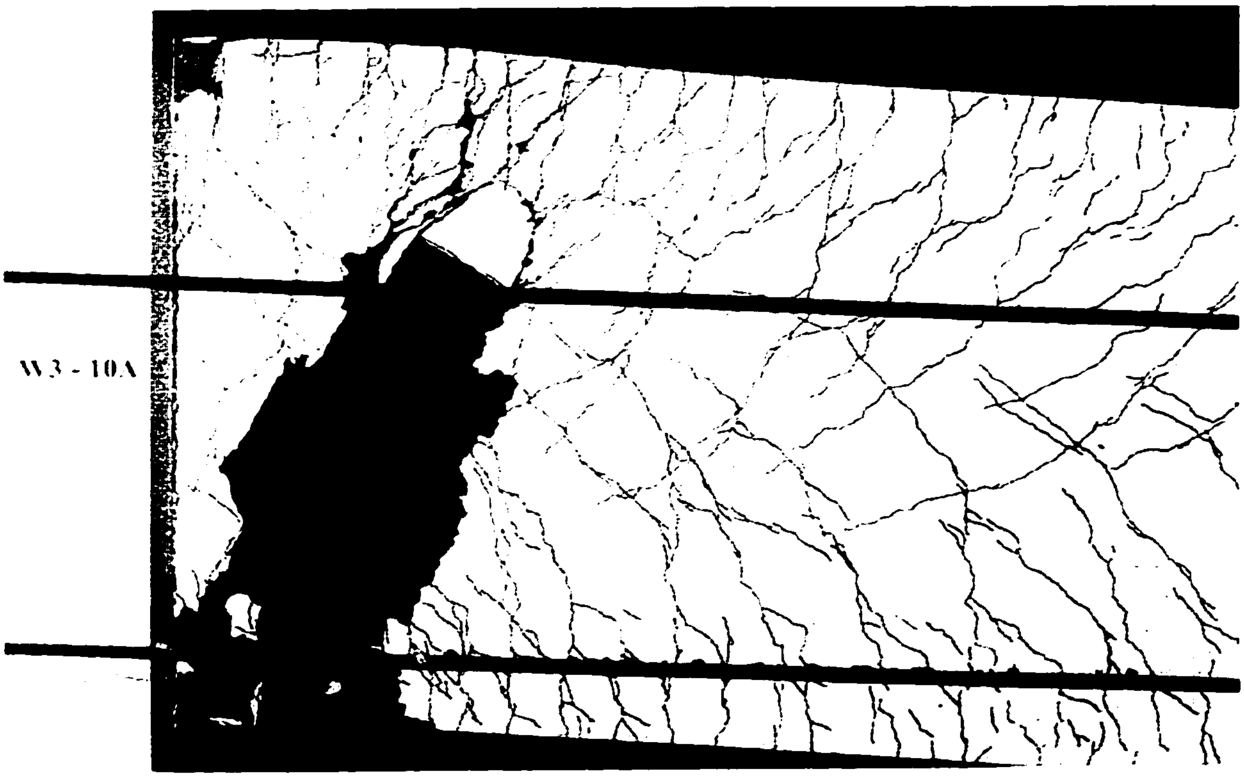

b) plastic hinge region at failure

Figure 3.18 Failure of Specimen W3

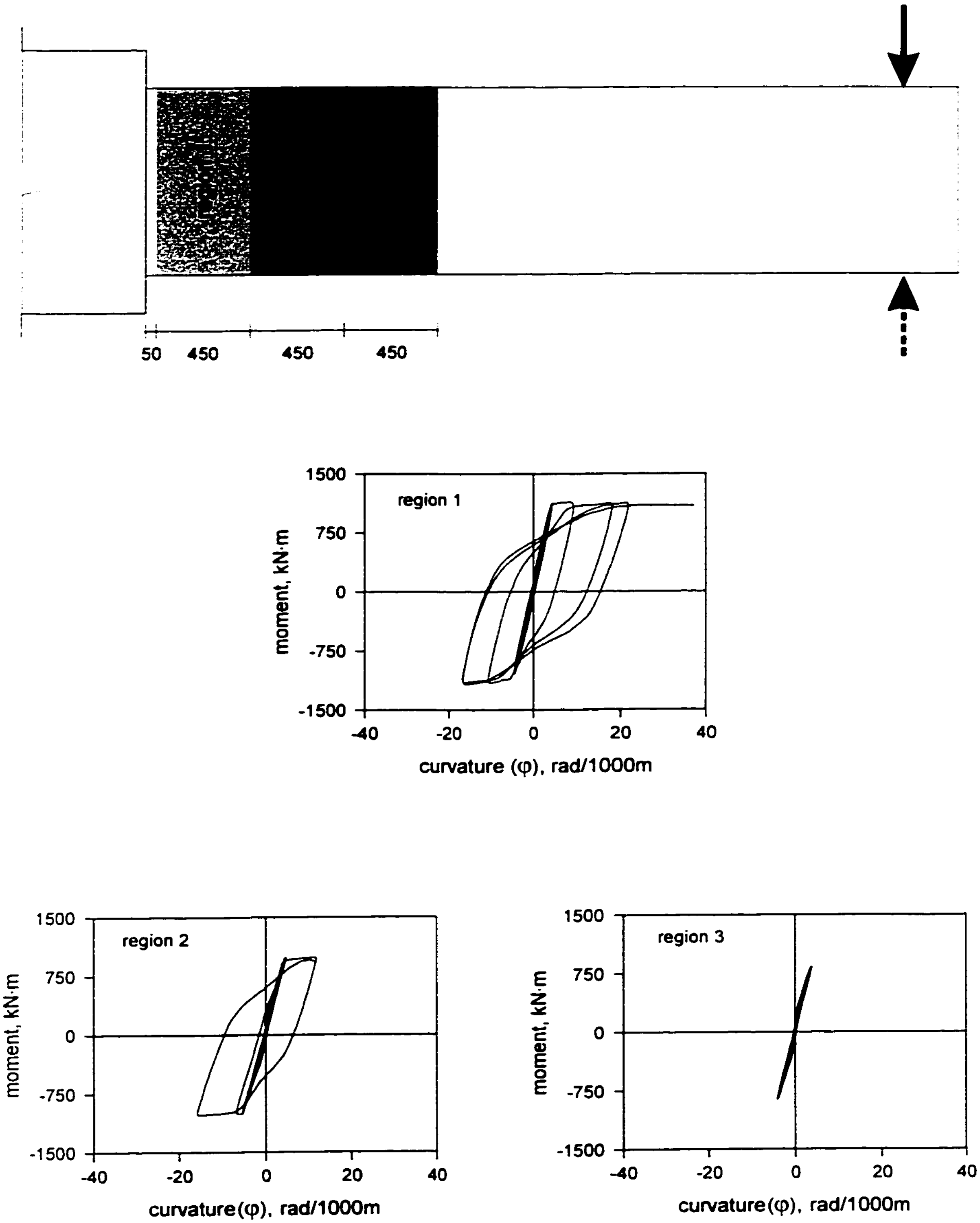

Figure 3.19 Curvature response of Specimen W3

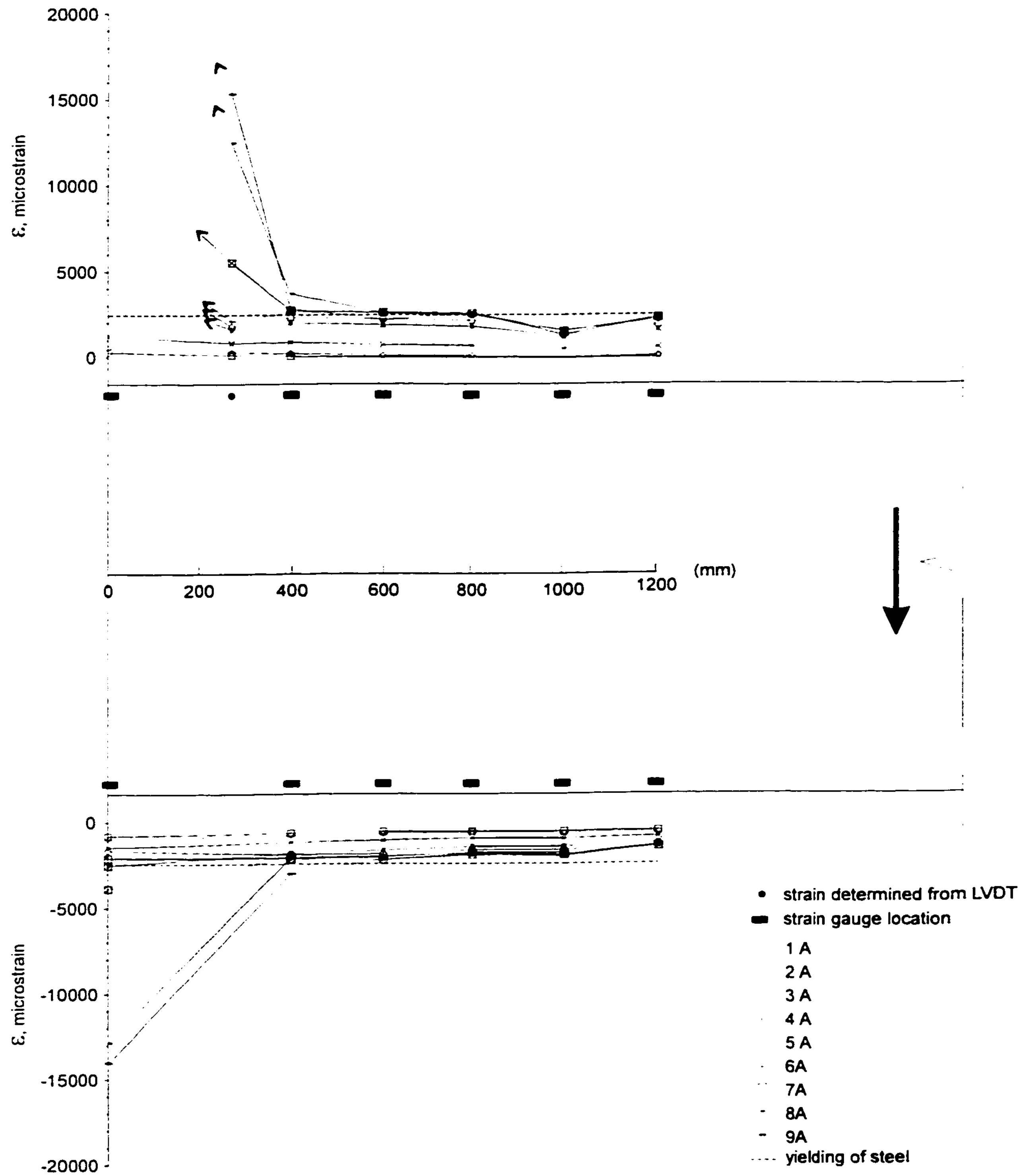

Figure 3.20 Reinforcing bar strain distribution at peak positive cycles for Specimen W3

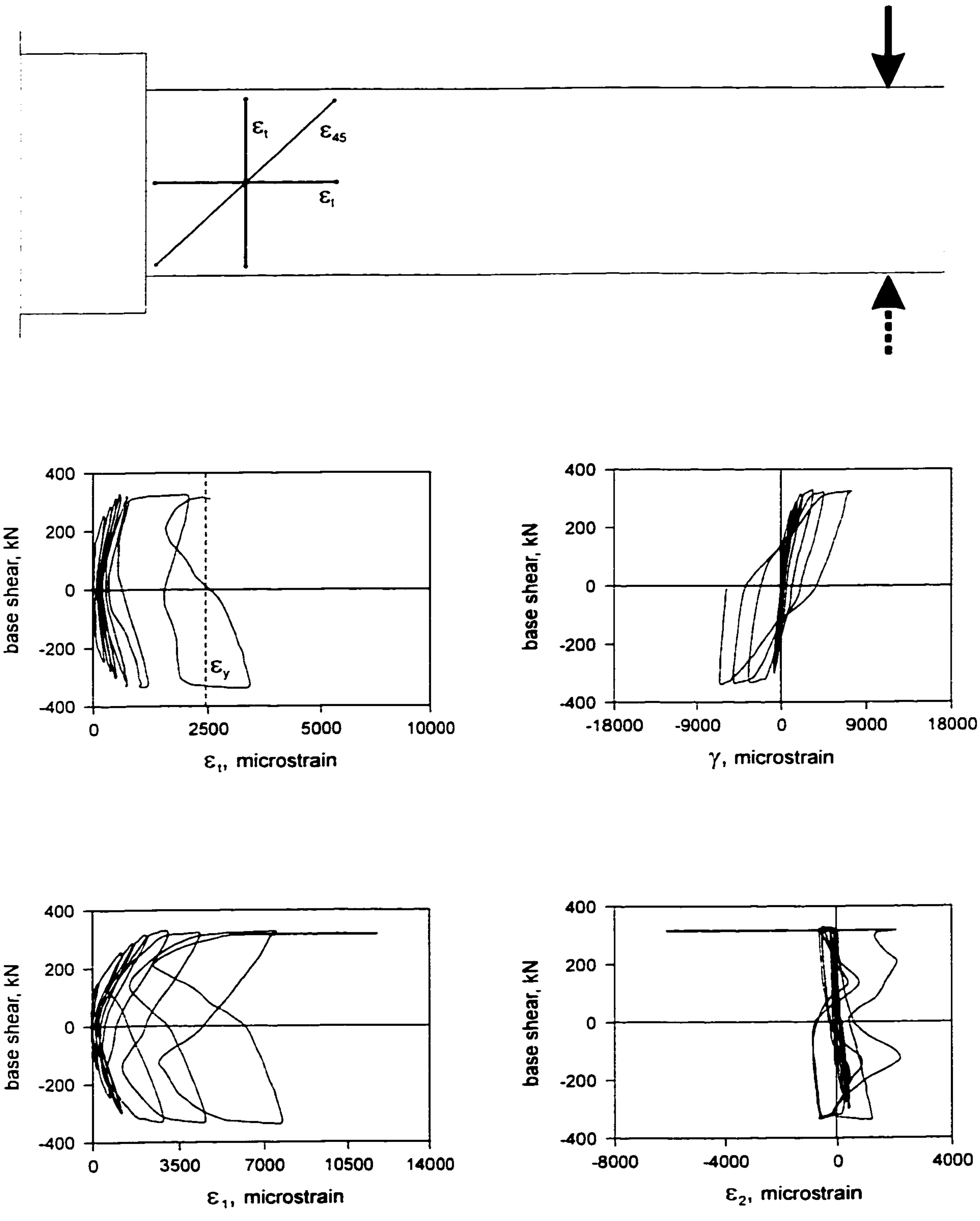

Figure 3.21 Strain conditions for Specimen W3

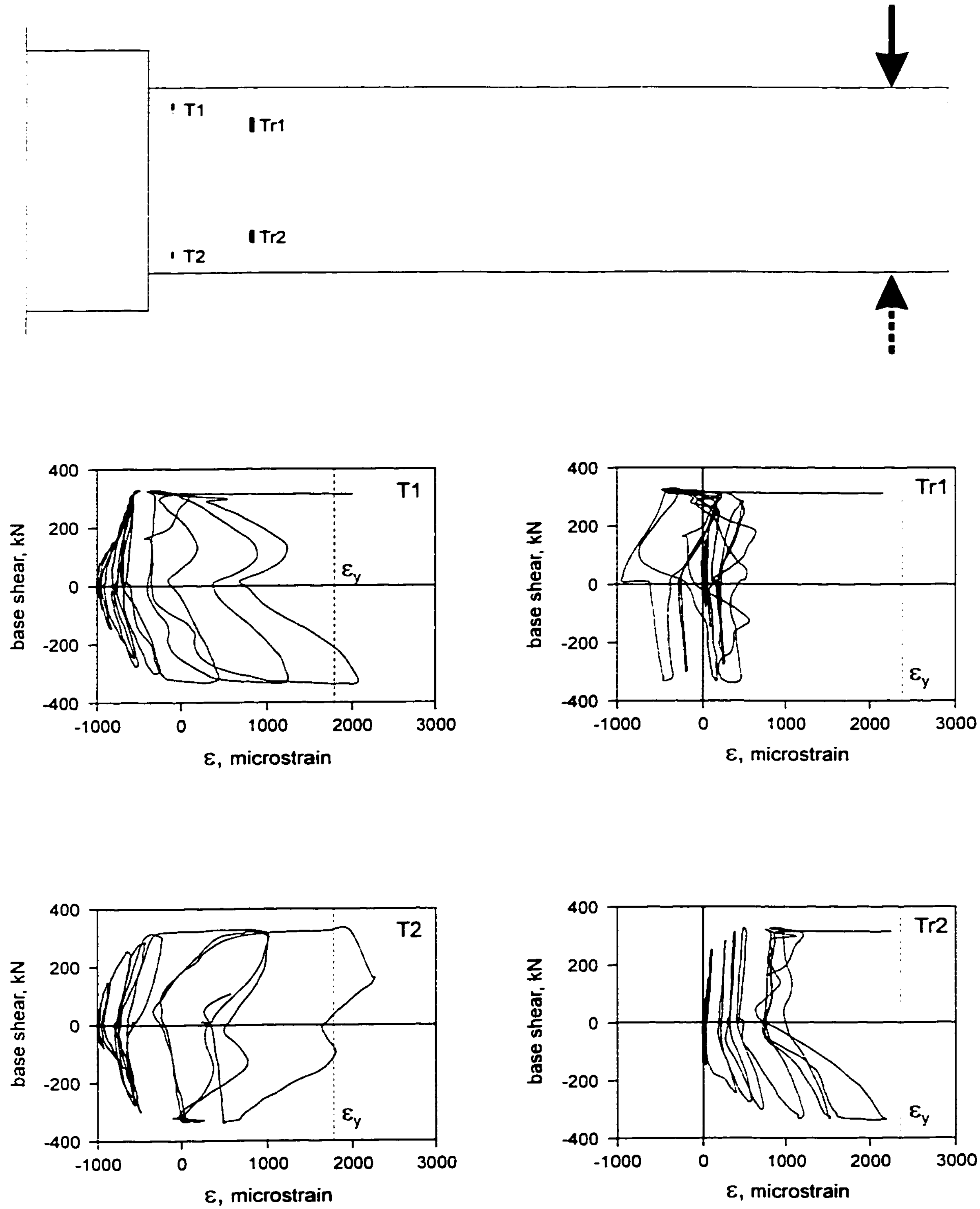

Figure 3.22 Response of Specimen W3 reinforcement

CHAPTER 4

ANALYSES AND COMPARISON OF RESPONSES

Analysis of the reversed cyclic responses, behavioural comparisons and a discussion of the differences in the construction techniques for the three shear wall specimens are presented in this chapter.

4.1 Construction Sequences

The construction of shear wall systems with boundary elements proved to have several advantages. The use of boundary elements eliminated the need for congested end reinforcement details that were necessary in the typical reinforced concrete wall. The end reinforcement required in Specimen W3 was difficult and labourious to construct accurately. As mentioned in section 2.3, the steel boundary elements served as the tension and compression chords, however, they also acted as formwork at the ends of Specimens W1 and W2. The main advantage of construction of walls with boundary elements is that considerable prefabrication is possible, reducing the on-site labour and hence reducing construction time.

Specimen W1 required a significant amount of welding and drilling which necessitated more labour than was needed for Specimen W2. Combining stud welding and prefabricated headed reinforcing bars was a concept that made Specimen W2 a reasonable alternative to conventional construction.

4.2 Predicted and Experimental Results

Monotonic responses for each wall were predicted using the computer programs RESPONSE (Collins and Mitchell, 1991) and RESPONSE 2000 (Bentz and Collins, 1998). The cross-section of each wall was discretized into ten concrete layers with the boundary elements simulated by several steel layers. Average values of the experimentally determined material properties (i.e., f'_c, f_y and ε_{sh}) were used in the predictions. The full non-linear responses of both the concrete and the steel, including strain hardening and confining effects were modeled. With the inclusion of the 600 kN compressive axial load, the nominal flexural capacity of each wall was determined. The predicted monotonic moment versus curvature responses are shown in Fig. 4.1, depicting the envelope of the reversed cyclic loading responses. The experimental moment versus curvature responses, plotted in Fig. 4.1, were determined from the curvature measurements taken from region 1 for each wall using the moment corresponding to the centre of region 1. As can be seen, the curvature predictions are very close to the envelope of the experimental results.

Predictions were made for the load versus deflection of each specimen. Figure 4.2 illustrates how the curvature diagrams were determined from the predicted moment-curvature responses for different stages in the response. The moment-curvature response was idealized by four key stages: first yielding (M'_y, ϕ'_y), general yielding (M_y, ϕ_y), maximum moment (M_m, ϕ_m) and ultimate curvature (M_u, ϕ_u). General yielding was determined from the predicted moment-curvature plot at the point where significant change in stiffness takes place. The ultimate curvature point corresponds to the maximum curvature predicted, while sustaining at least 80% of the maximum moment attained (see Fig 4.2a). For the conditions at first yield and general yielding linear curvature distributions were assumed (see Fig. 4.2b and c). For the conditions at maximum moment a concentrated plastic curvature of ϕ_m-ϕ_y over the plastic hinge length, ℓ_p, was superimposed on the general yielding curvature distribution (see Fig 4.2d). The length of plastic hinging was determined as follows:

$$\ell_p = h_w - \frac{M_y}{M_m} h_w \qquad (4\text{-}1)$$

where, h_w = wall height of 3750 mm

Figure 4.2e shows the assumed curvature distribution at ultimate conditions. It is assumed that the plastic hinge length is the same as that determined from Eq. 4-1.

The predicted plastic hinge lengths determined from Eq. 4-1 and length of tension steel yielding determined from the electrical resistance strain gauges (see Figs 3.6, 3.13 and 3.20) are compared in Table 4.1. It must be pointed out that the actual plastic hinge length is somewhat less than the length over which yielding of the tension steel was recorded.

Specimen	M_y, kN·m	M_n, kN·m	ℓ_p, mm (Eq 4-1)	yielding length, mm (from tests)
W1	986.5	1253.4	798	1200
W2	1079.8	1305.2	647	800
W3	1109.2	1285.0	513	750

Table 4.1 Predicted plastic hinge lengths and experimental yielding lengths

The predicted load-deflection response (see Fig. 4.3) of each wall was determined from the predicted moment curvature response by integrating the curvature distributions over the length of the wall. Since shear deformations were predicted to contribute only 2% to the deflection, they were neglected in the predictions. As can be seen from Fig. 4.3, the predictions give smaller deflections than the experimental values, particularly up to general yielding. This is most likely due to the debonding of the structural sections and the reinforcing bars inside the footing end block. In addition, the HSS and channel sections experienced local buckling at significant deflections, which was not accounted for in the predictions.

4.3 Hysteretic Responses

The hysteretic responses of the wall specimens are described using comparisons of the displacement ductility, ability to increase load beyond general yielding, peak-to-peak stiffness degradation and cumulative energy absorption. Table 4.2 summarizes the maximum values of each of these attributes and indicates the failure mode of each specimen. The deflection ductility is taken as the ratio of the ultimate positive tip deflection, Δ_u, to the positive tip deflection at general yield, Δ_y. The V_u/V_y ratio indicates a specimen's ability to increase its load and maintain the load after general yielding. V_u and V_y represent the loads corresponding to the maximum positive tip deflection, Δ_u, and the positive yield tip deflection, Δ_y, respectively. The third parameter, k_u/k_y, represents the stiffness degradation between general yielding and ultimate deflection. The stiffnesses, k_u and k_y, represent the slope of the line joining the peaks of the respective positive and negative load-deflection responses. The cumulative energy dissipation is obtained by integrating the areas under the load-deflection curves and hence is representative of the hysteretic damping.

Specimen	Mode of Failure	Δ_u/Δ_y	V_u/V_y	k_u/k_y	Energy. kN·m
W1	HSS local buckling	2.80	1.27	0.42	71.0
W2	Channel local buckling and concrete crushing	3.0	1.03	0.36	87.1
W3	Concrete spalling and crushing followed by bar buckling and rupture of confining tie	3.18	1.08	0.47	70.6

Table 4.2 Summary of specimen responses

4.3.1 Specimen Ductility

As shown in Table 4.2. all three specimens have comparable displacement ductility. averaging about 3.0. The ductility levels for each specimen at each peak load are given in Chapter 3. Tables 3.1 through 3.3.

Local buckling of the structural steel compressive chord was the cause of failure for Specimens W1 and W2. In both cases. the local buckling occurred between the first and second set of shear connectors closest to the base of the wall. Figures 4.3a and 4.3b indicate that buckling of the structural steel chords limited Specimens W1 and W2 from reaching their previous maximum load levels. Specimen W2 also experienced crushing of the concrete just prior to buckling. Failure of Specimen W3 was initiated by severe spalling and concrete crushing. followed by buckling of the longitudinal bars in the concentrated reinforcement zone and rupturing of one of the confining ties.

4.3.2 Load Sustainability

The ratio, V_u/V_y, indicates the ability of each specimen to increase and maintain a load after general yielding. Table 4.2 and Fig. 4.4 show that Specimen W1 reached the largest value of V_u/V_y, since the response of this wall was governed by the structural steel.

These tension and compression chords experienced significant strain hardening allowing Specimen W1 to maintain the load in the later stages. Specimen W2 began to lose its capability to sustain load in the last full cycle due to concrete crushing and buckling of the channel in compression. Specimen W3, after yield, maintained a constant V_{peak}/V_y ratio of approximately 1.1.

4.3.3 Stiffness Degradation

The ultimate stiffness ratios in Table 4.2 show that all of the specimens had a similar peak-to-peak stiffness ratio, k_u/k_y, at the end of their respective tests. Figure 4.5 illustrates the stiffness degradation of each specimen throughout the entire test. The most evident difference between the specimens is the significantly lower initial stiffness of Specimen W1 (see Fig. 4.5). Although Specimen W1 had comparable flexural strength to that of the other specimens its elastic stiffness was less.

4.3.4 Energy Dissipation

One of the most important characteristics is the ability of a shear wall to dissipate energy while subjected to reversed cyclic loading. Figure 4.6 compares the cumulative energy dissipation versus ductility and tip displacement for each wall. It is shown that Specimen W2 dissipated the greatest amount of energy, approximately 25% more energy than the other two specimens. The greater cumulative energy dissipation of Specimen W2 is due to the fact that the hysteretic loops are wider than the loops of the other two specimens (see Fig. 4.3).

4.4 Structural Steel Local Buckling

Various types of structural steel sections such as wide-flange, angle, channel and HSS can be used for the chord members of composite shear walls. An HSS is one of the most economical sections because it is capable of developing large compressive strains. This is due to a larger radius of gyration when compared with other sections with the same cross sectional area. There are concerns about the ductility of HSS brace members after local buckling occurs. However, HSS members serving as truss chords in a composite steel-concrete shear wall are subjected to much less severe strain gradients over their depth.

As described in Table 2.2, the width-to-thickness ratios and the height-to-web ratios all satisfy the requirements for Class 1 sections in the CSA S16.1 Standard. The strain measurements on the steel sections included local strain measurements using electrical resistance strain gauges and average strain measurements using LVDTs. The electrical resistance strain gauges were typically located just outside of the regions of most severe local buckling, however the LVDT readings captured the average strains across these regions. From the strain readings the following conclusions were made:

1) Initial signs of local buckling are apparent at strains of about 1%.
2) Both the HSS and the channel sections had strains greater than 2% and hence it is assumed that strain hardening was achieved prior to local buckling.

These reversed cyclic loading tests have indicated that in order for composite walls to get comparable behaviour to a reinforced concrete ductile flexural wall, Class 1 sections must be used, since local buckling must be delayed until reasonably high strains are reached. Another important aspect in the design is to provide adequate connection between the steel section and the concrete. The provision of a sufficient number of discrete shear connectors, such that their shear capacity would enable yielding of the HSS chord member, was found to be essential in achieving ductile response.

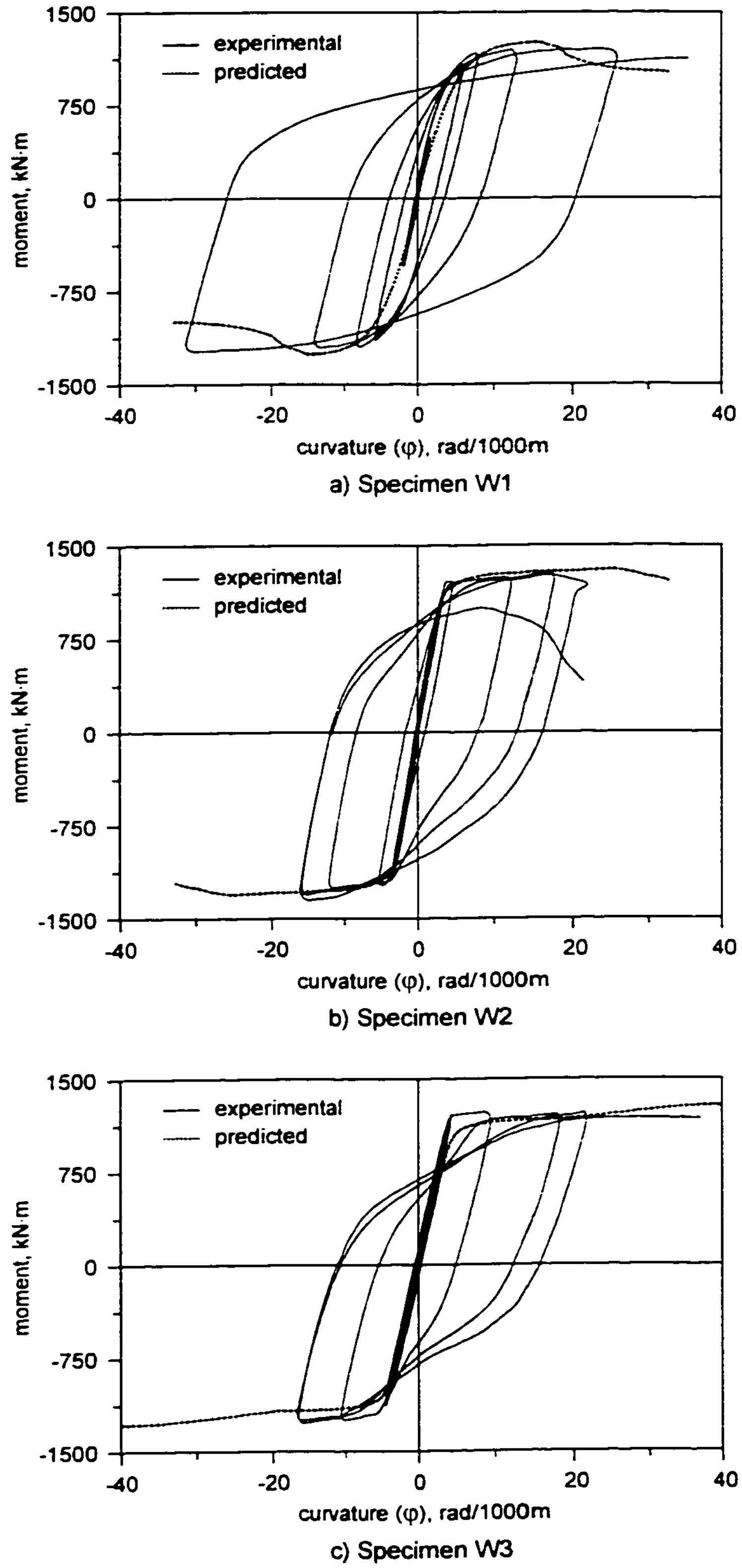

Figure 4.1 Experimental and predicted moment versus curvature plots

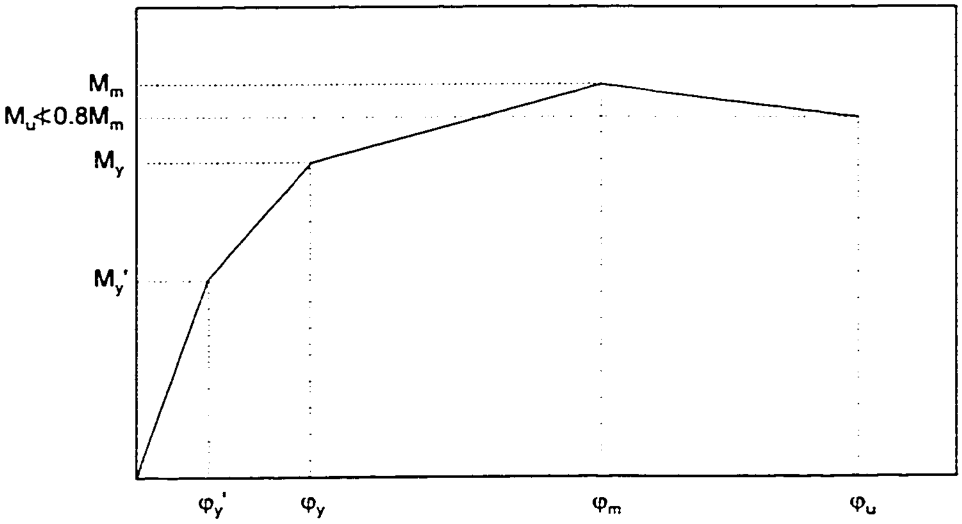

a) Monotonic moment-curvature prediction

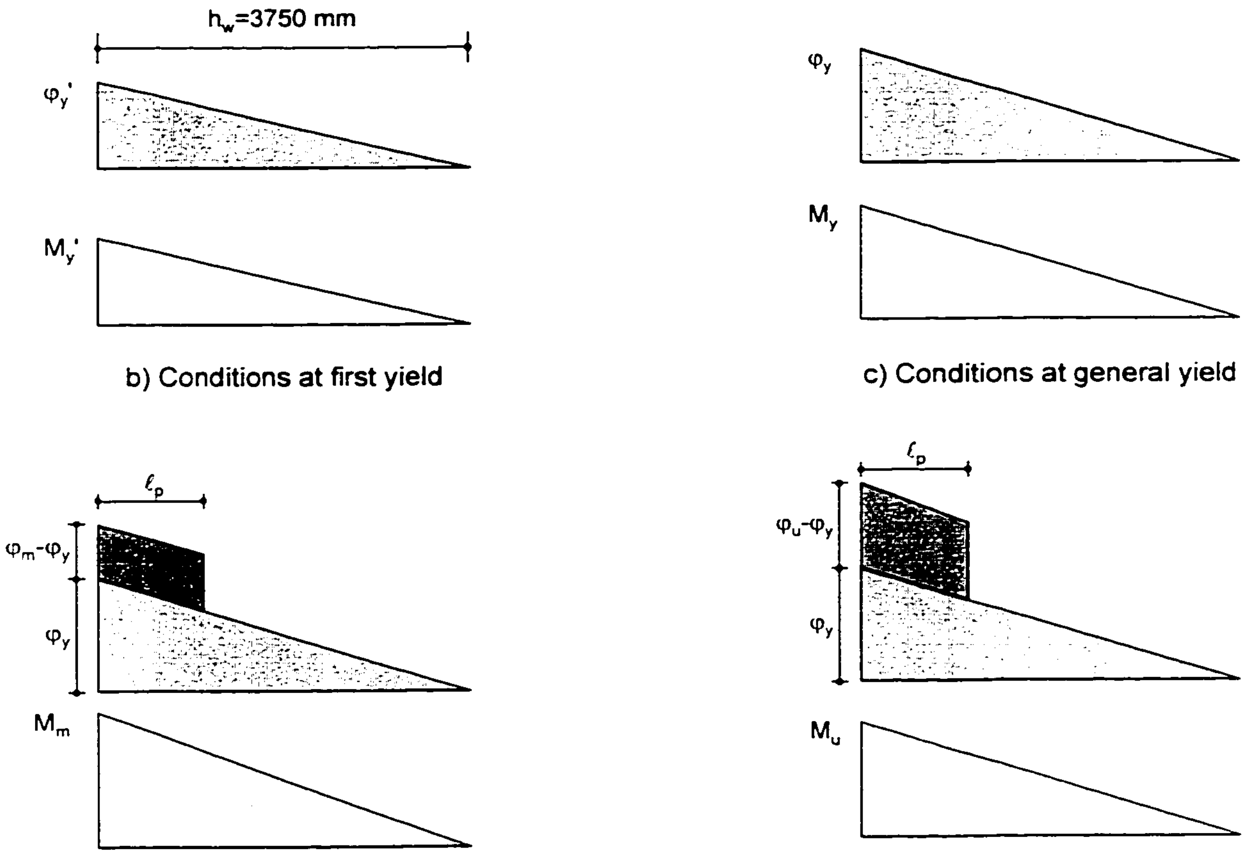

b) Conditions at first yield

c) Conditions at general yield

d) Conditions at maximum moment

e) Conditions at ultimate moment

Figure 4.2 Determination of curvature diagrams from moment-curvature predictions

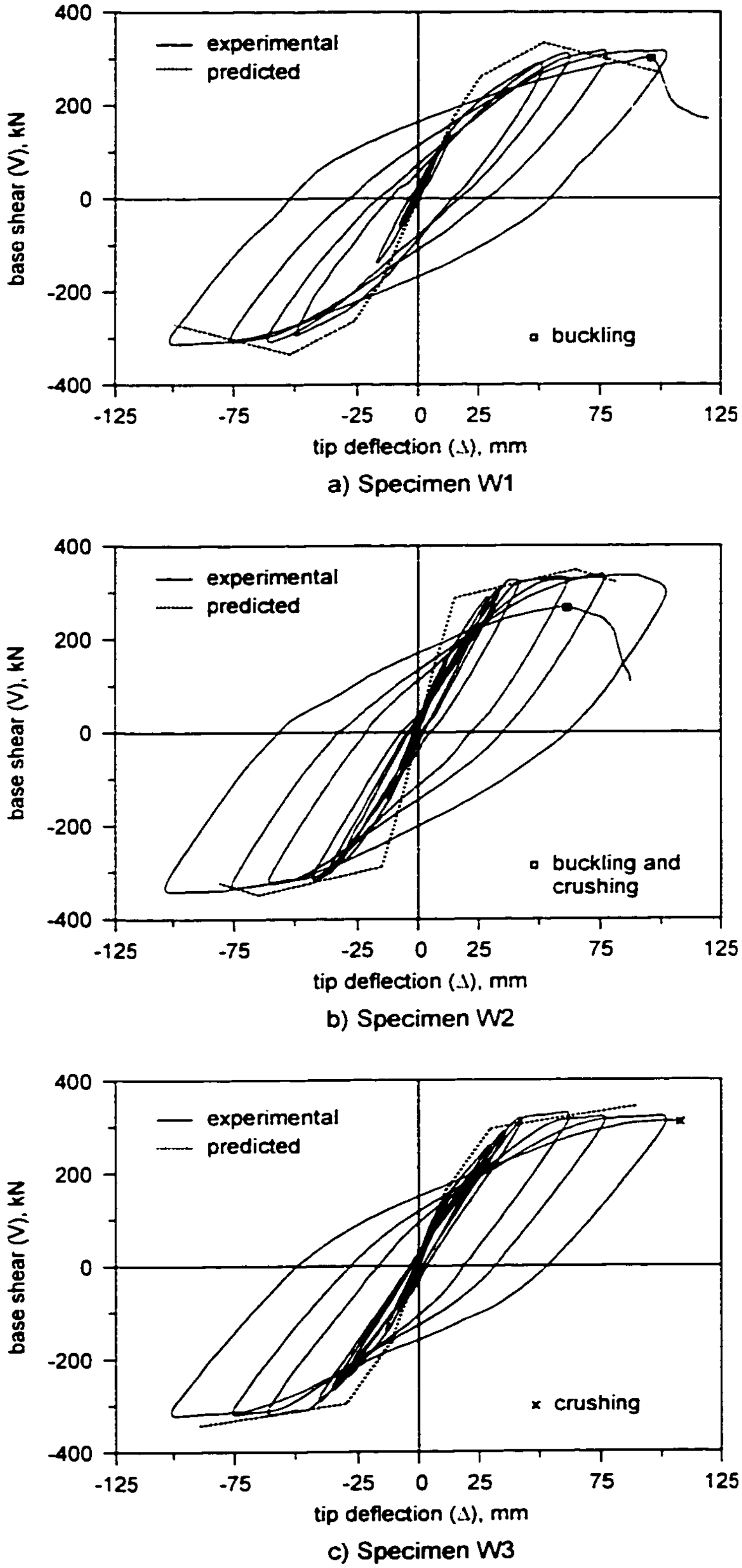

Figure 4.3 Experimental and predicted load-deflection curves

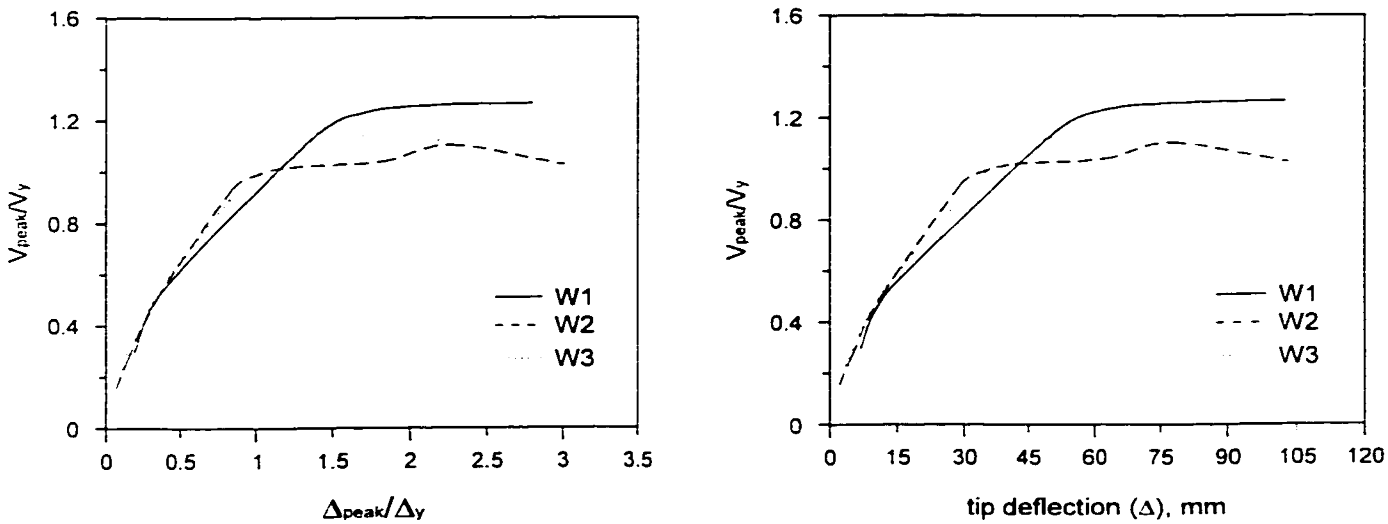

(a) Load ratio versus ductility ratio

(b) Load ratio versus tip deflection

Figure 4.4 Load sustainability of specimens

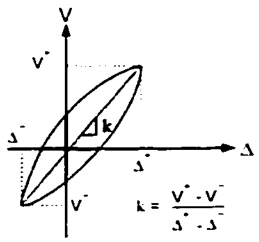

Loading stiffness, k

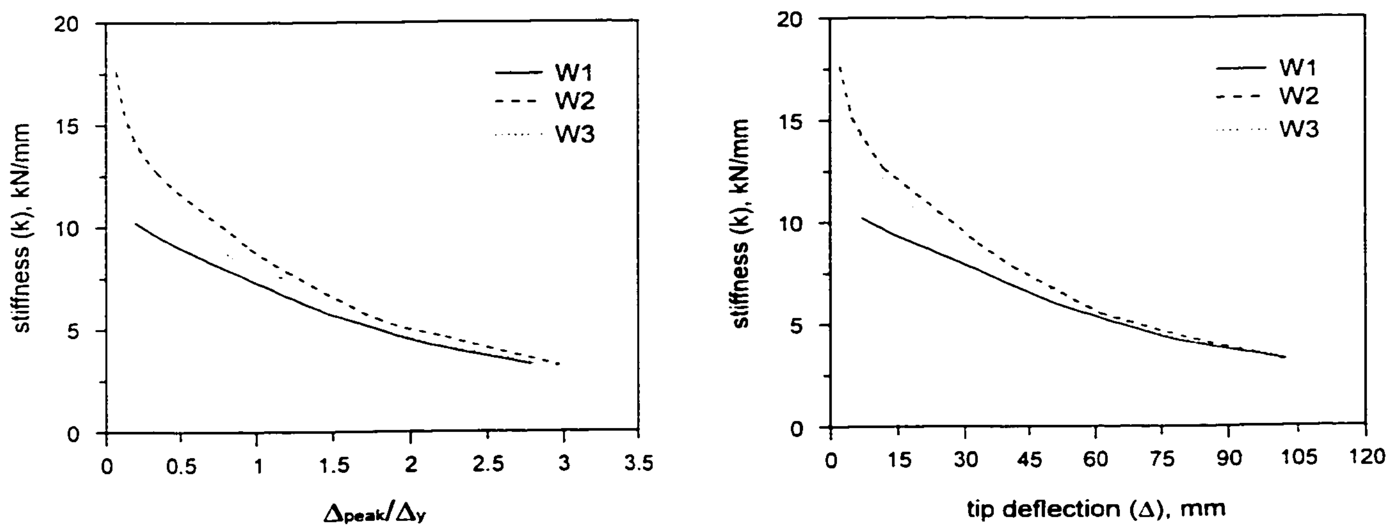

(a) Loading stiffness versus ductility ratio

(b) Loading stiffness versus tip deflection

Figure 4.5 Stiffness degradation of specimens

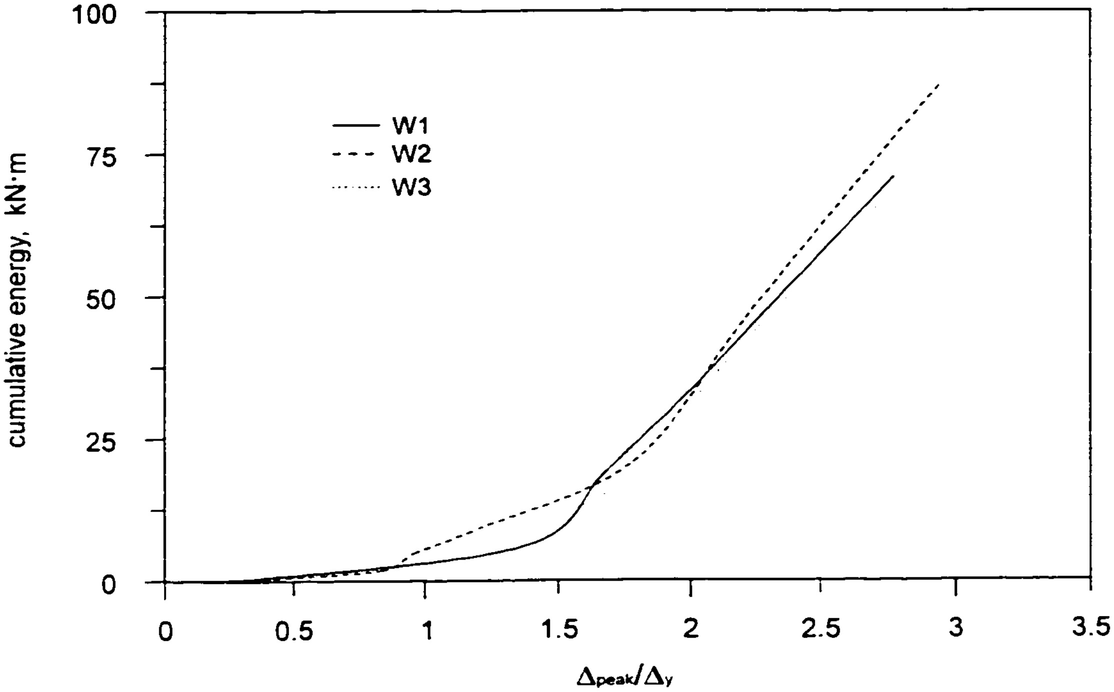

a) cumulative energy vs. ductility ratio

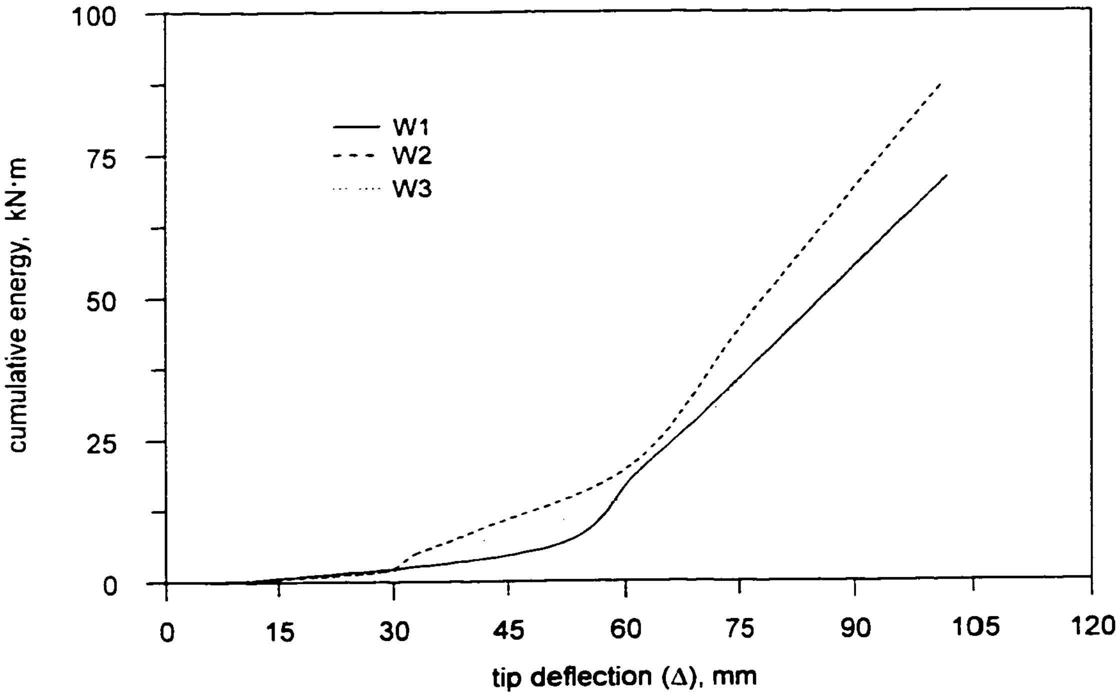

b) cumulative energy vs. tip deflection

Figure 4.6 Energy dissipation of specimens

CHAPTER 5

CONCLUSIONS AND RECOMMENDATIONS

5.1 Conclusions

This experimental programme evaluated the performance of three shear wall specimens subjected to reversed cyclic loading. The traditionally reinforced concrete ductile flexural wall was designed in accordance with the Canadian Standard for the Design of Concrete Structures CAN3-A23.3-M94 (CSA. 1994). The designs of the two composite shear walls were carried out following the same principals used for the design of ductile flexural walls. An additional requirement for the composite walls was included ensuring that the shear connection between the boundary elements and reinforced concrete was capable of developing full yielding of the boundary elements.

The primary objective of this study was to investigate the reversed cyclic loading responses of walls with structural steel boundary elements and compare these responses with the response of a reinforced concrete ductile flexural wall. In addition, the constructibility of the two composite walls and the reinforced concrete ductile flexural wall was compared. The conclusions based on the construction and tests are discussed below:

i. The hysteretic responses of the walls with boundary elements were very similar to that of the typical reinforced concrete ductile flexural wall. All of the walls were designed to have equivalent flexural capacities and displayed similar ductilities and cumulative energy dissipation. Composite wall Specimen W2 exhibited slightly better energy dissipation than the other two specimens.

ii. The welding of the transverse reinforcing bars directly to the hollow structural steel tubes in Specimen W1 provided excellent shear connection enabling the full development of yielding of the boundary elements. The shear connection in Specimen W2 consisted of studs welded to the steel channel boundary elements, together with overlapping transverse reinforcing bars with headed ends. This connection proved capable of developing the full yield of the steel channels. However, significant separation occurred between the steel channel and the reinforced concrete web.

iii. The failure mode of the composite walls was precipitated by local buckling of the structural steel boundary elements. While a reduced spacing of the shear connectors in the plastic hinge would help control local buckling, both composite walls achieved ductilities and energy absorption comparable to the reinforced concrete ductile flexural wall.

iv. The positioning of the channels in Specimen W2 provided some concrete confinement at both ends of the wall. The placement of the hollow steel sections at the extreme ends of Specimen W1 enabled this wall to resist flexure almost entirely by forces in the structural steel chords.

v. The use of prefabricated elements in the construction of the boundary element walls would significantly reduce on-site labour. The construction of Specimen W1 required more care during prefabrication of the reinforcement than Specimen W2. However, Specimen W2 requires more on-site placement of reinforcement than Specimen W1. Due to the intricate details of the confinement reinforcement at the ends of Specimen W3, this specimen requires the greatest amount of on-site labour.

This preliminary study indicates that structural concrete walls with steel boundary elements are comparable to reinforced concrete ductile flexural walls when subjected to reversed cyclic loading. In addition, the prefabrication of walls with steel boundary elements can significantly reduce the need for on-site labour.

5.2 Future Research Recommendations

Suggestions for future work on the feasibility and behaviour of composite walls include:

i. A study could be carried out to investigate the influence of both the flange-width-to-thickness ratio and the web-height-to-thickness ratio of the structural steel used as boundary elements. This study could also examine the influence of the shear connector spacing on local buckling of the structural steel boundary elements.

ii. Alternative shapes of structural steel sections (e.g.. channels with longer flanges). with more concrete confining ability. could be investigated to study the influence on the overall ductility of the wall.

iii. An investigation could be carried out to study ways in which the boundary elements could be interconnected over the height of a multi-storey building.

iv. An application of this alternative form of construction on an actual building would provide useful information of the feasibility of construction.

REFERENCES

ACI Committee 318, *Building Code Requirements for Reinforced Concrete (ACI 318-95)*, American Concrete Institute, Detroit, Michigan, 1995.

American Institute of Steel Construction (AISC), Seismic Provisions for Structural Steel Buildings, Chicago, Ill., April 1997.

Associate Committee on the National Building Code, National Building Code of Canada 1990 and Supplement to the National Building Code of Canada 1990, National Research Council of Canada, Ottawa, Ontario, 1990.

Associate Committee on the National Building Code, National Building Code of Canada 1995 and Supplement to the National Building Code of Canada 1995, National Research Council of Canada, Ottawa, Ontario, 1995.

Bentz, E., and Collins, M., RESPONSE 2000 Version 0.7.5 (Beta), University of Toronto, 1998.

Blakeley, R. W. G., Cooney, R. C., and Meggett, L. M., "Seismic Shear Loading and Flexural Capacity in Cantilever Wall Structures." *Bulletin of the New Zealand Society for Earthquake Engineering*, Vol. 8, No. 4, December 1975, pp. 278-290.

Bristowe, S., Cook, W. D., and Mitchell, D., *Seismic Response of Precast Concrete Wall Panels*, Masters Thesis McGill University, Montreal, 1994.

Bruneau, M., Uang, C., Whittaker, A., Ductile Design of Steel Structures, McGraw-Hill, New York, 1998.

Building Seismic Saftey Council, NEHRP Recommended Provisions for Seismic Regulations for New Buildings and Other Structures, Washington, D.C., 1997.

Canadian Institute of Steel Construction (CISC), Handbook of Steel Construction, CISC, Willowdale, Ontario, 1991.

Canadian Institute of Steel Construction (CISC), Limit States Design in Structural Steel, CISC, Willowdale, Ontario, 1990.

Canadian Standards Association, CAN/CSA-S16.1 - Limit States Design of Steel Structures, Rexdale, Ontario, December 1994.

Canadian Standards Association, CAN/CSA-G30.18 - Billet Steel Bars for Concrete Reinforcement, Rexdale, Ontario, December 1992.

Canadian Standards Association, CSA Standard A23.3-84 - Design of Concrete Structures, Rexdale, Ontario, December 1984.

Canadian Standards Association, CSA Standard A23.3-94 - Design of Concrete Structures, Rexdale, Ontario, December 1994.

Cardenas, A. and Magura, D., "Strength of High-Rise Shear Walls - Rectangular Cross Sections," ACI Special Publication 36, Response of Muiltistorey Concrete Structures to Lateral Forces, 1973, pp. 119-150.

Chrysostomou, C. Z., "Effects of Degrading Infill Walls on the Nonlinear Seismic Response of Two-Dimensional Steel Frames," (Dissertation), Cornell University, School of Civil and Environmental Engineering, Ithaca, NY.

Collins, M.P., and Mitchell, D., Prestressed Concrete Basics, Canadian Prestressed Concrete Institute, Ottawa, Ontario, 1987.

Collins, M.P., and Mitchell, D., Prestressed Concrete Structures, Prentice Hall, Response Publications, Toronto/Montreal, 1997.

Corely, W. G., Fiorato, A. E., and Oesterle, R. G., *Structural Walls*, ACI Publication SP-72, American Concrete Institute, Detroit, 1981, pp. 77-131.

Elghazouli, A.Y. and Elnashai, A.S., *Performance of Composite Steel/Concrete Members under Earthquake Loading. Parametric studies and design considerations.* Earthquake Engineering & Structural Dynamics, Vol. 22, April 1993, pp. 347-368.

Goodsir, W. J., *The Design of Coupled Frame-Wall Structures for Seismic Actions*, Research Report 85-8, Department of Civil Engineering, University of Canterbury, Christchurch, New Zealand, 1985, 383 p.

Goodsir, W. J., Paulay, T., and Carr, A. J., "A Study of the Inelastic Seismic Response of Reinforced Concrete Coupled Frame-Shear Wall Structures," *Bulletin of the New Zealand Society for Earthquake Engineering*, Vol. 16, No. 3, September 1983, pp. 185-200.

Hiraishi, H. and Kaminosono T., *Major Causes of Typical Damages of Reinforced Concrete Buildings due to the 1995 Hyogo-Ken Nanbu Earthquake*, Proceedings of the Eleventh World Conference on Earthquake Engineering, Acapulco, Mexico, July 23-28, 1996, Paper No. 878.

Iqbal, M., and Derecho, A. T., "Inertial Forces over Height of Reinforced Concrete Structural Walls During Earthquakes," in *Reinforced Concrete Structures Subjected to Wind and Earthquake Forces*, ACI Publications SP-63, American Concrete Institute, Detroit, 1980, pp. 173-196.

Mander, J. B., Priestley, M. J. N., and Park R., *Theoretical Stress-Strain Model for Confined Concrete*, ASCE Journal of Structural Engineering, Vol. 114, No. 8, August 1988, pp.1804-1827.

Markevicius, V.P., and Ghosh, S. K., *Required Shear Strength of Earthquake Resistance Shear Walls*, Research Report 87-1, Department of Civil Engineering and Engineering Mechanics, University of Illinois at Chicago, February, 1987.

Mitchell et al., *Damage to Concrete Structures Due to the January 17, 1995, Hyogo-Ken (Kobe) Earthquake*. Canadian Journal of Civil Engineering, Vol. 23, 1996, pp. 757-770.

Oesterle, R. G., Fiorato, A. E., and Corley, W. G., "Reinforcement Details for Earthquake-Resistant Structural Walls," *Concrete International Design and Construction*, Vol. 2, No. 12, 1980, pp. 243-273.

Park, R., *Accomplishments and Research and Development Needs in New-Zealand*, Proceedings from the Workshop on Earthquake-Resistant Reinforced Concrete Building Construction, University of California, Berkeley, July 11-15, 1977, Vol. 2, pp. 255-295.

Park, R., and Paulay, T., Reinforced Concrete Structures, John Wiley & Sons, New York, 1975.

Paulay, T., *Earthquake-Resisting Shearwalls – A New Zealand Design Trend*, ACI Journal, Vol. 77, No. 18, May-June 1980, pp. 144-152.

Paulay, T., and Priestley M.J.N., Seismic Design of Reinforced Concrete and Masonry Buildings, John Wiley & Sons, New York, 1992.

Paulay, T., and Uzurmeri, S. M., "A Critical Review of the Seismic Design Provisions for Ductile Shear Walls of the Canadian Code and Commentary," *Canadian journal of Civil Engineering*, Vol. 2, No. 4, 1975, pp. 592-601.

Standards Association of New Zealand, NZS 3101: 1982, Part 1: Code of Practice for the Design of Concrete Structures and Part 2: Commentary on the Design of Concrete Structures, Wellington, New Zealand, 1982.

Standards Association of New Zealand, NZS 3101: 1995, Part 1: Code of Practice for the Design of Concrete Structures and Part 2: Commentary on the Design of Concrete Structures, Wellington, New Zealand, 1995.

Tall Building Committee A41 (Committee A41 of the Council on Tall Building and Urban Habitat), *Mixed Construction*, Monograph on Planning and Design of Tall Buildings (SB-9)-ASCE, New York, 1979, pp. 617-804.

Viest et al. Composite Construction Design for Buildings, McGraw Hill and ASCE. New York. 1997.

Viest. I. M.. *Composite steel-concrete construction*. Journal Structural Division – ASCE. 100(ST-5). 1974. pp.1085-1139.

Wakabayashi. M. Earthquake-Resistant Buildings. McGraw-Hill. New York. 1986.

Wakabayashi. M., and Minami. K.. Experimental Studies on Hysteretic Characteristics of Steel Reinforced Concrete Columns and Frames. Proc. Int. Symp. Earthquake Struct. Eng.. University od Missouri-Rolla. St. Louis. 1. pp 467-480.

APPENDIX A

A.1 Determination of Axial Load

The level of axial compressive load acting on the wall specimens was determined by considering a twelve storey structure reinforced concrete prototype building. The following assumptions were made in determination the axial load level:

a) 5.5 m x 5.5 m tributary area
b) Floor slab width of 180 mm
c) Floor Dead Loads - 4.32 kN/m^2 self weight of concrete floor slab
1.0 kN/m^2 partition loading on all floors
0.5 kN/m^2 mechanical services on all floors
d) Floor Live Loads - 2.4 kN/m^2 on typical office floors

The unfactored gravity loading case consistent with the earthquake loading requirements of the NBCC for this office building are:

$$\begin{aligned} \text{Dead Loads} &= 4.32\ \text{kN/m}^2 + 1.5\ \text{kN/m}^2 &&= 5.82\ \text{kN/m}^2 \\ \text{Live Loads} &= 0.5 \times 2.4\ \text{kN/m}^2 &&= \underline{1.2\ \text{kN/m}^2} \\ & && \ 7.02\ \text{kN/m}^2 \end{aligned}$$

Therefore, the axial load is: (5.5 m x 5.5 m x 7.02 kN/m^2 x 12 storeys) = 2548 kN

Hence, for a half scale model, in order to have the same axial compressive stress, an axial load of 2548/4 = 637 kN would be required. In the experiments a 600 kN axial compressive load was applied to each wall.

A.2 Determination of Lateral Design Loads

Trial cross-sectional dimensions and material properties of each specimen were input in program RESPONSE, to determine a monotonic moment-curvature response. Table A.2.1 gives the probable moment resistance, M_p, for each of the walls, which includes effects for strain hardening. These probable moments were then divided by a lever arm of 3.75 m (distance from the wall base to the application of the lateral force) to determine the shear force, V_p, corresponding to hinging at the base of the wall.

	Probable Moment (M_p), kN·m	Design Shear (V_p), kN
Specimen W1	1365	364
Specimen W2	1320	352
Specimen W3	1283	342

Table A.2.1 Design loads

A.3 CSA Standard Design of Reinforced Concrete Wall (Specimen W3)

Check the design requirements for the detailing of Specimen W3 (see Fig. 2.6).

Step 1: Dimension Limitations (refer to Clause 21.5.3)

The wall thickness within the plastic hinge region must exceed $\ell_u/10$. unless the predicted depth of compression. calculated with factored loads. does not exceed the lesser of:

a) $4b_w = 4\,(152\text{ mm}) = 608\text{ mm}$

b) $0.3\ell_w = 0.3\,(1000) = 300\text{ mm}$

A frame preventing out-of-plane movement of the wall was located 2.25 m from the base of the wall, therefore. $\ell_u/10 = 225$ mm. The calculated depth of compression under factored loads (Step 4) is 365 mm.

It is noted that this dimensional limitation has been slightly exceeded in this test specimen.

Step 2: Concentrated Reinforcement (refer to Clause 21.5.4)

a) Anchorage and Development in accordance with Clause 12

minimum development length of No. 20 bars.

$$\ell_d = 0.45 k_1 k_2 k_3 k_4 \frac{f_y}{\sqrt{f_c'}} d_b \qquad \text{(A-1)}$$

where. $k_1 = 1.0$ for other cases
$k_2 = 1.0$ for uncoated reinforcement
$k_3 = 1.0$ for normal density concrete
$k_4 = 0.8$ for No. 20 and smaller bars
$f_y = 450$ MPa
$f_c' = 38.7$ MPa
$d_b = 20$ mm

Therefore. $\ell_d = 520.8$ mm and 2100 mm of length is provided for each No. 20 bar in the end block. therefore, required anchorage is adequate.

b) Maximum Reinforcement

i) the concentrated reinforcement must be ≤ 0.06 x area of concentrated concrete

$$\frac{\text{area of concentrated steel}}{\text{area of concentrated concrete}} = \frac{8(300\text{ mm}^2)}{(152\text{ mm})(232\text{ mm})} = 0.068$$

It is noted that this reinforcement is on the limit of the code requirement.

ii) size of reinforcement must not exceed $b_w/10 = 15.2$ mm

The uniformly distributed reinforcement in the wall consisted of No. 10 bars and the concentrated reinforcement consisted well tied No. 20 bars.

c) Spacing of Concentrated Reinforcement

minimum clear spacing shall equal or exceed

i) $1.4\ d_b = 1.4\ (20\ mm) = 28\ mm$

ii) $1.4\ d_A = 1.4\ (20\ mm) = 28\ mm$

iii) 30 mm - **governed**

A minimum clear spacing of 25 mm was used between the reinforcement. It is noted that is on the limit of the code requirements.

d) Hoop Requirements

Hoops shall be detailed as hoops in columns in accordance with Clause 7.6 and 21.5.6.5, satisfying the following:

i) minimum tie diameter - at least 30% of longitudinal bars = 0.3(20 mm) = 6 mm

ii) in plastic hinge region, tie spacing shall not exceed

a) $6\ d_b = 6(20\ mm) = 120\ mm$

b) $24\ d_t = 24\ (6\ mm) = 144\ mm$

c) $0.5\ b_w = 0.5\ (152\ mm) = 76\ mm$ - **governed**

iii)outside plastic hinge region, tie spacing shall not exceed

a) $16d_b = 16(20\ mm) = 320\ mm$

b) $48\ d_t = 48\ (6\ mm) = 288\ mm$

c) $b_w = 152\ mm$ - **governed**

iv)hook length shall equal or exceed

a) 60 mm - **governed**

b) $6\ d_b = 6\ (6\ mm) = 36\ mm$

Each of these governing requirements were met in Specimen W3.

Step 3: Vertical and Horizontal Distributed Reinforcement (refer to Clause 21.5.5)

Two curtains of reinforcement must be used if:

$$V_p \geq 0.2\lambda\phi_c\sqrt{f_c'}A_{cv} = 108\ kN$$

V_p is greater than 108 kN, therefore, two curtains of reinforcement were used.

a) Vertical Distributed Reinforcement

reinforcement spacing shall not exceed

i) 450 mm outside plastic hinge

ii) 300 mm in plastic hinge - **governed**

iii) steel/concrete ratio of 0.0025, giving spacing of 608 mm *b) Horizontal Distributed Reinforcement*

i) spacing of reinforcement shall not exceed

a) 450 mm outside plastic hinge
b) 300 mm in plastic hinge
c) steel/concrete ratio of 0.0025 = 608 mm

In addition, it is necessary to provide sufficient shear resistance. The shear resistance of the wall was determined from Eq. 2-1 by calculating the spacing, s_h, of the distributed transverse reinforcement spacing.

$$s_h = \frac{\phi_s A_{sh} f_y d}{V_p} \qquad (2\text{-}1)$$

where, d = 1000 - 15 - 6 - 20 - 65 - 10 = 884 mm

This gives a spacing, s_h of 215 mm, which governs the placement of the horizontal distributed reinforcement.

Hence, two No. 10 bars at a spacing of 215 mm were used.

ii) development of horizontal transverse reinforcement

The required development length is determined from the general expression from the CSA Standard, including the effects of confinement, as:

$$\ell_d = \frac{1.15 k_1 k_2 k_3 k_4}{(d_{cs} + k_{tr})} \frac{f_y}{\sqrt{f'_c}} A_b \qquad (A\text{-}2)$$

where, k_1 = 1.0 for other cases
k_2 = 1.0 for uncoated reinforcement
k_3 = 1.0 for normal density concrete
k_4 = 0.8 for No. 20 and smaller bars
f_y = 475 MPa
f'_c = 38.7 MPa
d_b = 20 mm
d_{cs} = 2/3 (60 mm) = 40 mm

$$k_{tr} = \frac{A_b f_y}{105sn} \qquad (A\text{-}3)$$

s = maximum stirrup spacing, 152 mm
n = number of bars being developed, 2

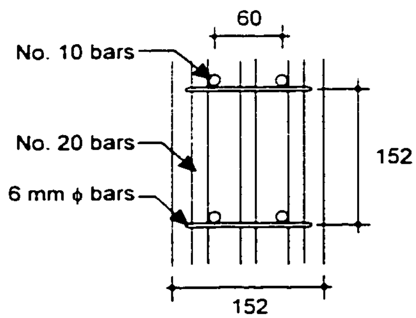

Figure A.3.1 Side view of Specimen W3

Therefore, the required embedment length is 160 mm

Since, the embedment length provided was 190 mm, sufficient development length is provided.

c) Clear Concrete Cover

The cover shall equal or exceed:

i) 20 mm for non-exposed wall

ii) 1.0 d_b = 20 mm

iii) 1.0 d_A = 20 mm - **governed**

The cover provided was 15 mm due to the specimen scale.

Step 4: Ductility (refer to Clause 21.5.7)

i) the depth of compression, c_c, shall not exceed 0.55 ℓ_w = 550 mm

From the factored loading predictions using program RESPONSE for the wall subjected to an axial load of 600 kN, c_c = 365 mm.

Since c_c exceeds 0.14 γ_w ℓ_w = 165.2 mm, confinement must be provided over a length greater than:

$$c_c(0.25 + c_c/\ell_w) = 224 \text{ mm} \qquad \text{(A-3)}$$

For this specimen confinement has been provide over a length of 232 mm.

A.4 Design of Reinforced Concrete Walls with Steel Boundary Elements (Specimens W1 and W2)

Check the design requirements for the detailing of the composite walls (see Figs 2.2 and 2.4).

Step 1: Dimension Limitations (refer to Clause 21.5.3)

The wall thickness within the plastic hinge region must exceed $\ell_u/10$, unless the predicted depth of compression, calculated with factored loads, does not exceed the lesser of:

a) $4b_w$ = 4 (152 mm) = 608 mm

b) $0.3\ell_w$ = 0.3 (1000) = 300 mm

A frame preventing out-of-plane movement of the wall was located 2.25 m from the base of the wall, therefore, $\ell_u/10$ = 225 mm. The calculated depth of compression under factored loads (Step 4) is 407 mm (i.e., a distance of 307 mm into the concrete) and 275 mm for Specimens W1 and W2, respectively. Since the compressed regions of concrete are close to the limit given above, than the wall thickness can be less than $\ell_u/10$.

Step 2: Steel Boundary Elements

a) Anchorage and Development

The composite shear connection in the wall should be sufficient to fully develop the yield strength of the steel boundary elements. From first principles, the development is based on the material properties of both the boundary element and the shear connectors. The necessary number of shear connectors is determined from the following:

$$N = \frac{A_{be} f_{yb}}{\mu \phi_s A_{sh} f_{yh}} \quad \text{(A-4)}$$

where,
- N = number of rows of shear connectors
- A_{be} = area of steel boundary element
- f_{yb} = yield stress of steel boundary element
- μ = coefficient of friction, 0.6
- ϕ_s = 0.85, material resistance factor
- A_{sh} = area of steel connectors in one row
- f_{yh} = yield stress of shear connectors

i) Specimen W1:
- $A_{be} = 2960$ mm^2
- $f_{yb} = 380$ MPa
- $A_{sh} = 200$ mm^2 (2 - No. 10 bars)
- $f_{yh} = 475$ MPa

Therefore, at least 24 rows of 2 - No. 10 bars are necessary to fully develop the HSS sections. Additional bars exceeding the shear resistance requirements (Step 3) were welded at the tip of the wall to ensure sufficient shear connection

ii) Specimen W2:
- $A_{be} = 2450$ mm^2
- $f_{yb} = 377$ MPa
- $A_{sh} = 253$ mm^2 (2 - 12.7 ϕ mm studs)
- $f_{yh} = 402$ MPa

Therefore, at least 18 rows of 2 - 12.7 ϕ mm studs are necessary to fully develop the channels. Additional studs were placed at the tip of the wall to ensure shear connection.

Step 3: Vertical and Horizontal Distributed Reinforcement (refer to Clause 21.5.5)

Two curtains of reinforcement must be used if:

$$V_p \geq 0.2\lambda\phi_c\sqrt{f_c'}A_{cv} = 108 \text{ kN}$$

V_p is greater than 108 kN for both walls, therefore, two curtains of reinforcement were used.

a) Vertical Distributed Reinforcement

reinforcement spacing shall not exceed

i) 450 mm outside plastic hinge
ii) 300 mm in plastic hinge - **governed**
iii) steel/concrete ratio of 0.0025, giving spacing of 608 mm

b) Horizontal Distributed Reinforcement

i) spacing of reinforcement shall not exceed

a) 450 mm outside plastic hinge

b) 300 mm in plastic hinge

c) steel/concrete ratio of 0.0025 = 608 mm

In addition, it is necessary to provide sufficient shear resistance. The shear resistance of the walls was determined from Eq. 2-1 by calculating the spacing, s_h, of the distributed transverse reinforcement spacing.

$$s_h = \frac{\phi_s A_{sh} f_{yh} d}{V_p} \qquad (2\text{-}1)$$

	effective depth, d (mm)	spacing, s_h (mm)
Specimen W1	847	180
Specimen W2	976	220

Table A.4.1 Composite specimen shear spacing

Hence, two No. 10 bars at a spacing of 180 mm and 220 mm were used in Specimen W1 and W2, respectively.

ii) development of transverse reinforcement

a) Specimen W1: determine necessary weld size to develop No. 10 bars

$$A_w = \frac{V_r}{0.67\phi_w X_u} \qquad (A\text{-}5)$$

where, V_r = nominal shear resistance of one No. 10 bar
= (475 MPa)(100 mm^2)
= 47.5 kN
ϕ_w = 0.67
X_u = electrode tensile stength, 300 MPa

Therefore, a minimum 7 mm by 7 mm weld was chosen to connect each No. 10 bar.

b) Specimen W2: determine area of headed plates to develop No. 10 bars
$A_h = 10\,(A_s) = (10)(100\text{ mm}^2) = 1000\text{ mm}^2$
and thickness greater than 7 mm

Therefore, 37 mm x 37 mm x 9 mm plate was used giving an area of 1451.6 mm^2.

Step 4: Ductility (refer to Clause 21.5.7)

i) the depth of compression, c_c, shall not exceed 0.55 ℓ_w = 550 mm

From the factored loading predictions using program RESPONSE for the walls subjected to an axial load of 600 kN, c_c = 407 mm (i.e., a distance of 307 mm within the concrete) for Specimen W1 and c_c = 275 mm for Specimen W2.

Since c_c exceeds 0.14 γ_w ℓ_w = 165.2 mm in both cases, confinement must be provided over a length greater than:

$c_c(0.25 + c_c/\ell_w)$ = 267 mm for Specimen W1
$c_c(0.25 + c_c/\ell_w)$ = 144 mm for Specimen W2

These requirements of confinement do not really apply to the situation with structural steel boundary elements. Instead, the steel boundary elements must be designed and detailed to provide adequate buckling resistance.

A.5 Cracking Moments

The cracking moments were calculated using the equation:

$$f_r = -\frac{P_{axial}}{A_{tr}} + \frac{M_{cr}}{S_{tr}} \qquad \text{(A-6)}$$

where, M_{cr} = applied moment that would crack the extreme concrete fibre
f_r = $0.6\sqrt{f_c'}$, where f_c' was assumed 35 MPa
P_{axial} = constant axial load, 600 kN
A_{tr} = transformed area of specimen
$S_{tr} = \frac{I_{tr}}{y_c}$
I_{tr} = transform moment of inertia of specimen
y_c = distance from neutral axis to extreme concrete fibre

The cracking moments are summarized in the following table:

	A_{tr}, mm^2	I_{tr}, x 10^{10} mm^4	y_c, mm	M_{cr}, kN·m
Specimen W1	161019	1.4239	398	260
Specimen W2	178895	1.9053	489	261
Specimen W3	179654	1.2667	500	175

Table A.5.1 Cracking moments